NAVAL POSTGRADUATE SCHOOL

MONTEREY, CALIFORNIA

THESIS

MODELING OF A DYNAMIC WAVE ENVIRONMENT FOR UNMANNED SURFACE VESSEL CONTROL

by

Joshua F. Malia

December 2018

Thesis Advisor: Brian S. Bingham
Co-Advisor: Joseph Klamo

THIS PAGE INTENTIONALLY LEFT BLANK

REPORT DOCUMENTATION PAGE			*Form Approved OMB No. 0704-0188*

1. AGENCY USE ONLY *(Leave blank)*	**2. REPORT DATE** December 2018	**3. REPORT TYPE AND DATES COVERED** Master's thesis

4. TITLE AND SUBTITLE MODELING OF A DYNAMIC WAVE ENVIRONMENT FOR UNMANNED SURFACE VESSEL CONTROL	**5. FUNDING NUMBERS**
6. AUTHOR(S) Joshua F. Malia	
7. PERFORMING ORGANIZATION NAME(S) AND ADDRESS(ES) Naval Postgraduate School Monterey, CA 93943-5000	**8. PERFORMING ORGANIZATION REPORT NUMBER**
9. SPONSORING / MONITORING AGENCY NAME(S) AND ADDRESS(ES) N/A	**10. SPONSORING / MONITORING AGENCY REPORT NUMBER**

11. SUPPLEMENTARY NOTES The views expressed in this thesis are those of the author and do not reflect the official policy or position of the Department of Defense or the U.S. Government.

12a. DISTRIBUTION / AVAILABILITY STATEMENT Approved for public release. Distribution is unlimited.	**12b. DISTRIBUTION CODE** A

13. ABSTRACT (maximum 200 words)

Modeling and simulation methods for the seakeeping dynamics of surface vessels vary widely. Higher fidelity models often demand high computational complexity that limits application to offline computation and are not applicable to all development cycles. These models are often based on solving nonlinear fluid flow equations, which cost time and computational power. Simplified models can reduce complexity, supporting rapid development. For developing control and autonomy of small unmanned surface vessels, choosing model fidelity requires a tradeoff between the accuracy of results and complexity of simulation. This thesis compares two methods for modeling and simulating the seakeeping of a small unmanned vessel: Gazebo—an open source, real-time robotics simulator, with an extension that integrates a model for the hydrodynamic wave forces into the rigid-body dynamics engine, and AEGIR —a nonlinear motion solver that leverages a high order boundary element method and numerical methods of motion integration. The forces, motions and runtimes are compared for various wave cases. The results suggest that the simplified models generate vessel motions of acceptable fidelity for the development of autonomy, but that for certain wave environments, the differences are significant. The results provide guidance for how the simplified Gazebo extension could be improved without adding significant computational load.

14. SUBJECT TERMS control systems, simulation, ROS, robotics, AEGIR, ocean waves	**15. NUMBER OF PAGES** 139
	16. PRICE CODE

17. SECURITY CLASSIFICATION OF REPORT	**18. SECURITY CLASSIFICATION OF THIS PAGE**	**19. SECURITY CLASSIFICATION OF ABSTRACT**	**20. LIMITATION OF ABSTRACT**
Unclassified	Unclassified	Unclassified	UU

NSN 7540-01-280-5500 Standard Form 298 (Rev. 2-89) Prescribed by ANSI Std. 239-18

THIS PAGE INTENTIONALLY LEFT BLANK

Approved for public release. Distribution is unlimited.

MODELING OF A DYNAMIC WAVE ENVIRONMENT FOR UNMANNED SURFACE VESSEL CONTROL

Joshua F. Malia
Lieutenant, United States Navy
BS, U.S. Naval Academy, 2012

Submitted in partial fulfillment of the
requirements for the degree of

MASTER OF SCIENCE IN MECHANICAL ENGINEERING

from the

NAVAL POSTGRADUATE SCHOOL
December 2018

Approved by: Brian S. Bingham
Advisor

Joseph Klamo
Co-Advisor

Garth V. Hobson
Chair, Department of Mechanical and Aerospace Engineering

THIS PAGE INTENTIONALLY LEFT BLANK

ABSTRACT

Modeling and simulation methods for the seakeeping dynamics of surface vessels vary widely. Higher fidelity models often demand high computational complexity that limits application to offline computation and are not applicable to all development cycles. These models are often based on solving nonlinear fluid flow equations, which cost time and computational power. Simplified models can reduce complexity, supporting rapid development. For developing control and autonomy of small unmanned surface vessels, choosing model fidelity requires a tradeoff between the accuracy of results and complexity of simulation. This thesis compares two methods for modeling and simulating the seakeeping of a small unmanned vessel: Gazebo—an open source, real-time robotics simulator, with an extension that integrates a model for the hydrodynamic wave forces into the rigid-body dynamics engine, and AEGIR—a nonlinear motion solver that leverages a high order boundary element method and numerical methods of motion integration. The forces, motions and runtimes are compared for various wave cases. The results suggest that the simplified models generate vessel motions of acceptable fidelity for the development of autonomy, but that for certain wave environments, the differences are significant. The results provide guidance for how the simplified Gazebo extension could be improved without adding significant computational load.

THIS PAGE INTENTIONALLY LEFT BLANK

TABLE OF CONTENTS

THIS PAGE INTENTIONALLY LEFT BLANK

LIST OF FIGURES

LIST OF TABLES

THIS PAGE INTENTIONALLY LEFT BLANK

LIST OF ACRONYMS AND ABBREVIATIONS

DOF	Degrees of Freedom
EOM	Equations of Motion
GUI	Graphical User Interface
ROS	Robot Operating System
URDF	Unified Robot Description Format
USV	Unmanned Surface Vessel
WAM-V	Wave Adaptive Modular Vessel
RTF	Real-Time Factor
NDW	Non-Dimensional Wavelength

THIS PAGE INTENTIONALLY LEFT BLANK

ACKNOWLEDGMENTS

I would like to thank every instructor that I have had at NPS who has enabled my progress along this graduate journey and armed me with the knowledge to complete this endeavor.

I would also like to thank my brother, Andrew, a student at NPS, for keeping me on the path and motivating me every day to keep working.

I would like to thank Dr. Joseph Klamo, my co-advisor, for always providing levity and enlightenment to every thesis meeting, and whose depth of knowledge in the field of Naval Architecture is a true value to NPS.

Finally, I offer my sincere thanks to my advisor, Dr. Brian Bingham, who from my third quarter at NPS has provided me with the academic and professional motivation to pursue this field. His dedication to this institution and his students is something I will always seek to live up to.

THIS PAGE INTENTIONALLY LEFT BLANK

I. INTRODUCTION

A. MOTIVATION

> The Department (of Defense) will invest broadly in military application of autonomy, artificial intelligence, and machine learning, including **rapid application of commercial breakthroughs, to gain competitive military advantages.** [1]

There is a clear impetus within the Department of Defense to leverage commercial technologies and increase the speed of the development cycle. The rapid progression of robotics in the commercial and military realms has demanded the use of low cost, moderate fidelity development tools to place robotics systems in service. This value of rapid development extends far beyond the DoD as the commercial world also seeks, and drives, a rapid development pace. In the pursuit of fielding robotics technologies faster than before, the role of simulation has become forefront in development.

1. Maritime Robotics

As technological advances have led to the ability to maintain distributed, reliable machines to perform a wide range of tasks, one of the applicable realms is in maritime robotics. There are a huge range of commercial [2-3] and military [1,4] applications where an autonomous machine would be able to provide consistent sensing, interaction and manipulation of the environment. In these pursuits, extensive research and resources have been dedicated over the last few decades to applying advanced in autonomy to the maritime environment and has introduced the advent of academic and industry competitions to advance education and proliferation of open source robotics ideas [5-8].

2. The Role of Simulation in Robotic Development

While most development projects expect implementation in hardware as part of their end goal, direct implementation of every autonomy or control idea to hardware and physical testing is not always ideal. Ideally, a simulation contains representations of every known interaction in nature, has perfect perception of that environment, and can consistently replicate results in real-time [9]. Because of the complexity of the maritime

environment, many efforts have been made to understand parts or all this environment and be able to replicate this in simulation [4,10-15]. The marine environment is more complex than a ground or air environment, as a ground vehicle generally deals with a static environment below it, and an air vehicle deals with only some external forcing in the way of wind, but neither the ground or air drives vehicle response and performance as much as wave loads do on a surface vessel. Because of the inherent cost, logistical challenges, and risk of loss of a vessel, live testing in the maritime environment, especially with unmanned vehicles, is too costly to be the sole source of testing and evaluation of a design. Simulation has been observed to be able to identify, replicate, and ultimately fix software bugs and errors that could have ultimately cost the loss of an unmanned vehicle or damage to property, and thus is incredibly invaluable [16]. Therefore, simulations are critical to development of any maritime USV, and while the challenge is always to make it an exact copy of the real world, the value of simulations cannot be overstated [17].

3. Maritime RobotX Challenge

The Maritime RobotX Challenge is an event that is hosted and sponsored by the Office of Naval Research and the Association for Unmanned Vehicle Systems International that invites academic teams from around the world to compete against each other in the realm of unmanned surface vessels [5,18]. RobotX acts as a platform to inspire the use of rapid development technologies that are accessible by academic teams to designed and implement a completely autonomous surface vessel to conduct a series of independent and dependent tasks [5,7]. These tasks are designed to mimic competencies that the next age of USVs would require. The competition requires the use of a standard vessel hull design that teams must acquire. This drives the focus away from the mechanical design of the system and focuses on the performance of the autonomy, control, and problem-solving abilities of each team's platform. In this development cycle at an academic level, teams must have the ability to simulate and test designs long before they enter the water and conduct live testing. The RobotX competition is also aimed at conducting a simulation only competition with the same principles and vessel model, further driving the need for cheap, fast, and accessible simulation tools specifically tailored for maritime robotics.

B. PROBLEM STATEMENT

Modeling and simulation methods for the dynamics of surface vessels vary widely, especially in the realm of seakeeping [4,10,13,19]. Higher fidelity models often demand such computational complexity that their application is usually limited to non-real-time computation, making them less applicable to rapid spiral development cycles [19]. Simplified seakeeping models can reduce the complexity, supporting more rapid design and development iteration.

This research aims to quantitatively and qualitatively compare two simulation methods applied to a USV hull form subject to external forcing from ocean waves: a high-fidelity method for non-real-time analysis and a lower fidelity approach suitable for real-time implementation.

C. APPROACH

To make this comparison between methods, we us the RobotX competition as an example of an application with a need for simulation support for development of software and algorithms for autonomy. RobotX competitors use a common base robotic platform, the Wave-Adaptive Modular Vessel (WAM-V). Therefore, in this study we create models of the WAM-V using each simulation approach. In order to generate directly comparable results, each model is generated with equivalent properties and characteristics. These models are then simulated in a series of equivalent scenarios in order to compare the resulting forces, moments and motions of the vessel. These scenarios include fixing the vessel in all DOF to analytically verify the results produced by each method, keeping the vessel fixed to investigate the effect of different wave conditions on the produced forces and moments, and allowing the vessel to move in certain DOF to investigate the effect of the forces on the motions of the vessel in each method.

THIS PAGE INTENTIONALLY LEFT BLANK

II. BACKGROUND

To investigate the relationship between the resultant motions from external forcing and the fidelity of the model, research was conducted into existing efforts towards unmanned vessel modeling, and the selected simulation tools that were to be used in comparison. Also crucial is a thorough understanding of the physical vessel that is being modeled—the WAM-V.

A. UNMANNED SURFACE VESSEL MODELING

The level of detail, number of inputs, demand for computing power, time for formulation, and directed application have governed the search for various ways of depicting the same physical object in a mathematical sense for simulation. In the development life cycle of a vessel, several different models, each formulated to support specific aspects of the design, may be used in the design or testing of several components that together would result in a finished product. Most unmanned surface vessel models fall into four categories: control, maneuvering, seakeeping, or simulation. These models have a wide variety of complexities and each are tailored to solve some aspect of development.

1. General Six Degree of Freedom Model

There is a mathematical formulation of a full matrix-vector equation for all six DOF of a surface vessel, that can be specifically tailored, reduced, or expanded to meet the application. Von Ellenrieder [20] uses a modified form of Fossen's [21] six DOF model that is expressed as

$$M\dot{\upsilon} + C(\upsilon)\upsilon + D(\upsilon)\upsilon + g(\eta) + g_0 = \tau_c + \tau_{external},$$

where υ is a vector of the vessel linear velocities *u*, *v*, and *w*, and angular velocities *p*, *q*, and *r*, represented as $\upsilon = [u, v, w, p, q, r]^T$, η is a vector of linear positions *x*, *y*, and *z*, and angular positions θ, φ, and ψ, represented as $\eta = [x, y, z, \theta, \phi, \psi]^T$, and τ_C is a vector of applied control forces *X*, *Y*, and *Z*, and moments *K*, *M*, and *N*, represented as $\tau_c = [X, Y, Z, K, M, N]^T$. The other term on the right side of this formulation is $\tau_{external}$,

which are any external steady or time varying forces acting on the vessel. The matrix M is the sum of M_{RB}, the rigid body mass inertia matrix, represented by

$$M_{RB} = \begin{bmatrix} m & 0 & 0 & 0 & mz_g & -my_g \\ 0 & m & 0 & -mz_g & 0 & mx_g \\ 0 & 0 & m & my_g & -mx_g & 0 \\ 0 & -mz_g & my_g & I_x & -I_{xy} & -I_{xz} \\ mz_g & 0 & -mx_g & -I_{yx} & I_y & -I_{yz} \\ -my_g & mx_g & 0 & -I_{zx} & -I_{zy} & I_z \end{bmatrix},$$

where m is the vehicle mass, x_g, y_g, and z_g represent the location of the center of mass in the body frame of the vehicle, and each I term represents the moment of inertia about each axis, and M_A, which is the added mass matrix, represented by

$$M_A = \begin{bmatrix} X_{\dot{u}} & X_{\dot{v}} & X_{\dot{w}} & X_{\dot{p}} & X_{\dot{q}} & X_{\dot{r}} \\ Y_{\dot{u}} & Y_{\dot{v}} & Y_{\dot{w}} & Y_{\dot{p}} & Y_{\dot{q}} & Y_{\dot{r}} \\ Z_{\dot{u}} & Z_{\dot{v}} & Z_{\dot{w}} & Z_{\dot{p}} & Z_{\dot{q}} & Z_{\dot{r}} \\ K_{\dot{u}} & K_{\dot{v}} & K_{\dot{w}} & K_{\dot{p}} & K_{\dot{q}} & K_{\dot{r}} \\ M_{\dot{u}} & M_{\dot{v}} & M_{\dot{w}} & M_{\dot{p}} & M_{\dot{q}} & M_{\dot{r}} \\ N_{\dot{u}} & N_{\dot{v}} & N_{\dot{w}} & N_{\dot{p}} & N_{\dot{q}} & N_{\dot{r}} \end{bmatrix}.$$

C is the Coriolis and centripetal matrix. D is the drag matrix, which is the sum of the linear damping matrix D_l, represented by

$$D = -\begin{bmatrix} X_u & X_v & X_w & X_p & X_q & X_r \\ Y_u & Y_v & Y_w & Y_p & Y_q & Y_r \\ Z_u & Z_v & Z_w & Z_p & Z_q & Z_r \\ K_u & K_v & K_w & K_p & K_q & K_r \\ M_u & M_v & M_w & M_p & M_q & M_r \\ N_u & N_v & N_w & N_p & N_q & N_r \end{bmatrix},$$

and the nonlinear damping matrix D_{nl}, which is represented by

$$D_{nl} = -\begin{bmatrix} X_{u|u|} & X_{v|v|} & X_{w|w|} & X_{p|p|} & X_{q|q|} & X_{r|r|} \\ Y_{u|u|} & Y_{v|v|} & Y_{w|w|} & Y_{p|p|} & Y_{q|q|} & Y_{r|r|} \\ Z_{u|u|} & Z_{v|v|} & Z_{w|w|} & Z_{p|p|} & Z_{q|q|} & Z_{r|r|} \\ K_{u|u|} & K_{v|v|} & K_{w|w|} & K_{p|p|} & K_{q|q|} & K_{r|r|} \\ M_{u|u|} & M_{v|v|} & M_{w|w|} & M_{p|p|} & M_{q|q|} & M_{r|r|} \\ N_{u|u|} & N_{v|v|} & N_{w|w|} & N_{p|p|} & N_{q|q|} & N_{r|r|} \end{bmatrix}.$$

Surface vessel models usually consider up to the quadratic terms for nonlinear damping, as shown. However, not every term has applicability to this model and end up becoming negligible or zero. This generalized model represents the full dynamic system of a six DOF surface vehicle. Individual motion planes can be computed, and a variety of forms for the disturbances can be used to compute control forces, motions, or estimate the damping of an observed system.

2. Models for Seakeeping

This six DOF model can be modified to account for the time varying disturbances presented by the sea surface and other environmental effects such as currents or wind. This formulation redefines the term $\tau_{external}$, which is now made up of $\tau_{FK+diff}$, which is the Froude-Krylov and diffraction forces from the incident waves, and τ_{drift}, which are the wave forces pushing the vessel in the horizontal plane. Also, typically included in a full seakeeping model is the effect of currents, $\tau_{currents}$. The formulation of the seakeeping model is now

$$M\dot{\upsilon} + C(\upsilon)\upsilon + D(\upsilon)\upsilon + g(\eta) + g_0 = \tau_c + \tau_{FK+diff} + \tau_{wind} + \tau_{current}\,.$$

This is different from previous models as the wind and wave induced forces are not just prescribed as disturbances but are calculated over time and depend on the history of the vessel motion and its instantaneous position and velocities in the environment with respect to the wind and waves. Computation of the Froude-Krylov and Diffraction forces is usually done using a potential flow solver, which uses fluid dynamics and potential theory to compute the forces on a body moving relative to a fluid. These forces are then

added to the model as time-varying disturbances to determine the next motion state for each time step [21].

3. Models for Maneuvering

Maneuvering models consider the necessary equations of motion typically for one plane of interest. For surface vessels, this is the horizontal plane tangent to the Earth's surface, and thus the maneuvering model consider only the DOFs of surge, sway, and yaw. For a non-holonomic vessel which cannot independently move in any direction, the six DOF model can be reduced and expanded to a three DOF model only containing terms for surge, sway and yaw [21]. The surge equation then becomes

$$M_{RB}\dot{u} - M_{RB}x_g r^2 - M_{RB}vr = X_{\dot{u}}\dot{u}_r + Y_{\dot{v}}v_r r + Y_{\dot{r}}r^2 + X_u u + X_{u|u|}u|u| + \tau ,$$

which is uncoupled from the Yaw equations, whose formulation is

$$I_z\dot{r} + M_{RB}x_g\dot{v} + M_{RB}x_g ru - Y_{\dot{r}}\dot{v} - N_{\dot{r}}\dot{r} - Y_{\dot{v}}v_r u + X_{\dot{u}}u_r v - Y_{\dot{r}}ru - N_v v + N_{v|v|}v|v| + N_r r + N_{r|r|}r|r| = \tau$$

4. Models for Control

Models utilized from control development will most often focus on certain isolated aspects of the vessel and determining the necessary input parameters to achieve a desired output. Examples of this are tuning propulsion parameters, designing systems for controlling vessel rotations along any axis, or basic control input following for speed or heading. Most of these types of models will center on a specific plane of movement at a time and are often reduced. An example of this formulation is the equation for vessel thrust [22], which only considers the surge of the vessel, and is formulated as

$$M_{RB}\dot{u} + X_{u|u|}u|u| + X_u u = X_c ,$$

where X_c is the force from propulsion, or the decoupled steering equation [22], where N_c is the steering torque and whose formulation is

$$I_z\ddot{\psi} + (N_r + N_{r|r|}|\dot{\psi}|)\dot{\psi} = N_c .$$

5. Models for Simulation

Models that are considered for full simulation call into use many other details beyond just the vessel. These models consider replication of every aspect of the vessel and the environment. These models consider environmental disturbances, lighting, weather, and focus on rendering and visuals. These models typically leverage several components of control, maneuvering, or seakeeping models to replicate interactions with the environment. Examples including actual ship bridge simulations [17], training systems [11], and potential use to replicate sea trial conditions for further system identification and development [4].

B. SIMULATION TOOLS

Out of the many models and tools available, two distinct suites were selected for use in this study. These were selected based on their availability, required learning curve, previous use in the field, and existence at opposite ranges of complexity and fidelity of result.

1. Robotic Operating System and Gazebo

ROS is an open-source, Linux-based system that is a "collection of tools, libraries, and conventions that aim to simplify the task of creating complex and robust robot behavior across a wide variety of robotic platforms" [23]. It provides a meaningful, adaptable platform to handle robotic functions and can be tailored and modified to achieve any number of robotic functions at the software level. It can interface with many other programs that expand its capability, namely the simulation environment Gazebo. Gazebo is a three-dimensional simulation environment that can handle numerous objects and robots and provides a convenient GUI for visualization and rendering [23].

Gazebo currently supports modeling and simulation in a variety of domains, but the basis of the robot modeling and motion generation is done using one of four physics engines to solve rigid body equations of motions. In order to capture the motions and environmental forcing for a USV, our research group has developed a Gazebo plugin to extend the simulator with two essential functions for the simulation of USV seakeeping.

First, it accepts inputs on wave parameters to that generate a wave environment by superimposing any number of monochromatic waves. Second, it handles the hydrodynamic calculations of the incident and generated wave loads on the vessel and produces the forces and moments needed to generate motions. ROS and Gazebo are generally able to handle computations near-real-time, depending on the complexity of the equations of motion and the number and complexity of bodies being simulated. The fidelity of this modeling is generally considered low, as the way it calculates the forces from the waves does not consider all forces that a wave can impart on a vessel.

2. NavaSim and AEGIR

NavaSim is a module-based software system that allows for the interconnecting of several different software packages that independently handle a variety of computations associated with naval architectural design and analysis. It provides an interface to handle the importation of vessel three-dimensional models in a standard format. It also houses a file system, visualization GUI, and input file generation mechanics to set up and run projects. AEGIR is the steady and time-domain seakeeping code that NavaSim utilizes for the calculation of forces, moments, and motions of a vessel in a defined wave field [24]. AEGIR models both the wave field and the vessel with variations of B-Splines and utilizes a high-order boundary element method for the computation of steady and unsteady forces. Unsteady forces include diffraction, wave, and Froude-Krylov forces. The parameters of each simulation are developed into an input file called a Namelist, which are loaded into the executable code and run via the NavaSim GUI. While generally considered being faster than many computational fluid dynamics codes, such as large-eddy simulation, Reynolds averaged Navier-Stokes, and direct numeric simulations, AEGIR is usually expected to run far slower than real time [19]. This type of model is generally considered a higher fidelity, as it not only can calculate very accurate forcing from wave action, but also the impact that the vessel can have on the wave field itself, and how the vessel can displace the wave field around it. Of note, this program also computes the transient responses of the vessel when a new wave is introduced into calm water. To avoid impulse-like responses, the program automatically applies a ramp to the generated wave amplitude of the first several waves, which is easy to see in the time histories presented in this research. This program is best

suited for detailed studies in the interaction between a vessel and waves and comparison to scale model testing, as well as a design tool for complex hulls.

C. WAVE-ADAPTIVE MODULAR VESSEL

1. WAM-V Description

The RobotX competition selected a single surface platform for every team to use in the competition. The selected platform is the WAM-V 16, made by Marine Advanced Research, Incorporate [25].

a. Vessel Specifications

The WAM-V is a small catamaran built for autonomous, near shore applications. As evident in the name, the vessel features a proprietary wave adaptive suspension that allows each pontoon to independently pitch up and down as the vessel travels over waves [14]. This is a passive system, consisting of several joints, springs, and dampeners that connect the platform to the forward strut. It also has a large platform used for sensor payloads, cameras, computers, and communications equipment. With this design, the payloads will stay level for a range of waves that can be compensated for by the wave adaptive system, allowing for greater sensor accuracy and would specifically benefit vision or line of sight-based identification or navigation systems [2]. The vessel is typically powered by two stern mounted, steerable motors. The catamaran hull and length-to-beam ratio provide the vessel with significant transverse, longitudinal, and directional stability. Figure 1 is a picture of the vessel.

Figure 1. WAM-V Operating in Waves. Source: [25]

For a vessel of this size, it has a relatively small static displacement, and can carry a payload of almost 150% of that displacement [25]. Even at the maximum load, the vessel has a very shallow draft, allowing deployment in a variety of shallow water applications, while benefiting from the stability of the platform [2]. Table 1 lists the three standard loading conditions for the vessel, and Table 2 contains data pertaining to the physical dimensions of the vessel.

Table 1. Loading Conditions for the WAM-V. Adapted from [25].

Load Condition	Mass [kg]	Draft [cm]
Base Hull	154	8.9
Design Load	180	9.2
Maximum Load	374	16.5

Table 2. Principle Characteristics of WAM-V. Adapted from [25].

Parameter	Value
Length (L)	485 cm
Beam Overall (BOA)	244 cm
Length to beam ratio (L/B)	1.988
Centerline-to-centerline hull separation (B)	1.83 m
Demi-hull radius (R)	21.3 cm
Maximum Payload	220 kg
Design Volumetric Displacement (V)	0.5 m^3
Design Waterplane Area (A_{wp})	3.4 m^2
Mass Moment of Inertia about z-axis	250 kg-m^2

b. Mass and Inertia Properties

For the defined design load condition, the mass and inertia properties were previously derived [20, 26]. From the definition of the rigid body mass matrix, M_{RB} for the WAM-V is represented as

$$M_{RB} = \begin{bmatrix} 180 & 0 & 0 & 0 & 16.6 & 0 \\ 0 & 180 & 0 & -16.6 & 0 & 92 \\ 0 & 0 & 180 & 0 & -92 & 0 \\ 0 & -16.6 & 0 & 120 & 0 & 0 \\ 16.6 & 0 & -92 & 0 & 393 & 0 \\ 0 & 92 & 0 & 0 & 0 & 446 \end{bmatrix},$$

where inertia terms are in units of kg-m^2, mass terms are in units of kilograms, and terms that define the location of the center of gravity of the vessel are in terms of meters.

c. Damping Coefficients

The damping coefficients, previously defined in matrix form as the linear and nonlinear damping matrices D_l and D_{nl}, are the tunable coefficients that are introduced in the six DOF seakeeping model to transform an input forcing into the resultant motion. For this vessel, there are assumed to be linear and quadratic components of the coefficients in

most DOF. Using the definitions for D_l and D_{nl}, and the appropriate equations from von Ellenrider [20], the damping terms are now represented as

$$D_l = \begin{bmatrix} 51.3 & 0 & 0 & 0 & 0 & 0 \\ 0 & 40 & 0 & 0 & 0 & 0 \\ 0 & 0 & 500 & 0 & 0 & 0 \\ 0 & 0 & 0 & 50 & 0 & 0 \\ 0 & 0 & 0 & 0 & 50 & 0 \\ 0 & 0 & 0 & 0 & 0 & 400 \end{bmatrix},$$

where X_u, Y_v, and Z_w are in units of N/(m/s) and K_p, M_q, and N_r are in units of (N-m)/(rad/s). Because the only term identified in the paper is in the surge direction, the full damping term for surge, including the linear and quadratic term is

$$D = 72.4u|u| + 51.3u .$$

2. Modeling in Gazebo

Within the Gazebo simulation environment, an object is defined by specifying the visual, physical and collision properties. Additionally, for the USV, the hydrodynamic and buoyancy parameters also must be specified to be used by the custom plugin to generate external forces due to the wave field. A series of Unified Robot Description Format (URDF) files describes each of the physical characteristics of the vessel and represents the vessel within the environment.

a. WAM-V Model Characteristics

The URDF model used for this application contains several important components. First it contains a complex meshing that is used as the visual representation within the environment. It also contains collision information, where simple boxes are built around the main components of the visual representation, which is how the vessel interacts with other modeled objects within the environment. The number and complexity of the collision representations directly impacts the computational performance of the simulation, as at ever time step, the simulation must check for intersections between every collision volume represented in the simulation space [23]. The URDF also contains the mass properties of

the vessel, adapted from the actual mass properties of the WAM-V. Using each of these descriptors, a vessel model with a visual representation, mass and the ability to take up space and interact with other simulation objects is created. Figure 2 shows the visual representation of the WAM-V in the Gazebo environment, and the body-fixed coordinate convention used in Gazebo. Coordinates are referenced where X is Surge, Y is Sway, Z is Heave, θ is Roll, φ is Pitch, and ψ is Yaw.

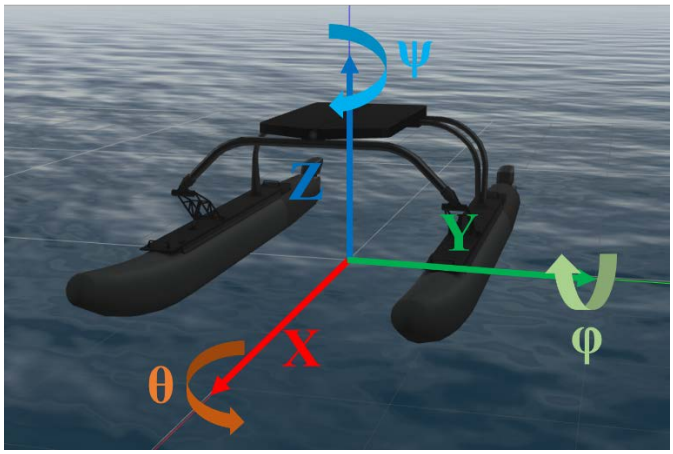

Figure 2. Render of WAM-V in Gazebo Simulation Environment

b. Mathematical Model Formulation

While the vessel model is described in a way that allows interactions with other objects in the environment, it also needs a way to interact with the environment itself. For this environment, the vessel needs the ability to interact with the water surface, whether calm or disturbed by waves. This external environmental force is implemented using a software plugin that interacts with the Gazebo environment. The plugin allows the generation of a wave field in the simulation domain and can be made up of any number of component waves that are added to make a complex wave environment or can be used to generate a regular wave field in one direction. The standard monochromatic wave equation describes the wave elevation as

$$\zeta(t) = \zeta_0 \sin\left(\frac{2\pi}{T}t\right),$$

where ζ_0 is the peak amplitude of the wave, T is the wave period, and t is time. The wave direction is also given as a vector referenced to the world frame [26].

The plugin represents each of the demi-hulls as a rectangular box. Each hull is described by the waterplane area, the length of the vessel, and the distance between the center of each pontoon. Each of the demi-hull boxes are then divided into two box elements. The resulting four discrete grid points specify the locations where, at each step in the simulation, the wave force is calculated and then applied to the rigid body. This results in a four-box element representation of the waterplane, each rigidly connected, shown in Figure 3.

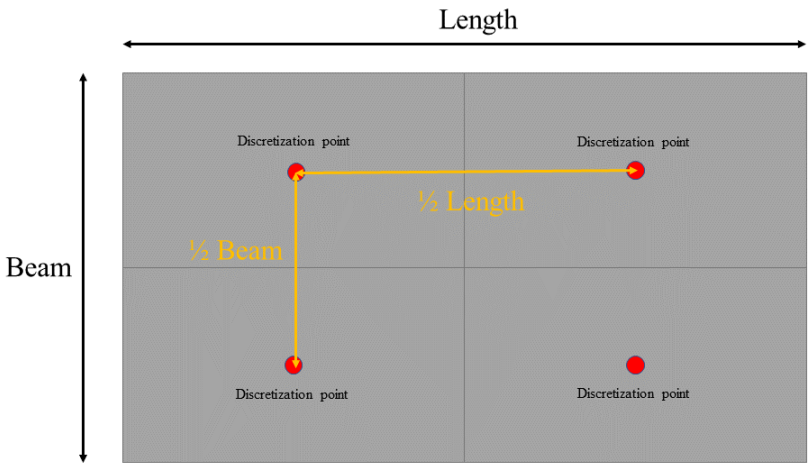

Figure 3. Discretization of Waterplane in Gazebo

The external wave force at each grid point on the vessel is calculated in the following steps:

1. The wave height for an instance in time is evaluated at the grid point,
2. The vertical location of the grid point is evaluated based on the current position and attitude of the vessel,

3. The distance between the wave height and the grid point vertical location is used to calculate a static buoyancy force due to the estimated hull displacement at the grid point location.

4. The static buoyancy force is applied at the grid point.

When each grid point has a resultant force calculated at the center of each box, combinations of forces can impact each DOF. Any forces result in a net motion, and any imbalance of forces between discretization boxes result in moments, and thus rotations.

The plugin configuration also contains information on the linear and quadratic damping terms. With the body-frame forces and damping coefficients, the resultant motions are calculated for each time step, the body is moved, the wave field is progressed, and the next set of wave heights are calculated, and motions induced. Gazebo typically does these types of computations at 100 Hz, unless otherwise specified.

c. Description of Outputs

One distinct feature of the ROS and Gazebo suite is that it can output as much or as little data as desired. Information that is exchanged between the various elements of the simulation are published as topics, which are information streams about anything related to the simulation, if it is written to publish information on that topic. The information can be accessed, recorded, and used for further calculations. This open type of architecture allows easy access to the forces, moments, motions, and wave measurements that are necessary for analysis.

(1) Forces

The forces that are reported from Gazebo are available on the “wave_force” topic in ROS. The forces are measured in units of Newtons and are resolved in the vessel body frame.

(2) Moments

The moments that are reported from Gazebo are available on the “wave_moment” topic in ROS. They are measured in Newton-meters. These are also resolved in the vessel body frame about each principle axis.

(3) Motions

The motions that are reported from Gazebo are available on the “gazebo/model_states” topic in ROS. This topic contains information about the position and orientation of the vessel, and includes motions and rotations in each axis, resolved in the world frame. Translational motions are measured in meters, and rotational motion is measured in radians.

3. Modeling in AEGIR

NavaSim and AEGIR can accept incredibly complex geometries, if they follow very specific rules and conventions for their formulation. These geometries are typically required to be made up of surfaces that can be mapped to rectangular panels, and each panel that is mapped must be either completely or partially wetted. While there are many different structural elements that make up the WAM-V, only the individual demi-hulls are modeled for this application [24].

a. WAM-V Model Characteristics

The WAM-V representation in AEGIR has been modeled to best represent the actual hull form and is based directly from drawings and rendering of the three-dimensional hull. The hull geometries for were independently developed by Navatek, the designers of the NavaSim program, and a copy was provided for this research. Each hull is made up of several panels and are mathematically identical. A rendered depiction of the hull in the NavaSim GUI is shown in Figure 4.

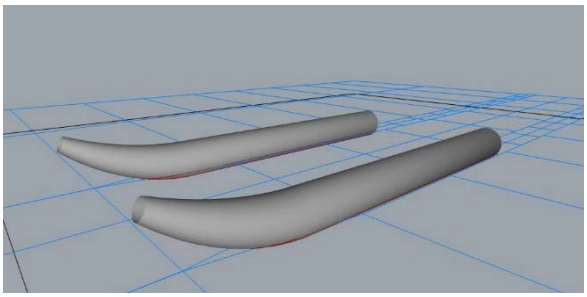

Figure 4. WAM-V Hull Render in NavaSim GUI

The coordinate frame for AEGIR is oriented like Gazebo, except for the Y axis, which points in the opposite direction. Figure 5 is the graphical depiction shown in the NavaSim GUI that denotes the orientation of each principle axis and the associated rotation. The symbolic notation is the same as used for Gazebo, where X is Surge, Y is Sway, Z is Heave, θ is Roll, φ is Pitch, and ψ is Yaw.

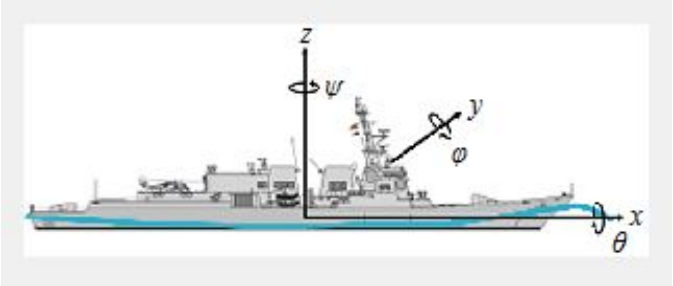

Figure 5. NavaSim and AEGIR Coordinate Frame Conventions.
Source: [24]

b. Mathematical Model Formulation

AEGIR utilizes a nonlinear boundary element method for solving the fluid flow interaction between the vessel and water surface. The vessel, and the water, are modeled using B-splines. Everything is modeled with the assumption that the flow is inviscid and incompressible. It also restricts the wave fields to be irrotational and that they do not cause spray or break. The flow is described with a velocity potential function that is then modeled as B-splines [27].

c. Description of Outputs

When AEGIR runs a time-domain simulation, it creates several output files where all the information for that type of simulation is recorded. Each of these are text files that contain columns of data associated with time, wave height, and each of the DOFs.

(1) Forces

The forces that are reported from AEGIR are divided into individual components, dependent on how those force components are created, and how they interact with the hull. There are three component forces that are calculated by the AEGIR program.

- Incident—This force component is also known as the Froude-Krylov forces. These are due to the direct interaction between the hull and the wave field.
- Wave—This force component is the total force generated by the vessel pushing wave energy away from itself as it displaces water and breaks up individual encountered waves. This is the vessel putting energy back into the wave field.
- Hydrostatic—This force component represents the hydrostatic restoring force of the displaced water volume.

(2) Moments

The moments results are reported in the same way as the forces, where each degree of freedom has each of the components broken out individually. These are measured in Newton-meters and are also contained within the Modal Force History text file [24].

(3) Motions

The motions resulting from each simulation are recorded in what is known as the Body Force History file or the Modal Force History file. Each of these files contains information for each degree of freedom as a time history. Displacements are measured in

meters and rotations are measured in radians. These files also contain information on the displacement, velocity, and accelerations for each degree of freedom [24].

D. GENERAL WORKFLOW

While all the information is available from each simulation method, each of the sets of data must be recorded and collated in a way to allow comparison, truncation, and calculations to be performed, as well as create visual graphics and plots to represent the data and draw both qualitative and quantitative conclusions. All data is eventually transferred to MATLAB for processing.

1. Gazebo

As Gazebo is running a simulation, ROS can record a selection of or all topics that are actively being published to. These topics, along with time information, is recorded to what is called a "bag file." This bag file is then processed in MATLAB using the Robotics System Toolbox and custom developed functions. When processed, the results are converted into a MATLAB workspace file, which contains the time, wave height, forces, moments, and motions in a MATLAB structure. Using this structure, the data for each individual simulation can be used for comparison.

2. AEGIR

As AEGIR runs each simulation, the information is automatically recorded in a series of text-based files. These text files read into MATLAB, which converts the series of data columns into a MATLAB structure. This is done for every type of file that is saved by NavaSim for each simulation, and each result is converted to a MATLAB workspace file. These workspace files are then imported for use in comparisons.

THIS PAGE INTENTIONALLY LEFT BLANK

III. VERIFICATION

To help establish an understanding of the consequence of regular wave forcing on the vessel, an examination of the forces on the vessel is conducted first. The vessel is completely fixed in all DOF and run through several iterations of wave cases, in both AEGIR and Gazebo. This verification, as it is referred to, is meant to understand how hull geometry changes the resulting forces from identical wave cases, and to see how close simple calculation can come to predicting the forces generated from the waves for a very simple, long period wave case.

A. APPROACH

To accomplish this verification, the simplest case that can be geometrically approximated is a very long period wave case, where the period of the wave produces a wavelength that is significantly longer than the vessel length.

1. Verification Scenario

In this scenario the vessel is constrained to be static, fixed in all six DOFs. This isolates the external forcing of the incident waves from the motion dynamics. Furthermore, the monochromatic incident waves considered have a wavelength much longer than the vessel length. For this scenario, analytical predictions of the wave forces on the vessel allows us to verify that the two simulation approaches (Gazebo and AEGIR) are providing results consistent with the analytical prediction and provides a first comparison between the methods.

The model will be setup in a fashion that allows a given wave to pass the vessel without resulting in the vessel moving or rotating in any degree of freedom. This will result in the direct calculation of the forces on the vessel created by each wave. Thus, the vessel will not be allowed to translate in surge, sway or heave, and cannot rotate in roll, pitch or yaw.

2. Verification Steps

As part of this verification, several methods will be employed to calculate the expected forces on the vessel when subject to the incident waves. The simplest case, and the most predictable, is that when a monochromatic regular wave is significantly longer than the hull, and where the slope of the wave is also small. As such a wave passes the hull, the effect can be approximated as a static increase in the draft of the vessel, equal both fore and aft. Using AEGIR, Gazebo, and geometric principles, the heave force generated by a wave of various amplitudes can be approximated.

3. Cases of Interest

To identify the long wave case, the physical characteristics of the vessel must be considered. The goal in selecting a very long wave is to keep the wave steepness at a minimum across the range of tested amplitudes. For this verification, a wavelength of 20 times the length of the vessel is selected, which corresponds to a wavelength of 96.7 meters. Each of the simulation methods requires the period of the wave as the input value. Using the deep water, first-order dispersion relationship,

$$T = \sqrt{\frac{2\pi\lambda}{g}},$$

where g is the acceleration due to gravity, and λ is the wave length.

There are several cases of interest that are associated with the long wave case. This long wave is tested at a variety of amplitudes, chosen as fractions or multiples of the draft of the vessel. The full range of test cases is contained in Table 4. There are three interesting cases within the test matrix—a very small wave, a medium sized wave, and a very large wave. The small wave is where the amplitude of the wave is less than the draft of the vessel. The medium wave case is where the wave amplitude is larger than the draft but does not extend above the available freeboard. As the vessel is completely fixed in all DOF, the wave crest will extend up to the freeboard, and the wave trough will fall below the keep of the vessel, causing it to be suspended in space. The large wave case is where the amplitude of the wave extends above the freeboard. This would cause the vessel to be suspended in

space in wave troughs and would become completely submerged when encountering a wave peak. The three wave cases that were explored in detail are highlighted in yellow within Table 3. This also introduces two descriptors of each wave case, namely the wave steepness,

$$k = \frac{2\zeta_0}{\lambda},$$

as well as the non-dimensional wave amplitude, which is

$$\zeta_{ND} = \frac{\zeta_0}{h},$$

where h is the vessel draft.

Table 3. Verification Wave Cases

Non-Dimensional Wave Amplitude	Wave Amplitude (ζ)	Wave Length (λ)	Wave Period (T)	Wave Steepness
[-]	[m]	[m]	[s]	[-]
0.1	0.0092	96.7	7.87	0.0002
0.5	0.0462	96.7	7.87	0.0010
1	0.0924	96.7	7.87	0.0019
2	0.1847	96.7	7.87	0.0038
2.5	0.2309	96.7	7.87	0.0048
3	0.2771	96.7	7.87	0.0057
3.5	0.3232	96.7	7.87	0.0067
4	0.3694	96.7	7.87	0.0076
4.5	0.4156	96.7	7.87	0.0086
5	0.4618	96.7	7.87	0.0096
7	0.6465	96.7	7.87	0.0134

B. ANALYTIC VERIFICATION

Approximating the long period wave as a static increase in draft, it is possible to calculate the expected heave force caused by a very long wave of any given amplitude using the geometry and basic physics. This geometric approximation only accounts for the increase in instantaneous hydrostatic buoyancy, or the physical volume of water that is

displaced by the wetted hull. Two models of the hull were selected for this validation—a rectangular prism and a cylindrical representation. A simple representation of these hulls is contained in Figure 6.

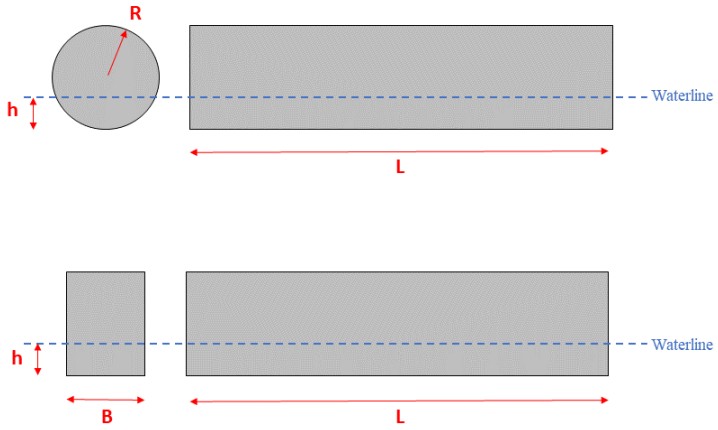

Figure 6. Geometric Demi-Hull Approximations

1. Rectangular Approximation

As Gazebo uses a simple rectangular prism shaped approximation for the hull, the calculation for a static increase in draft caused by a passing wave can be performed in relatively few steps. The dimensions used for the rectangular approximation are contained in Table 4.

Table 4. Rectangular Hull Approximation Dimensions

Dimension (symbol)	Value	Unit
Length (L)	4.832	[m]
Demi-hull Beam (B)	0.352	[m]
Static Draft (h)	0.0923	[m]

Applying the definition of a regular wave to Archimedes Principle results in the

$$F_z(\zeta_0, T, t) = \rho g L B \left[\left(\zeta_0 \sin \frac{2\pi}{T} t \right) + h \right],$$

which shows that for any wave period, if all parameters except for time are constant, the result is also sinusoidal. Thus, the maximum value of the force,

$$F_{z,\max}(\zeta_0) = \rho g L B\left(\zeta_0 + h\right),$$

which indicates that the resulting relationship between the wave amplitude and the magnitude of the heave force is linear. The Gazebo formulation has this rectangular shape have infinite height and does not impose a limit on the extent of the height of the freeboard, thus the buoyancy increases linearly for all positive values of NDW. Applying this equation to the selected wave parameters that will be examined produces the expected linear representation, that has a zero-amplitude heave force equal to the static displacement of the vessel, as approximated as a rectangular prism, shown in Figure 7.

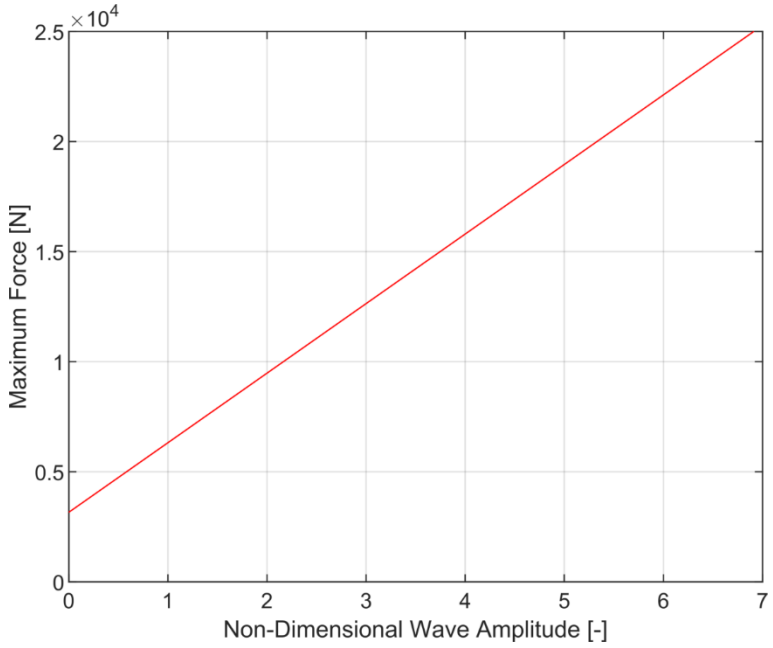

Figure 7. Rectangular Hull Approximation Heave Force for Long Period Wave

2. Cylindrical Approximation

Although the box shaped approximation is easier computationally, the shape of the vessel is more accurately represented using a cylinder. Without accounting for the bow

shape, each demi-hull can be approximated as a simple cylinder. The dimensions used for this approximation are included in Table 5.

Table 5. Cylindrical Hull Approximation Dimensions

Dimension (symbol)	Value	Unit
Length (L)	4.832	[m]
Demi-Hull Radius (R)	0.213	[m]
Static Draft (h)	0.0923	[m]

Since the submerged volume of a circular cylinder does not increase linearly as the depth of submergence increases, the relationship between wave amplitude and buoyancy is not linear. If all vessel parameters remain constant, the maximum buoyancy force induced by a passing wave on a fixed cylinder is represented by

$$F_{z,\max}(\zeta_0) = \rho g L\left[R^2 \cos^{-1}\left(\left(\frac{R-(\zeta_0+h)}{R}\right)-\left(R-(\zeta_0+h)\right)\sqrt{2R(\zeta_0+h)-(\zeta_0+h)^2}\right)\right]$$

This calculation is based on the area of a section of a circle combined with Archimedes principle. The entering assumption is that the wave amplitude is measured from the static draft. Also assumed is that once the wave amplitude is large enough to cover the hull completely, the buoyant force will no longer increase. Applying the equation across the test case wave periods results in the expected heave force for the cylindrical approximation, depicted in Figure 8.

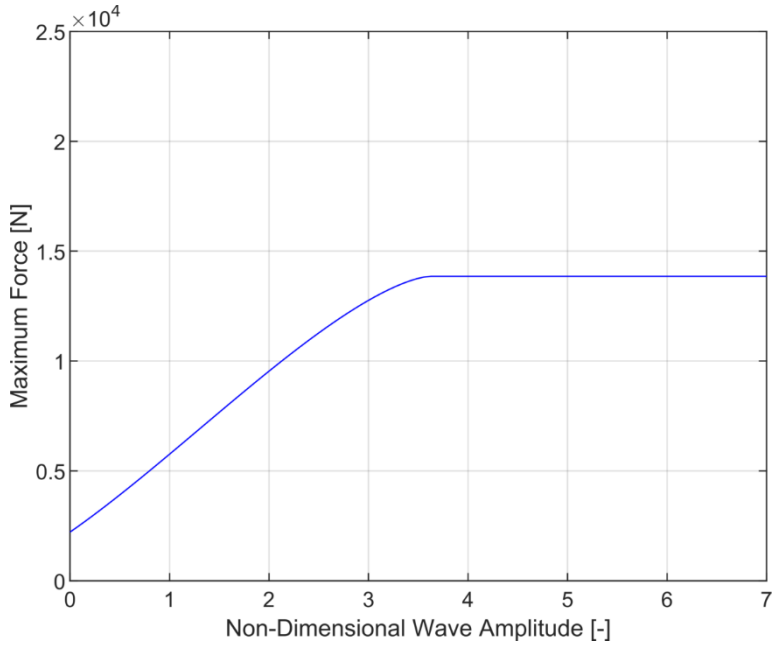

Figure 8. Cylindrical Hull Approximation Heave Force for Long Period Wave

This approximation for the cylindrical hull shows a nearly linear relationship between the wave amplitude and the force, up through a certain non-dimensional wave amplitude. The model then levels off to a maximum force once the cylindrical hull is submerged.

C. HEAD SEAS VERIFICATION

The first step in the verification is to test the vessel in seas that have relative wave headings of 180 degrees, or head seas. Each of the input wave cases are identical for both AEGIR and Gazebo, as well as the fixed location of the vessel in the vertical plane.

1. AEGIR Verification

Each wave case is developed into an input file for the AEGIR program and run individually to generate the resultant heave forces. All eight cases are developed in AEGIR to run simulations. Each simulation is run for thirty-five seconds of simulation time, as recommended by the best practices.

a. Setup

AEGIR requires a specific input setup to be able to implement the constraints and test conditions. Within the program, each degree of freedom, or mode, are set to "Fixed." Each wave case is entered as a combination of the period and amplitude. The vessel is fixed at the design draft, where it will remain within the domain. Wave amplitudes that are input into AEGIR are in reference to the waterplane of the vessel at the design draft. The last major setting that is changed in AEGIR is the method that it uses to solve for the component forces. The method that is selected in the GUI is an efficient, nonlinear equation solver.

b. Small Amplitude Case

The small amplitude case is the case that would be expected to perform very close to the analytical geometric verification methods. The case examined is where the wave amplitude is 1/10th of the draft of the vessel. Figure 9 shows the time history over the simulation duration for this case.

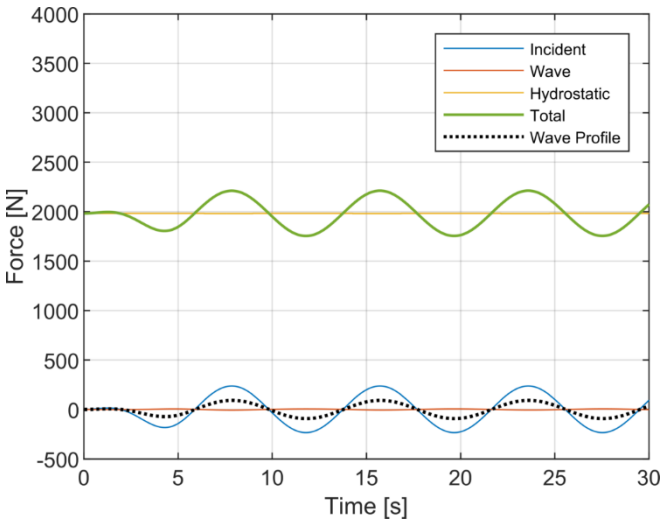

Figure 9. AEGIR Heave Force for Small Amplitude Head Wave

From this the total heave force follows the shape of the wave and is in line with the peaks and troughs. The hydrostatic component of the force remains at the static buoyancy of the vessel throughout the simulation. It is also apparent that the force from the Wave

component is insignificant compared to the Incident component of the force, and it is out of phase with the Incident force component. The total force behavior is expected to be in line with the geometric approximations.

c. Medium Amplitude Case

The medium amplitude case should highlight an artifact of the implemented setup. As the medium case is where the wave amplitude is equal to the draft of the vessel, it is a limiting case where the buoyancy goes to zero in the wave trough since the displaced volume goes to zero. The time history from this simulation is shown in Figure 10.

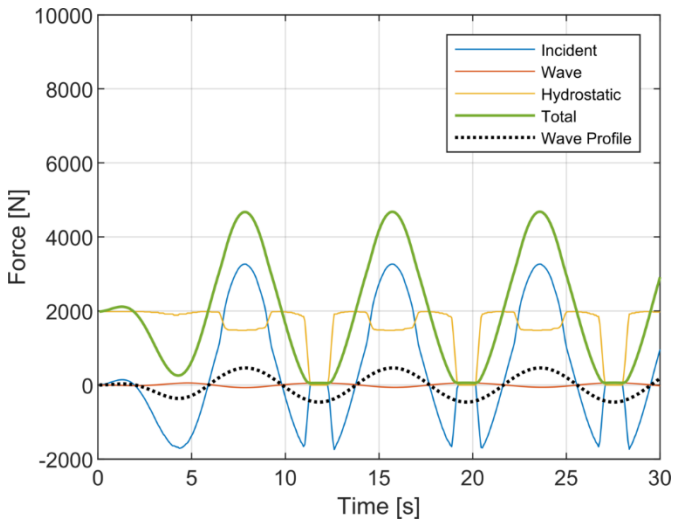

Figure 10. AEGIR Heave Force for Medium Amplitude Head Wave

For this case, the most notable result from the data is the behavior of the hydrostatic component of the heave force. For example, when the vessel reaches a wave trough, at approximately 11.0 seconds of simulation time, the hydrostatic forces fall to zero. All other force components also fall to zero, leaving no total force on the vessel. This is generally expected, as at this point the vessel is floating in space above the free surface and is subject to no wave interaction. The total force, however, does maintain its sinusoidal behavior and appears to be clipping in the trough of the wave. Here it is also noted that the Wave component is still much smaller than the Incident component and remains out of phase.

d. Large Amplitude Case

The large amplitude case should also highlight another observation of the implemented setup, as the vessel will become completely submerged during the peak of each wave. Figure 11 is the time history of this simulation.

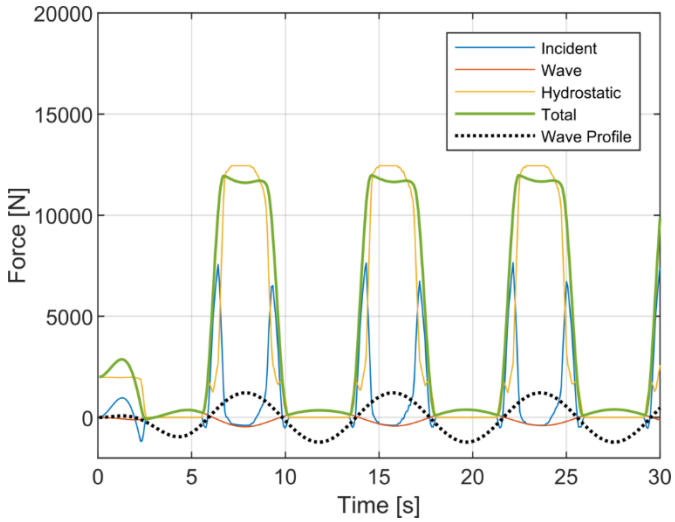

Figure 11. AEGIR Heave Force for Large Amplitude Head Wave

This total force behavior is different than previous wave cases but is still expected. The total force falls to zero when the vessel is at a wave trough and is clipped in the maximum value when the vessel is submerged by the wave peak. Also, when submerged, the Incident component of the force decreases as the vessel is no longer interacting with the free surface of the wave, and the hydrostatic force takes over.

2. Gazebo Verification

The same verification of wave cases is conducted in Gazebo. Each wave case is entered into the dynamics plugin, and the wave forces and wave height are recorded via ROS.

a. Setup

In Gazebo, the vessel model is also fixed. To do this, the source code for the hydrodynamics plugin was modified to calculate the forces and moments on the vessel, but none of the actual motions are calculated or implemented at each time step. Each of the wave cases is input as a combination of amplitude and period, input into the configuration file for the dynamics plugin. Each Gazebo simulation is run independently and only the time, wave amplitude and forces are recorded. All wave parameters are identical to the AEGIR counterpart.

b. Small Amplitude Case

The small amplitude wave case in Gazebo has identical input parameters and has the greatest likelihood of matching the behavior of the same AEGIR case. Figure 12 shows the result of the simulation. Note that the simulation does not begin with the same transient behavior as in AEGIR, and the wave case will not line up in phase.

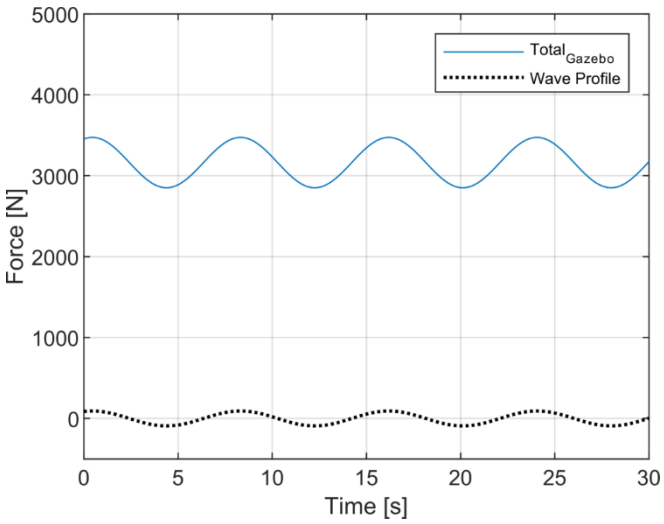

Figure 12. Gazebo Heave Force for Small Amplitude Head Wave

As evident in the results, the behavior of the heave force is sinusoidal, as with the regular input wave. It is oscillating about the expected static buoyancy and is in phase with the wave profile.

c. Medium Amplitude Case

The medium amplitude case is also expected to display an artifact of the setup. Figure 13 shows the simulation results from the medium wave case.

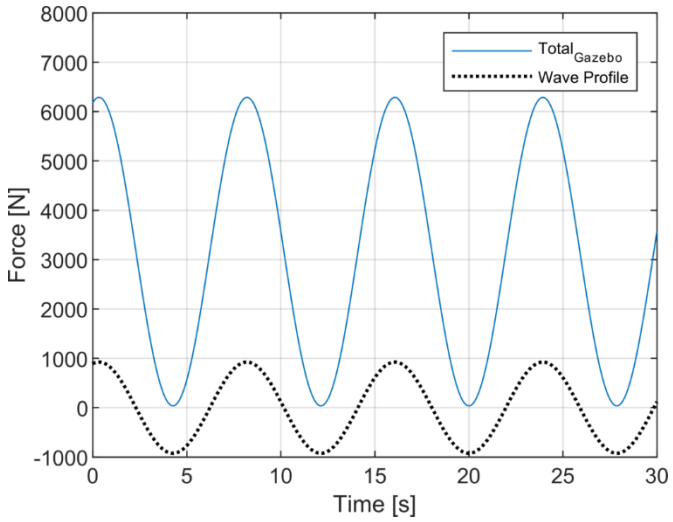

Figure 13. Gazebo Heave Force for Medium Amplitude Head Wave

As expected, the total heave force is in phase with the wave profile. The Gazebo model is also able to show the zero-heave force that occurs at the trough of each wave.

d. Large Amplitude Case

The large amplitude case in Gazebo is not expected to show one of the primary behaviors that was evident in AEGIR and would be realistically evident, as the model has a specific limitation. Figure 14 shows the results of this simulation.

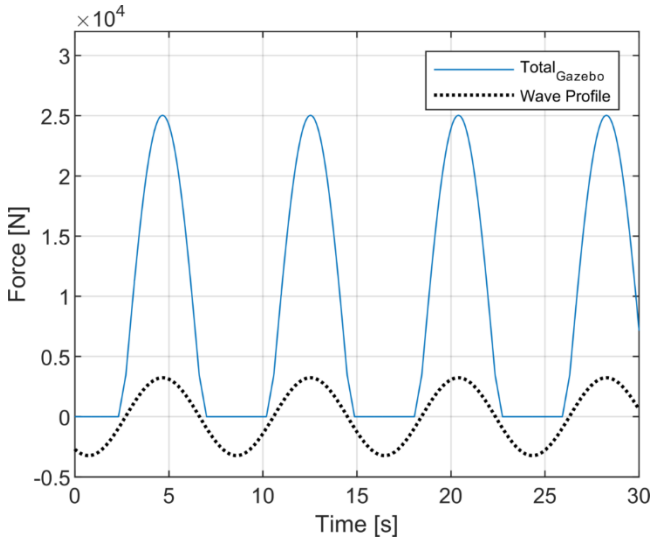

Figure 14. Gazebo Heave Force for Large Amplitude Head Wave

Here, we see the full result of the wave dropping beneath the hull, as the heave force result drops to zero for several seconds during each trough of the wave. While it is expected that the force would reach a ceiling as the vessel becomes submerged, this result does not show that behavior, and the force keeps increasing as the wave passes further over the hull. This is directly due to the way Gazebo determines the wave height at each discretization point. It directly measures the wave height and applies that to the waterplane section to find the volume, and thus the buoyancy, of that section. Essentially, the freeboard of the hull is not considered, and it can be infinitely tall. This deviation is important when comparing the two results.

3. Comparison

To make a comparison between each step of the verification, the maximum value of the heave force is calculated from each test. For the geometric verifications, this can be calculated from where the amplitude is maximum. For Gazebo, as the total force is already calculated and reported for each degree of freedom, the maximum value is determined at the wave peak. For AEGIR, each of the components of the force are summed in the time history, and the maximum value is extracted. The Non-Wave Component Sum is the sum of the time histories of the Incident and Hydrostatic Forces on the vessel. Figure 15 shows each of these results for comparison.

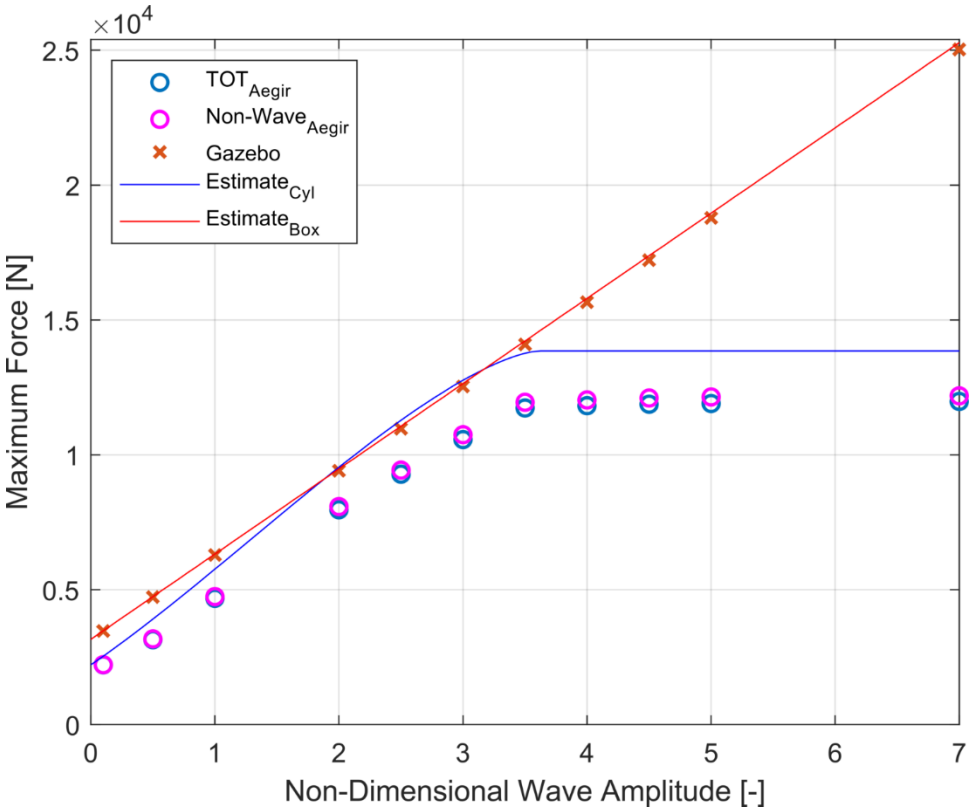

Figure 15. Comparison of Verification Methods in Head Seas

Layering each result shows the overall behavior of each model across the range of the test cases. The first striking comparison is between the results produced by Gazebo and the rectangular, or box hull approximation. Both results are equal. Because the geometry employed by gazebo is a box shape, the direct equivalence is expected. However, because this is not the actual shape of the hull, the difference between the cylindrical approximation and the AEGIR result are smaller than the difference between AEGIR and the rectangular approximation across the entire range of test amplitudes. It does appear that the box approximation, the cylindrical approximation, and the actual AEGIR results are all similar for wave amplitudes that are less than the height of the freeboard. The steady difference between the cylindrical results and the AEGIR results is likely due to the bow shape being unaccounted for in the cylindrical approximation.

D. BEAM SEAS VERIFICATION

To ensure that the long wave buoyancy assumption is sound, each of the verification steps should work regardless of the approach angle of the incident wave. The same verification is therefore completed with seas approaching from the beam of the vessel, at the wavelength and period, as well as the same test amplitudes.

1. Setup

In AEGIR, the setup is accomplished the same as the head seas test. The only change is the angle of incidence, which is set to 90 degrees, or an approach from the starboard beam.

2. AEGIR Results

Each wave case is created as an input file into AEGIR, and each simulation is run for thirty-five seconds. The maximum value derived from each result is expected to be the same as the head seas testing.

a. Small Amplitude Case

It is evident that for the small wave case that AEGIR produces very similar results. Because the small amplitude wave and thus very shallow wave steepness, the direction of the seas still manifests as a static increase in the vessel draft. The results for the small amplitude beam seas test are included in Figure 16.

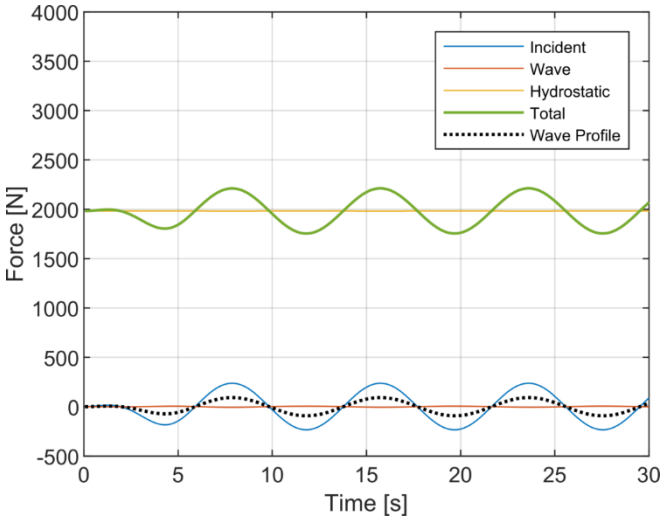

Figure 16. AEGIR Heave Force for Small Amplitude Beam Wave

b. Medium Amplitude Case

The results for the medium amplitude case for beam seas are also very similar to the head seas test, with one exception. The Hydrostatic component of the force, and thus the overall total, has what appears to be a small step when the wave is approach a peak or trough, and when the peak or trough has just passed. This step is likely due to the panel discretization of the hull and has not impacted the overall maximum total of the heave force. The medium amplitude wave results are shown in Figure 17.

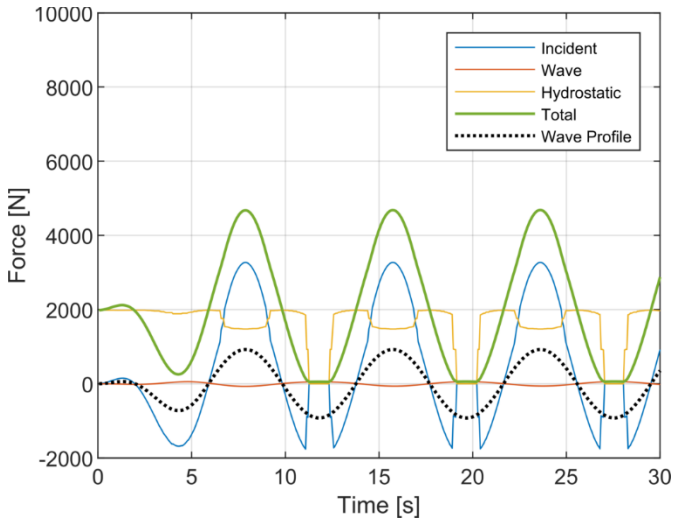

Figure 17. AEGIR Heave Force for Medium Amplitude Beam Wave

c. Large Amplitude Case

These results are also very similar to the head seas results, with one exception. As seen when the wave is approaching a peak, the upper plateau of the total force is now symmetric on either side of the wave peak, where the head seas results were not symmetric. This is due to the vessel being symmetric about the centerline plane, which the waves travel perpendicular to. The large amplitude results for beam seas are contained in Figure 18.

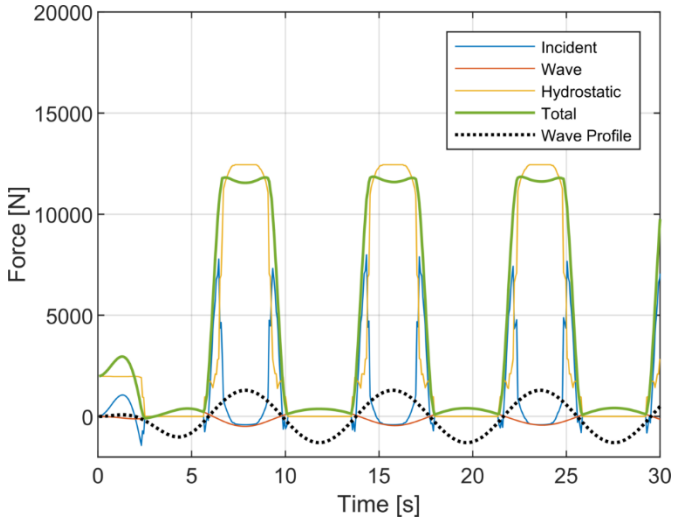

Figure 18. AEGIR Heave Force for Large Amplitude Beam Wave

3. Gazebo Results

Because of the discretization of the Gazebo Hull, the results for beam seas testing in Gazebo is not expected to be different than the head seas testing. Each of the wave cases is input into the plugin configuration file and all simulations were run for thirty-five seconds. The only change to the wave case is the direction of the incident wave.

a. Small Amplitude Case

Results for the small amplitude wave case are contained in Figure 19. This result shows the sinusoidal behavior of the total force, in phase with the wave profile.

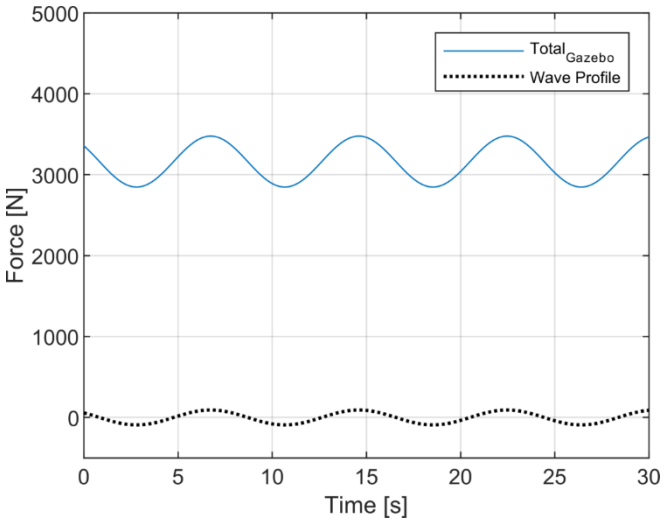

Figure 19. Gazebo Heave Force for Small Amplitude Beam Wave

b. Medium Amplitude Case

Results for the medium amplitude case are contained in Figure 20. The total force is also in line with the expected sinusoidal behavior, and still reflects the drop to zero force when the vessel it at a wave trough.

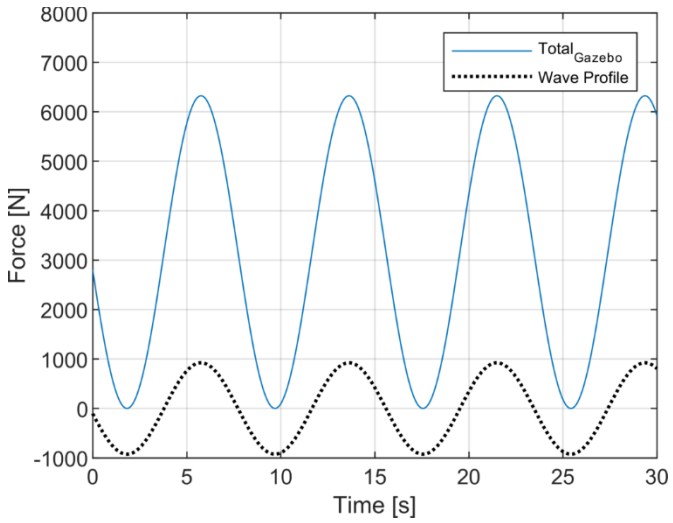

Figure 20. Gazebo Heave Force for Medium Amplitude Beam Wave

c. Large Amplitude Case

The results for the large amplitude wave case are contained in Figure 21. This result matches the shape of the head seas result and reflects the zero-force condition when the vessel is suspended over a wave trough.

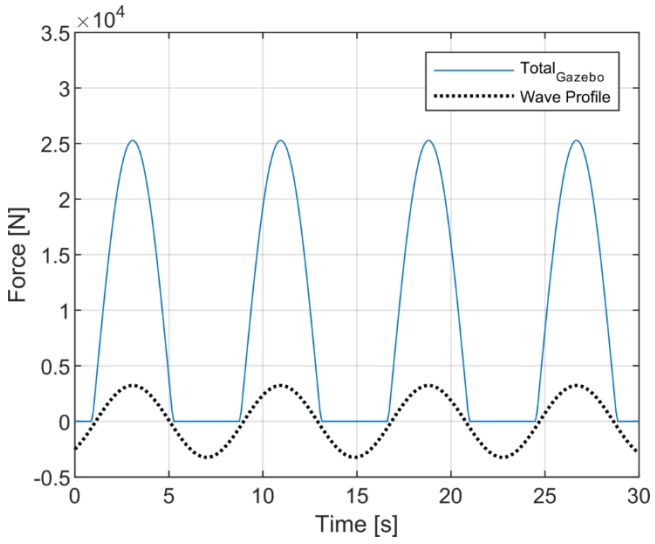

Figure 21. Gazebo Heave Force for Large Amplitude Beam Wave

4. Comparison

The method of comparison for the beam seas condition is the same as the head seas. Figure 22 shows each of the verification methods compared. As the geometric estimations do not account for the wave direction, as they expect an equal increase of fore and aft draft for the long wave case, the estimated values are the same as the head seas condition. As is evident in the results, the beam seas verification data follows the same trends as the head seas testing. Gazebo performed exactly on the rectangular box approximation, and the AEGIR results followed the shape of the cylindrical approximation.

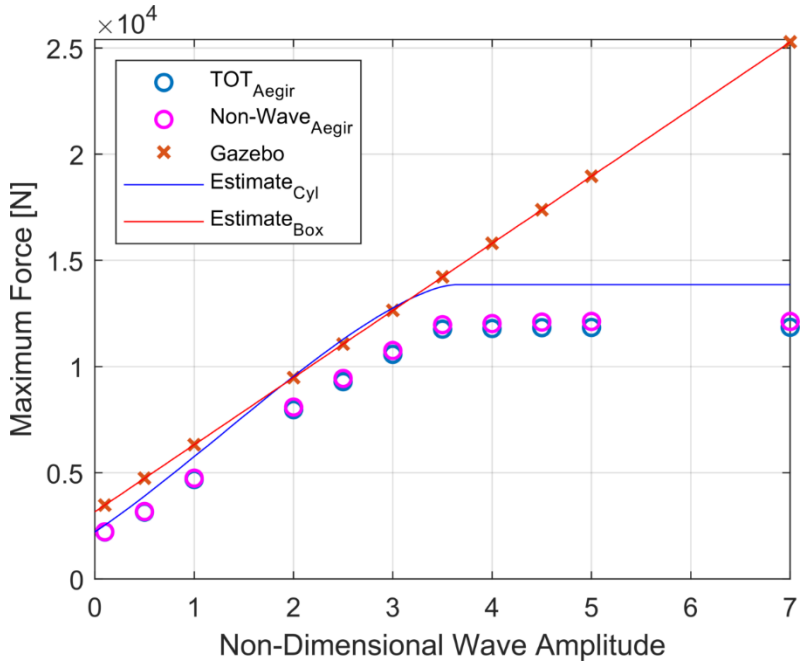

Figure 22. Comparison of Verification Methods in Beam Seas

E. CONCLUSION

This verification of the long wave case has highlighted several important points that will be crucial to understanding and qualifying any results produced by different wave conditions. First, it is evident that the rectangular approximation directly mirrors the way Gazebo works. If this box were not to be of infinite height, as implemented in Gazebo, and accounted for the freeboard of the vessel, the resulting forces would better mirror the other

methods. Without changing the Gazebo mathematical implementation, it can be concluded that there is a general limit to the acceptable wave cases that can be used in Gazebo. Second, even at the long wave case there are wave induced forces that are not accounted for by Gazebo, even if a cylindrical model is implemented, which in effect over-estimates the forces on the vessel. This also would likely only be able to be accounted for in waves that are longer than the vessel length. Third, the difference between the head seas testing and the beam seas testing is very small. Figure 23 shows the percent difference between the predicted forces for the head seas vs. beam seas scenarios – for both the AEGIR solution and the Gazebo solution.

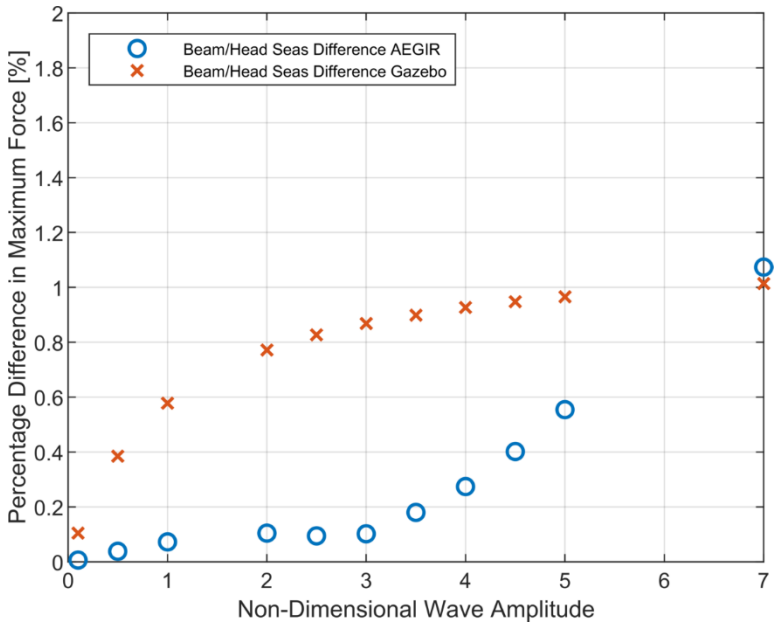

Figure 23. Difference in Results between Beam Seas and Head Seas

These differences are because the wave steepness is increasing as the amplitude increases, since the wave period is held constant throughout the test. While the long wave case that was selected is significantly long, the largest amplitude wave case still has a wave steepness of about $1/75^{th}$. This means that when a wave peak is directly in the center of the vessel, the wave amplitude at each end of the vessel will be less. However, the difference between the beam and head seas is so small (less than 2% across the entire test range), it is

assumed that the long wave assumption holds true, and thus the geometric checks are assumed to be accurately calculated for the long wave case regardless of the wave direction. Finally, from all these results, it is seen that for the cases where the wave amplitude is less than the draft, the average difference between the Gazebo and AEGIR results is about 35 percent.

IV. COMPARISON OF SIMULATED BODY FORCES AND MOMENTS

The next step is to fully investigate the impacts of wave amplitude and wave period combinations on the vessel, beyond cases that can be analytically approximated geometrically.

A. APPROACH

These tests are conducted generally the same as the long wave case described in Chapter III. However, applying the limitations discovered in the long wave case will limit the range of wave amplitudes that will be used across a wide range of wave periods. This process also considers the moments acting on the vessel. These were previously not analyzed, as the assumption with the long wave period held that the wave was encountered as a static increase in draft both fore and aft, thus no moment would be produced.

The forces and moments in two vessel planes are investigated; the heave force and pitch moment from head seas, and the heave force and roll moment from beam seas.

1. Model Setup

The model will be setup in a fashion that allows a given wave to pass the vessel without resulting in the vessel moving or rotating in any degree of freedom. This will result in the direct calculation of the forces on the vessel created by each wave. Thus, the vessel will not be allowed to translate in surge, sway or heave, and cannot rotate in roll, pitch or yaw.

2. Comparison of Forces and Moments on Static Body

This test investigates heave force, pitch moment, and toll moment, as they are the perturbations that have a restorative component. Results from AEGIR testing and Gazebo are compared side by side across the range of test cases, and in some instances the difference is computed and analyzed.

B. TEST CASES

This test looks at a range of amplitudes and periods that will be selected based on the vessel geometry. They are spaced such that they will cover a large range of wave geometries incident on the hull. This section will focus on three specific cases that present representative results for a range of wave cases. The first case is where the wavelength of a set of regular waves is less than the hull length. The second is where the wavelength of a wave is equal to the vessel length, and the last is where the wavelength is equal to twice or more of the vessel length. Figure 24 is a graphical depiction of these interesting wave cases, which will be examined in reference to specific simulations.

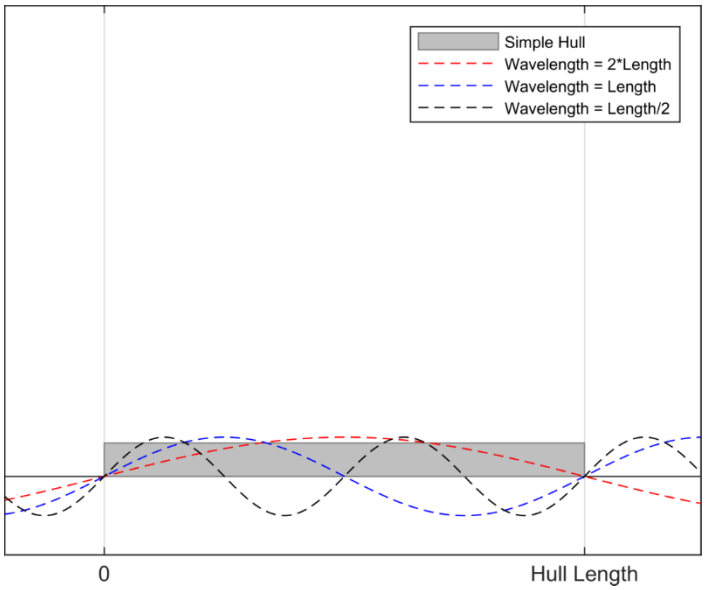

Figure 24. Graphical Depiction of Interesting Wave Cases

1. Amplitude Selection

The amplitudes selected for this case are more restricted than the long wave case. To avoid the geometrically unpredictable behavior in the forces caused by an incident wave dropping below the hull, or that of a wave swamping over the freeboard, amplitudes that are greater than the draft will not be used. Instead, the focus will remain on new amplitudes selected at 10, 25, 50, 75, and 95 percent of the draft. These will be large enough to provide

meaningful differences in the output force and moments, while staying within the amplitude restrictions.

2. Period Selection

The wave period selection is also made as a function of the vessel geometry, and in this case the wave period will indirectly be a function of the length of the vessel. Using the long wave case as the upper bound, which was 20 times the length of the vessel, the other cases that are investigated are fractions of that. The non-dimensional wavelengths (NDW) that are selected are ¼, ½, 1, 2, 4, 8, 12, and 20 times the length of the vessel.

3. Wave Steepness

To check that each of these test cases are physically possible and represent realistic wave cases on the vessel, the metric of wave steepness is used. The theoretically steepest wave that is possible in nature is about 1/7, which is the upper limit of acceptable waves. Any steepness of wave can exist below this, but the typical lower limit of steepness that is considered in seakeeping studies is about 1/200. Of note, more common wave steepness are 1/30, 1/60, 1/90, and 1/120. Using these two metrics, the wave steepness is calculated for each wave case.

Table 6. Force Testing Wave Cases

λ/L [-]	λ [m]	Wave Period [s]	Wave Amplitudes [m]				
			0.00924	0.02309	0.04618	0.06927	0.08774
0.25	1.21	0.88	0.015	0.038	0.076	0.115	0.145
0.5	2.42	1.244	0.008	0.019	0.038	0.057	0.073
1	4.83	1.76	0.004	0.010	0.019	0.029	0.036
2	9.66	2.488	0.002	0.005	0.010	0.014	0.018
4	19.33	3.519	0.001	0.002	0.005	0.007	0.009
8	38.66	4.976	0.000	0.001	0.002	0.004	0.005
12	57.98	6.095	0.000	0.001	0.002	0.002	0.003
20	96.64	7.868	0.000	0.000	0.001	0.001	0.002

Wave Steepness:	Flat	Realistic	Too Steep

Clearly, all cases except one fall within a range that is physically feasible. The one steep case is just outside of the 1/7 steepness range and may still be considered in the results.

C. HEAD SEAS TESTING

The first set of tests will again involve testing wave cases that approach the vessel from the bow. Here the heave force and pitch moment are recorded and analyzed in both AEGIR and Gazebo, and compared side by side, and for select cases.

1. Heave Force

For each wave case, the heave force result from AEGIR and Gazebo are investigated individually and compared against one another.

a. AEGIR Results

The expectation for the AEGIR heave force results is that starting with the long wave case and decreasing in wave period, the force will gradually decrease for waves longer than the vessel, and then level off and approach the static buoyancy for waves shorter than the vessel. This trend should then scale based on the wave amplitude. The results of each wave case run in AEGIR is shown in Figure 25.

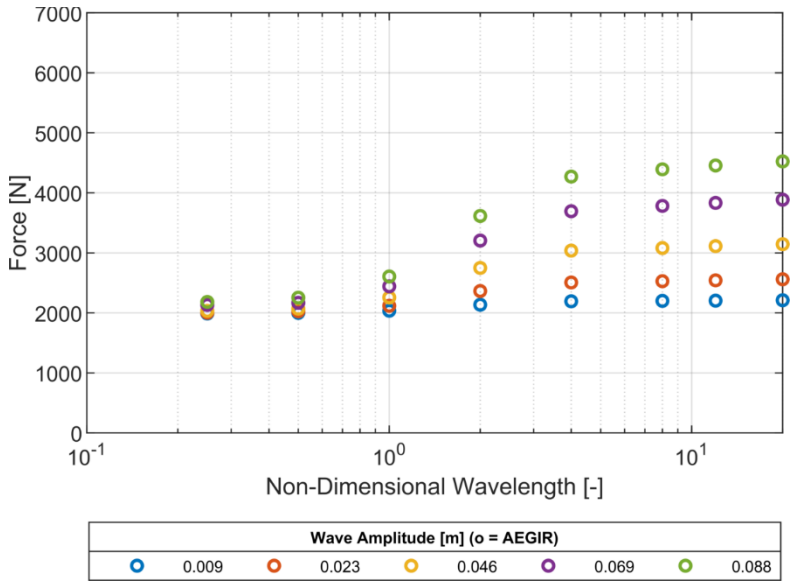

Figure 25. AEGIR Heave Results for each Test Case Amplitude

As is evident from the data, the expectation holds true. The waves with more energy, the longer period waves, manifest a greater heave force than the shorter period waves. The longest period wave case in this run also match with the verification tests. Looking deeper at the time histories of the three interesting wave cases can levy some more insight into the components of the wave forces that are affecting the vessel.

As the long wave case is known, the next most interesting case is where the wavelength is twice that of the vessel length. When the vessel is fixed, the vessel could have a wave peak at the center of the hull and zero wave height at the bow and stern, or the inverse of that condition. Figure 26 depicts the time history of such a case, for the 0.088-meter wave.

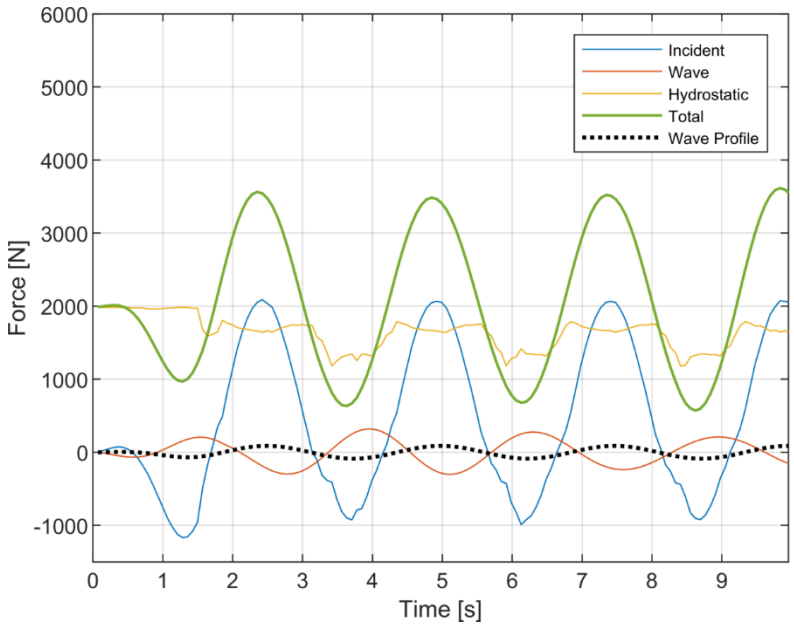

Figure 26. AEGIR Heave Force for NDW=2

This depicts similar results in one respect to the very long wavelength case. With the regular wave, sinusoidal input, the total output represents a nearly in phase sinusoid. The hydrostatic result does exhibit clearly non-sinusoidal, but repetitive behavior. For this case and longer wavelength, the total heave force behavior exhibits larger and longer sinusoids.

The next interesting case is where the wavelength is equal to the length of the vessel. At certain times that are multiples of the wave period, the vessel could have a wave peak or trough present at both the stern and bow, with the opposite at the center of the vessel. The physical result of this is that the amount of the wave above the calm waterline is exactly cancelled by the amount of water below the calm waterline. Figure 27 depicts the time history of such a case.

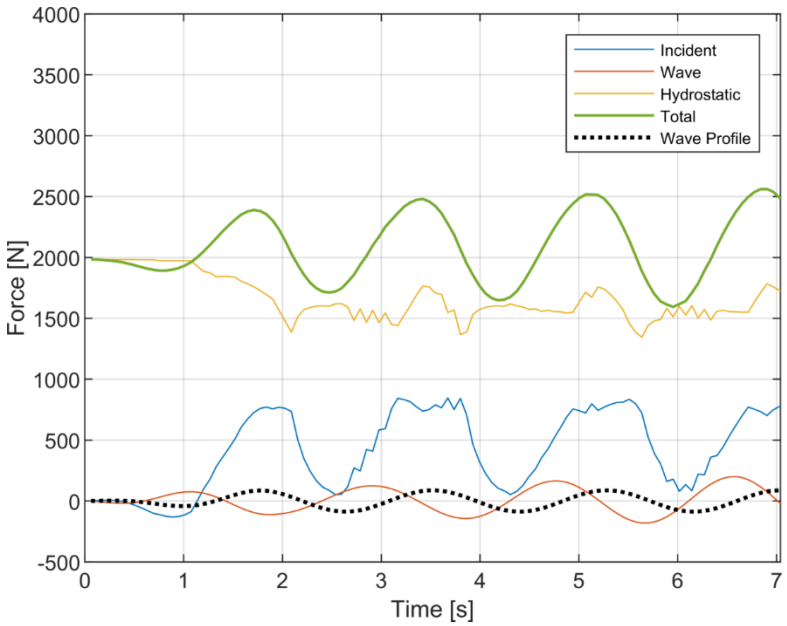

Figure 27. AEGIR Heave Force for NDW=1

This case is where the input is sinusoidal, but the resultant forcing is no longer sinusoidal. Here it is evident that the total heave force is not in phase with the encountered wave profile, which results in a jittery behavior in both the incident component and the hydrostatic component.

There also exists a phenomenon when the wavelength is less than the vessel length. With several waves appearing along the length of the hull, the hull bridges across these waves. If there is an even number of waves along the hull, each end is supported by a peak or trough. If there is an odd number of waves alone the hull, one end it supported by a peak, and the other is encountering a trough. Figure 28 depicts a case where the number of waves along the hull is even.

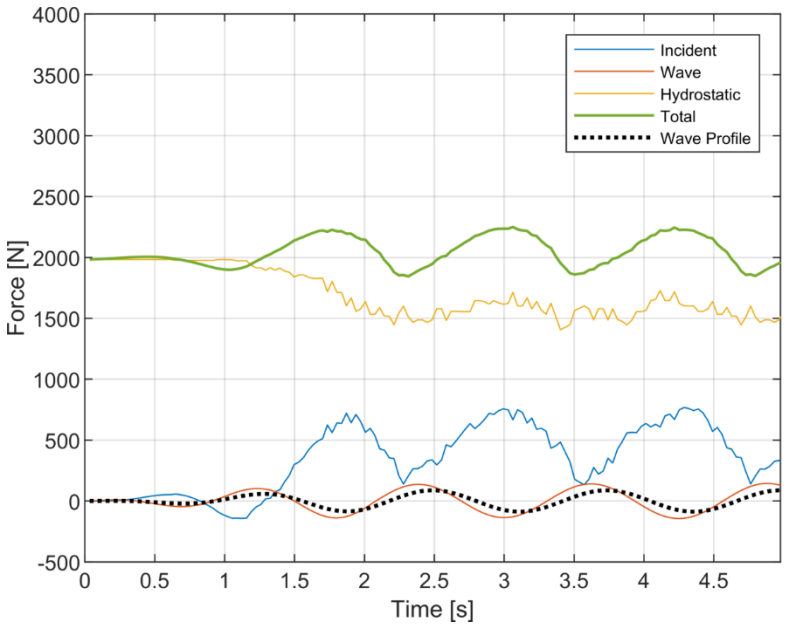

Figure 28. AEGIR Heave Force for NDW=0.5

This case can best be visualized as where the vessel is bridged across several wave peaks, and the heave force again exhibits jittery behavior, out of phase with the input wave. Some of the erratic behavior of the Incident and Hydrostatic components is likely also due to a lack of refinement in the time step used for this case, but the maximum value and general behavior are still qualitatively and quantitatively useful.

This behavior leads to a periodic result in the maximum value of the heave force across wave periods less than one. For the middle amplitude case this was examined in finer detail. The maximum value of the heave force values for this refined set of periods is contained in Figure 29.

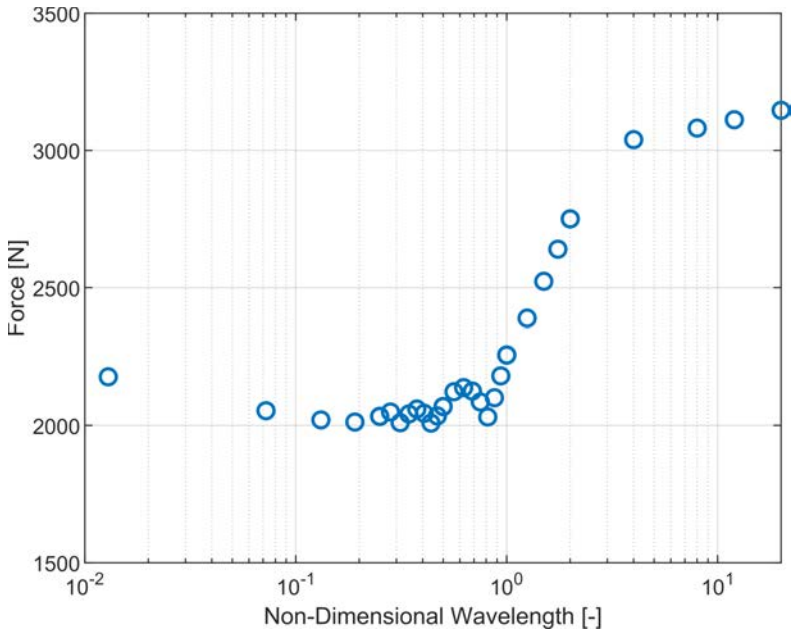

Figure 29. Detailed Results for AEGIR Heave Force with Wave Amplitude of 4.6 cm

This clearly shows the periodic nature of the maximum value of the heave force at wavelengths less than the hull length, as well as the eventual flattening of the heave force value at longer wavelengths.

b. Gazebo Results

For the Gazebo results, the same behavior is also expected, but as seen in the verification, with a significant difference in the magnitude of the heave force. Figure 30 contains the data from the Gazebo runs.

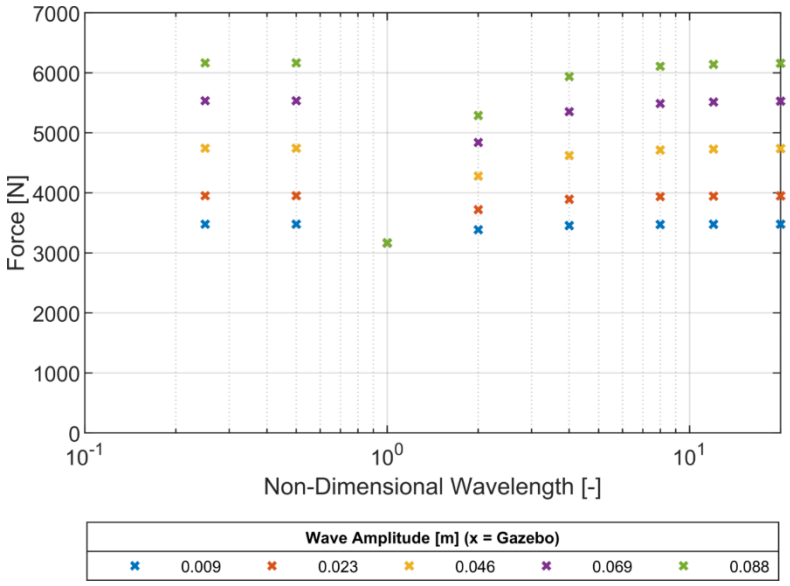

Figure 30. Gazebo Heave Force Results for each Test Case Amplitude

The Gazebo results highlight two artifacts of the way Gazebo calculates the heave force. First, for wavelengths equal to the vessel length, each wave amplitude results in the exact same heave force. The value of this heave force is exactly equal to the static buoyancy of the vessel sitting in calm water. This is because at the two points along the length of the vessel that the wave height is measured to calculate the force are spaced apart by half the vessel length. This means that for any instance in time, the wave height at each of these two points are equal in magnitude, but opposite in sign. Therefore, the total wave height, and thus force, that is calculated is only the hydrostatic buoyancy. The second artifact that is evident is that both the extremely small wavelength case and the long wave length case that were investigated result in the same force for each wave case. This also seems to be the result of using just two measurement points. Because the NDW of these cases are even fractions of the vessel length, the measurement points will both read the exact same wave height, as if it were just a very long wave, or a static increase in draft. Thus, the result is the same as the long wavelength.

Looking again at three specific wave cases assists with understanding how the results came to be. Both the wave case that is twice the length of the vessel and half the length of the vessel result as expected, a sinusoidal regular wave input resulting in a

sinusoidal force output. The case where the wave length is equal to the vessel length does show a force value equal to the buoyancy of the vessel, as seen in Figure 31.

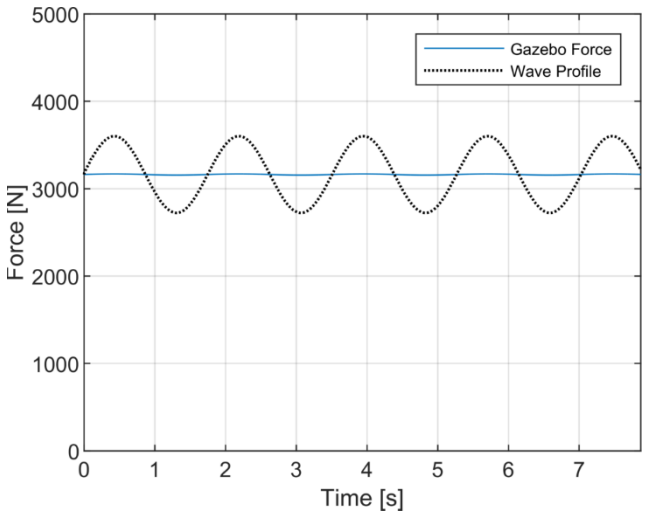

Figure 31. Gazebo Heave Force for NDW=1

Because of the rough discretization that Gazebo uses, the periodic nature of the maximum value of the heave force will also be present at wavelengths less than the vessel length. But, as seen in the overall Gazebo results, the even fraction peaks are equal to the long wavelength case heave force. Using a more detailed set of NDW, the periodicity in the result can be seen. The flattening of the maximum value of the heave force at longer wavelengths can also be seen. Figure 32 shows the results of the more detailed set of NDW runs.

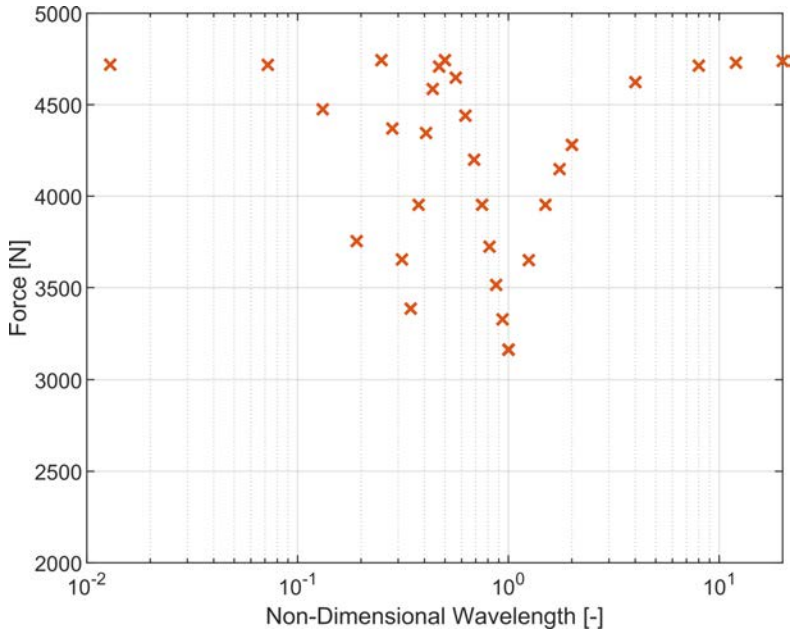

Figure 32. Detailed Results for Gazebo Heave Force with Wave Amplitude of 4.6 cm

c. Comparison

Comparing the results from Gazebo and AEGIR side by side can begin to highlight a range of amplitudes and more importantly, wave periods, where the heave force behavior is similar. Looking at one of the selected wave amplitudes, the 4.6 cm wave, some of the behavior is similar. Figure 33 shows the detailed wave period investigation for this selected wave amplitude. For a more quantitative comparison, the percent difference is calculated and displayed in Figure 34. Because there is no true or theoretical value for the heave force in these cases, the mean is used to compute that the

$$\%Diff = 100 * \frac{|Gazebo - Aegir|}{(Gazebo + Aegir)/2}.$$

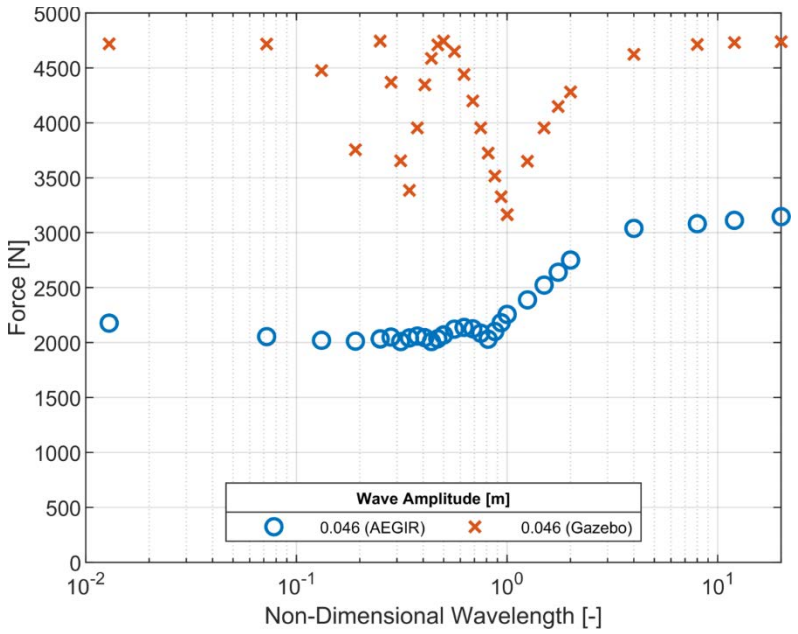

Figure 33. Heave Force Comparison of 4.6-cm Wave Test

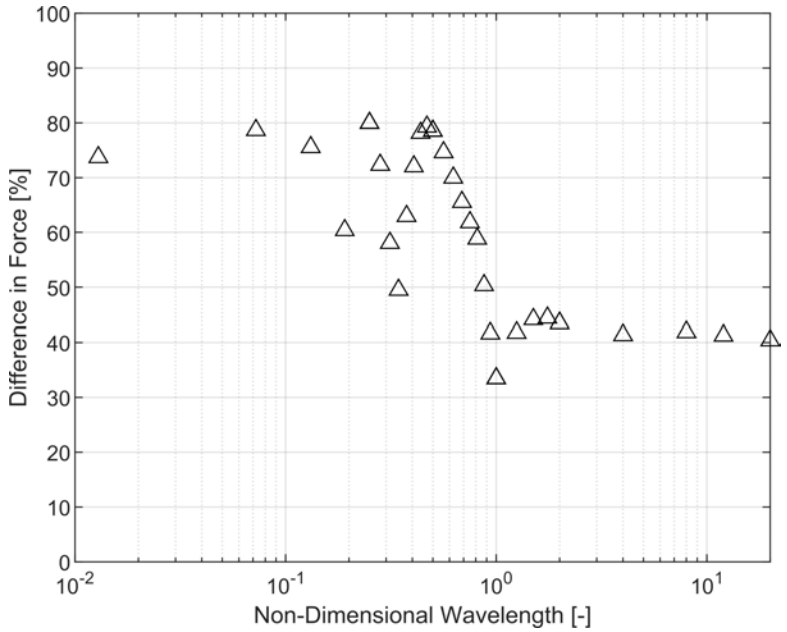

Figure 34. Percentage Difference in Heave Force for 4.6-cm Wave

The difference in performance of each program is substantial, but there are some interesting highlights to the differences. First, for NDW values of greater than one, the percentage difference between the two programs is steady between 40% and 45%. This is

almost completely due to Gazebo using a rectangular geometry, while AEGIR uses a more cylindrical geometry. This shows that for heave, decreasing the wave period from the longest wave case to a case where the wavelength is equal to vessel length has very little impact on the produced heave force. This leads to the likelihood that most of the force from the waves is due to hydrostatic and incident components of the force, which are generally captured by Gazebo with the instantaneous buoyancy model. It is also evident that both models exhibit the periodic behavior at small wavelengths, though Gazebo manifests this behavior in a much more exaggerated fashion. However, it can be noted that the percent difference between the two are the most unpredictable and erratic for the very short wavelengths, at NDW between 0.1 and 1.0. As the wavelength becomes infinitely shorter, it is expected that the results would behave more and more like calm water for small amplitudes waves up to the maximum theoretical wave steepness, as reflected in the AEGIR result.

With knowledge of the more detailed wavelength investigation, the impact of wave amplitude would most likely present itself as a scaling factor to the maximum value of the heave force. Each of the five wave cases is shown for comparison in Figure 35.

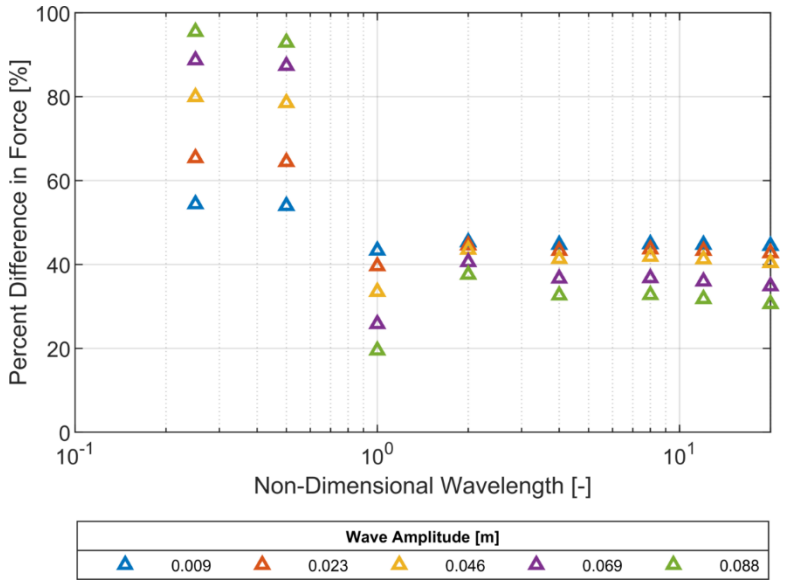

Figure 35. Percentage Difference in Heave Force for all Wave Cases

2. Pitch Moment

The next degree of freedom that is investigated, distinctly coupled with heave, is pitch, and thus the pitch moment in this fixed case. The pitch moment is calculated from the same head seas runs that resulted in the heave force values, thus for the exact same wave cases.

a. AEGIR Results

In AEGIR, the pitch moment should directly reflect the behavior of the forces throughout the set of wave cases. When the wave is significantly shorter than the length of the vessel, the pitch moment is also expected to be very small, as the forces are small. When the waves are significantly longer than the vessel and the wave steepness is decreasing, the pitch moment is also expected to be very small. By examining the same three cases from the heave force, these behaviors should be evident, and the largest value of the pitch moment should exist somewhere in between. Figure 36 shows the first case.

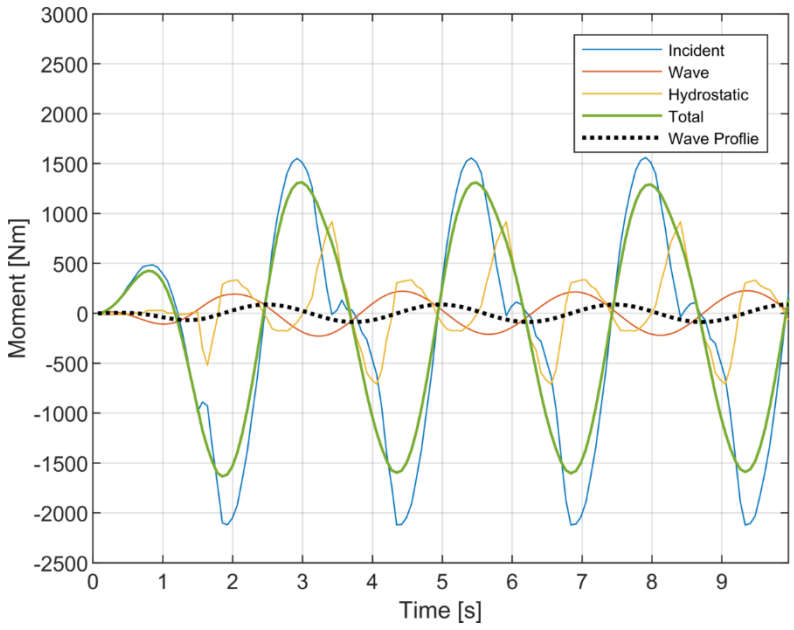

Figure 36. AEGIR Pitch Moment for NDW=2

Here is it clear that the pitch is 90 degrees out of phase with the wave profile and has a larger value in pitch in one direction over the other. This is directly due to the bow shape of the vessel, which would lead to an asymmetric pitch moment. The larger magnitude peak will be the one used to represent the case in comparisons. Figure 37 shows the next case.

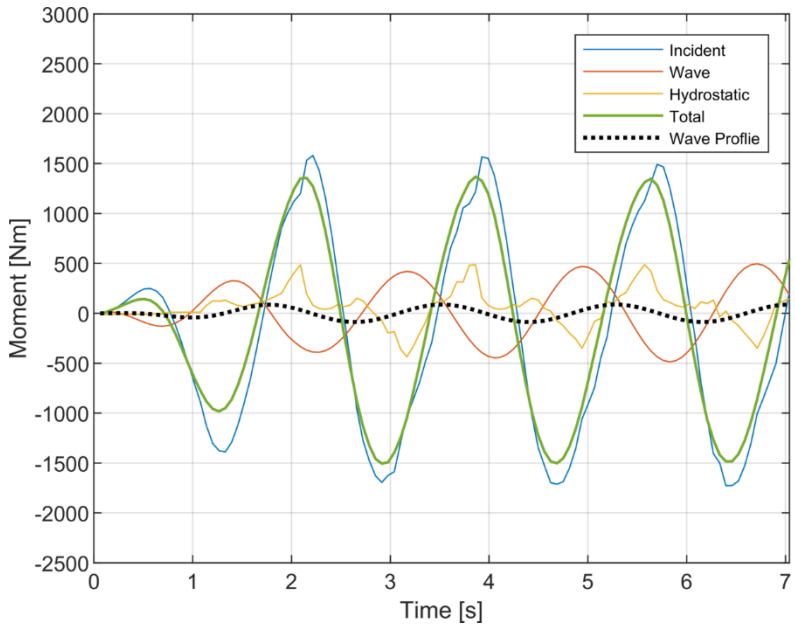

Figure 37. AEGIR Pitch Moment for NDW=1

Again, this same behavior is exhibited, while slightly less asymmetric. Finally, the last case in shown in Figure 38.

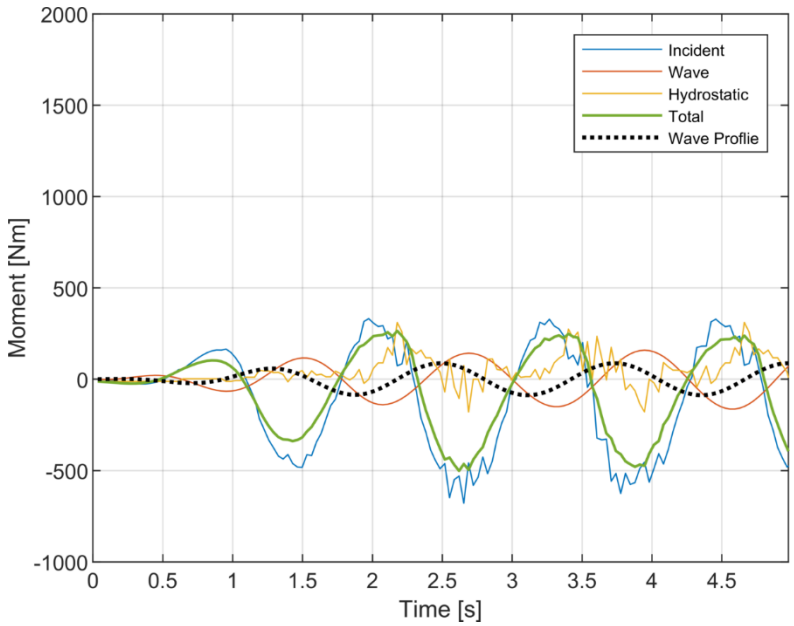

Figure 38. AEGIR Pitch Moment for NDW=0.5

Again, the result shown appears to be slightly numerically unstable, but highlights both the phasing and maximum value of the pitch moment. For each of the wave cases investigated, the maximum value of the pitch, regardless of sign, is considered. The results are as expected and follow the heave forces. Every result exhibited the asymmetric behavior see in the example case amplitude, thus reinforcing the idea that is stems from the bow shape and the vessel's asymmetric shape fore and aft. The pitch moment result does show that the pitch moment is very small for wavelengths less than the vessel length, as the vessel is supported by several wave peaks. It also shows that as the waves become longer, the pitch moment decays as the wave steepness decreases. All pitch moment results from these wave cases are contain in Figure 39. A more detailed look into the periodic nature of the pitch moment for wavelength less than the vessel length is show in Figure 40.

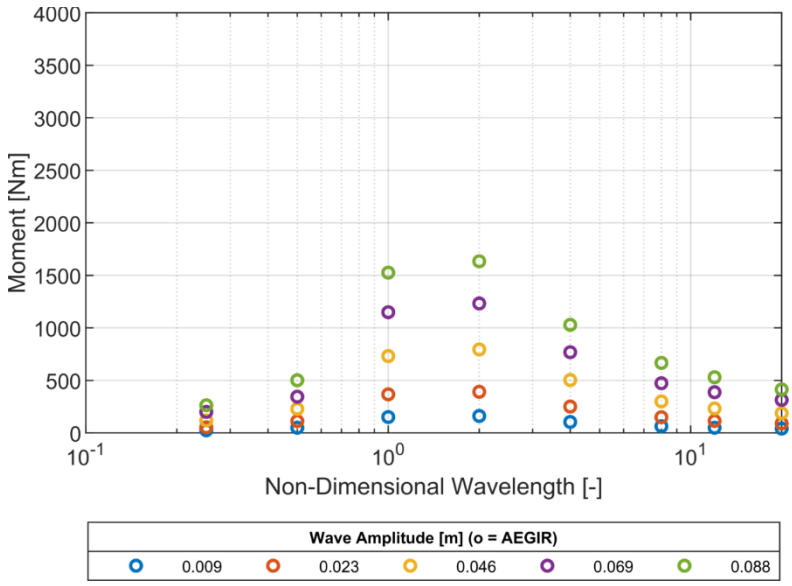

Figure 39. AEGIR Pitch Moment Results

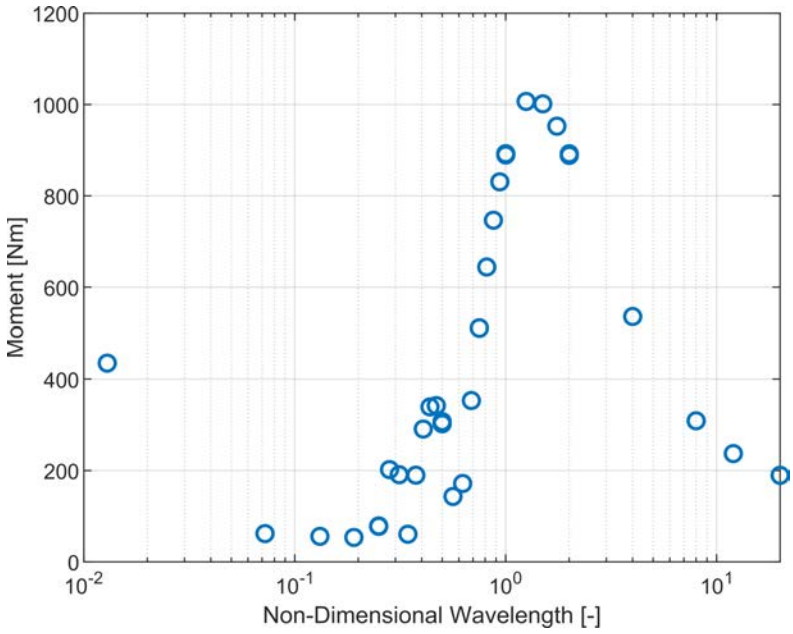

Figure 40. Detailed AEGIR Pitch Moment Result for 4.6-cm Wave

b. Gazebo Results

Because of the discretization of the Gazebo model, and how pitch is based on the force balance between two points that are equidistant from the center of the vessel, the Gazebo pitch result is relatively simple to predict. The result is expected to be maximum when the wavelength equals the vessel length, resulting in the greatest difference in force between the fore and aft discretization points. It then should decrease for increasingly long waves, as each of the point values will become closer and closer in value to each other. At wavelengths less than the vessel length, the expected pitch moment will be near zero, as each of the discretization points should be reading exactly opposite values for an even number of waves along the hull. Each of the wave case results are shown in Figure 41.

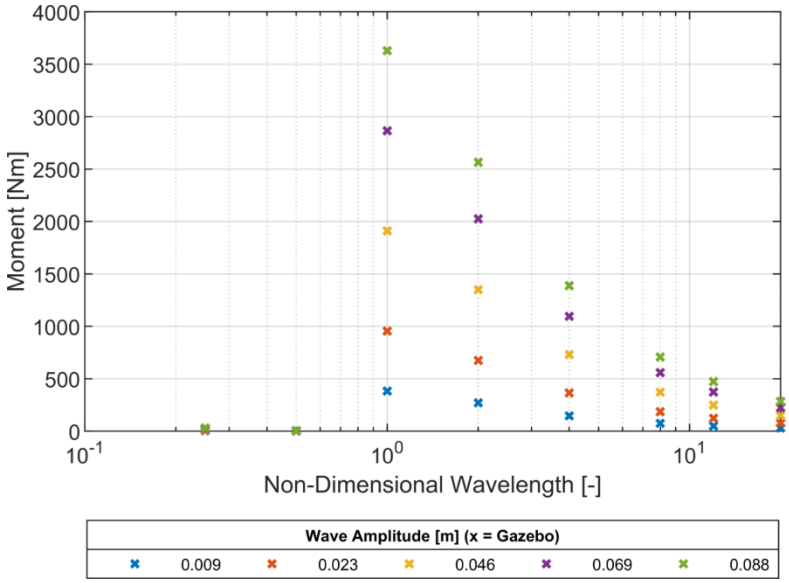

Figure 41. Gazebo Pitch Moment Results

This clearly shows the expected behavior. Because both cases selected for wavelengths less than the vessel length were even fractions of the vessel length, both results are nearly zero. The maximum pitch moment exists when the wavelength is equal to the vessel length and decreases as the wavelength increases. The periodic nature of the pitch moment was also investigated for wavelengths less than the vessel length, which can be seen in Figure 42. This shows the two points where the pitch moment is nearly zero, but a

slight increase or decrease in the wavelength subjects the vessel to a much larger pitch moment. It is seen that selecting a value between the two points results in a pitch moment nearly the same as the maximum moment for this selected amplitude case, which is clearly a result of the discretization spacing.

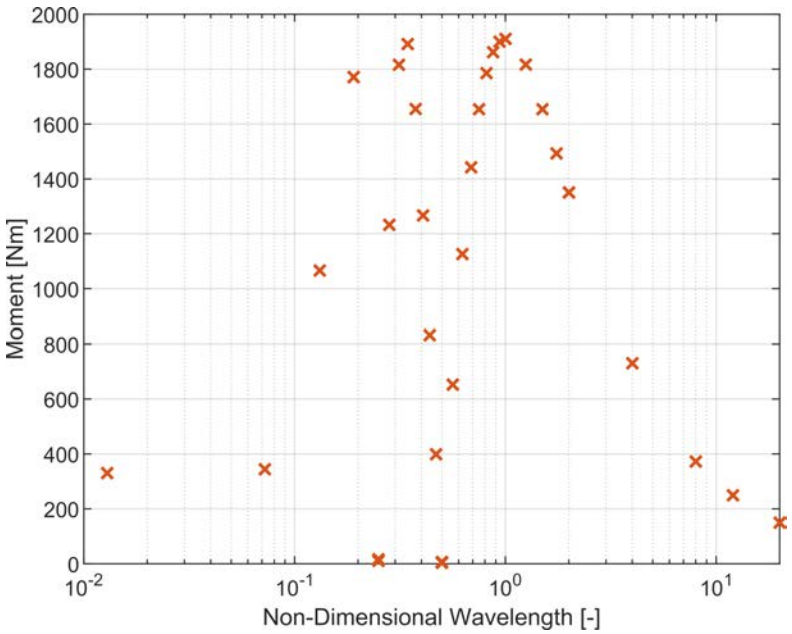

Figure 42. Detailed Gazebo Pitch Moment Results for 4.6-cm Head Wave

c. Comparison

With all the wave case data acquired for the pitch moment, they can now be compared side by side to see if the result is close to the difference seen in the heave force result. Looking at the selected amplitude detailed case, which highlighted the same result from the heave force, the difference in pitch moment is very evident. These results are contained in Figure 43, and the difference is highlighted in Figure 44.

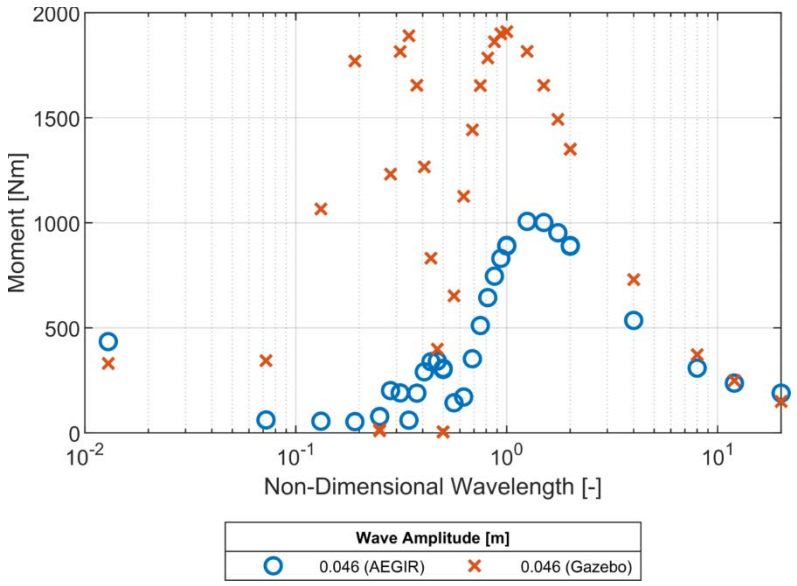

Figure 43. Detailed Pitch Moment Comparison for 4.6-cm Head Wave

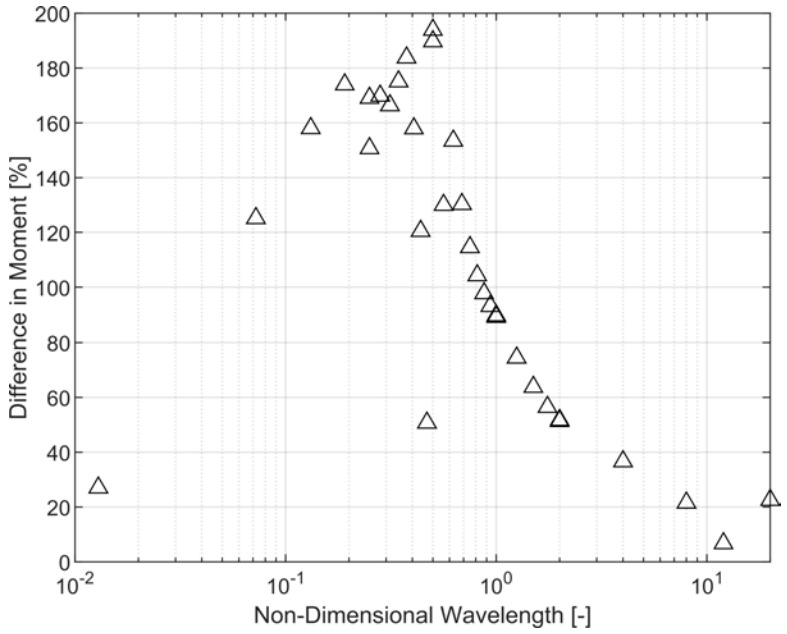

Figure 44. Detailed Pitch Moment Difference for 4.6-cm Head Wave

Clearly, the impact of the discretization of the Gazebo model is much greater in terms of pitch moment than in heave force. As the wavelength increases, however, the results converge to a much more comparable value to the heave force, nearing about 40%. With the maximum difference being about 200%, it is expected that any pitch motions

generated by Gazebo would be artificially large for the same wave cases. Gazebo also clearly has more issues capturing the pitch moment for wavelengths less than the vessel length. Comparison of each wave case across all amplitudes is shown in Figure 45.

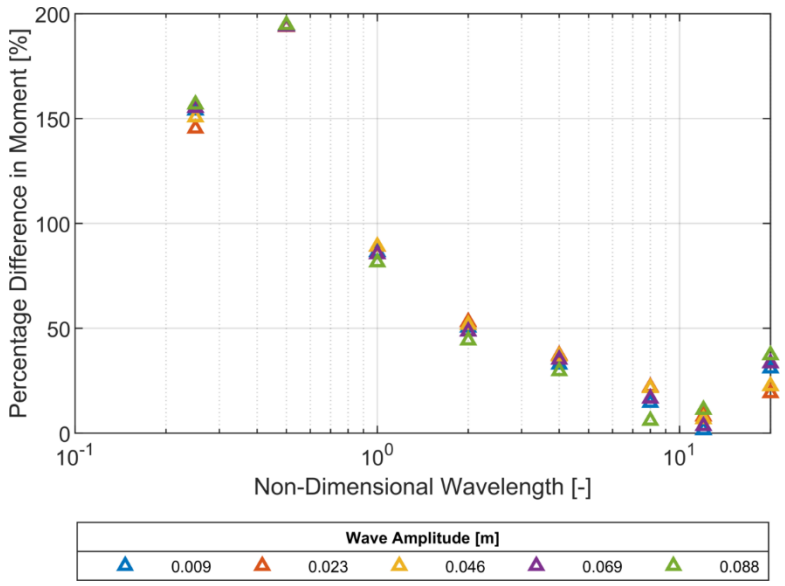

Figure 45. Pitch Moment Comparison for All Head Seas Cases

An extremely notable result here is that the difference in the pitch moment seems independent of the wave amplitude at each of the test wavelengths, and that most of the wavelengths that are longer than vessel length differences exist below 50%.

D. BEAM SEAS TESTING

Each of the wave test cases are run again with one modification—the direction of the waves. Testing the beam sea condition will allow the determination of the forces and moments about another principle axis. From this test both the heave force and the roll moment are determined.

1. Heave Force

The heave force for the beam seas cases are computed to make the direct comparison between the head seas results and the beam seas. As seen in the verification, there is expected to be a very small difference for the long wave case and will be looked at

for shorter and shorter waves. The detailed wave cases to investigate waves shorter than the vessel length were not investigated, however, there is expected to be a similar relationship when looking at waves that are shorter that the vessel beam. All results are still shown as NDW against the vessel length instead of the vessel beam.

a. AEGIR Results

The same wave cases are run through AEGIR with the only change being the wave direction. Figure 46 shows the resulting heave force from the same waves with the different incident direction.

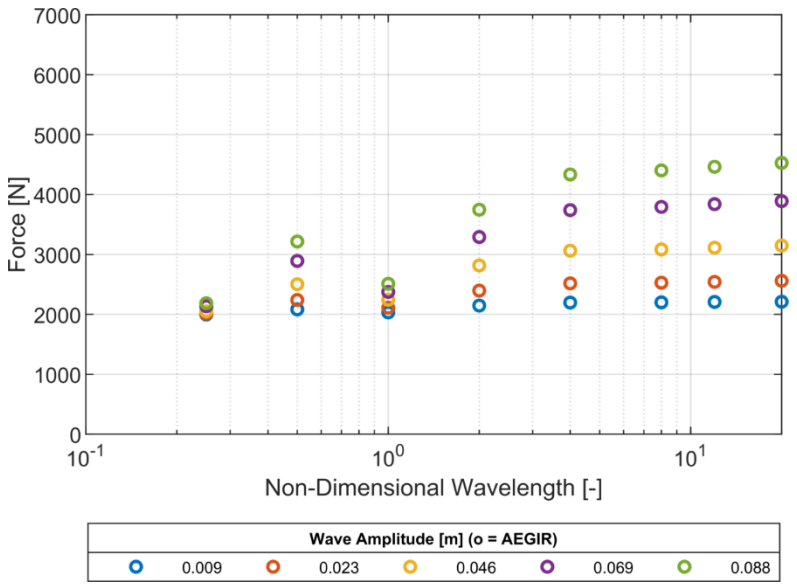

Figure 46. AEGIR Heave Force Results for Beam Seas

Here it is evident that the short wavelength peak in heave force occurs when the wavelength is equal to the beam of the vessel, instead of the length, with the new wave orientation. Increases or decreases in the wavelength result in a decreased heave force. As expected, the heave force asymptotes as the wavelength increases far beyond the length of the vessel.

b. Gazebo Results

Each wave case is used in Gazebo with the change in wave direction. Figure 47 displays the results across all wave cases

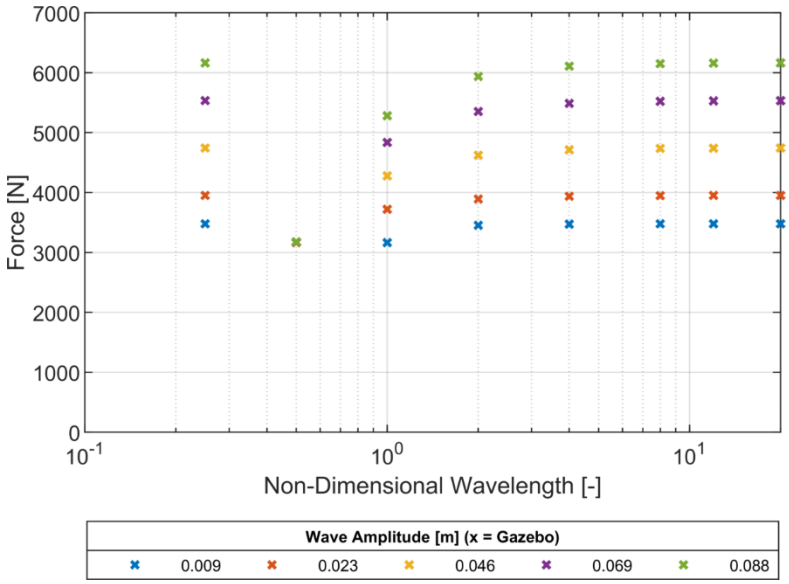

Figure 47. Gazebo Heave Force Results for Beam Seas

Again, it is evident that when the wavelength equals the spacing between the discretization points, in this case the beam-wise spacing, that the heave force returns to the vessel's static buoyancy. This effect was also seen in the head seas case. Again, the heave results for very short wavelengths are artificially high based on the discretization. As the wavelength increases far beyond the length of the vessel the same asymptotic behavior is also noted.

c. Comparison

Comparing the results between AEGIR and Gazebo is expected to yield a similar result to the head seas test and suggest a strong limitation based on the rough Gazebo discretization. Figure 48 contains the differences between each wave case.

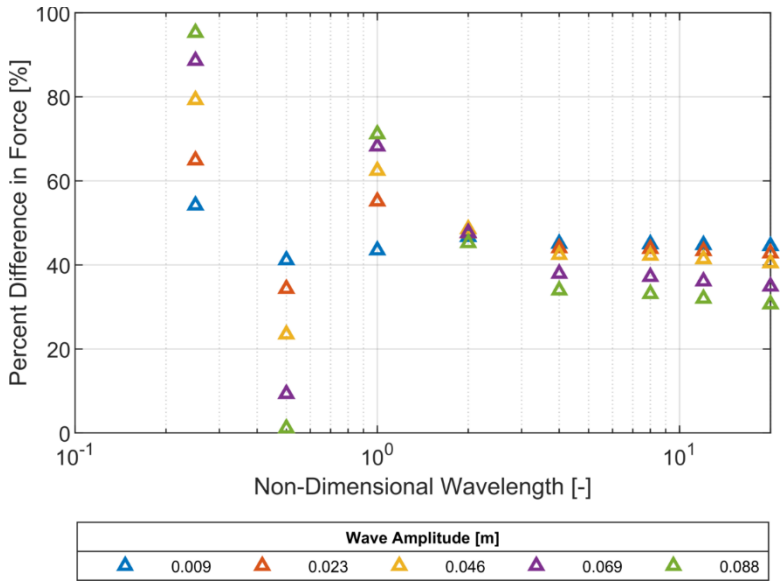

Figure 48. Heave Force Difference for Beam Seas

This clearly highlights the large differences exhibited at shorter wavelengths, and how much the wave amplitude also affects the range of differences. However, this also highlights a very similar range of differences at larger wavelengths, around 40%, which remain relatively steady for NDW greater than twice the beam.

2. Roll Moment

The roll moment is also directly computed during the beam seas testing, using the same exact wave parameters. Each wave case is replicated in AEGIR and Gazebo.

a. AEGIR Results

Again, as seen in Figure 49, the roll moment results follow the peaks and asymptotes of the heave force results. As expected, increases in the wave amplitude have a corresponding effect on the magnitude of the roll moment.

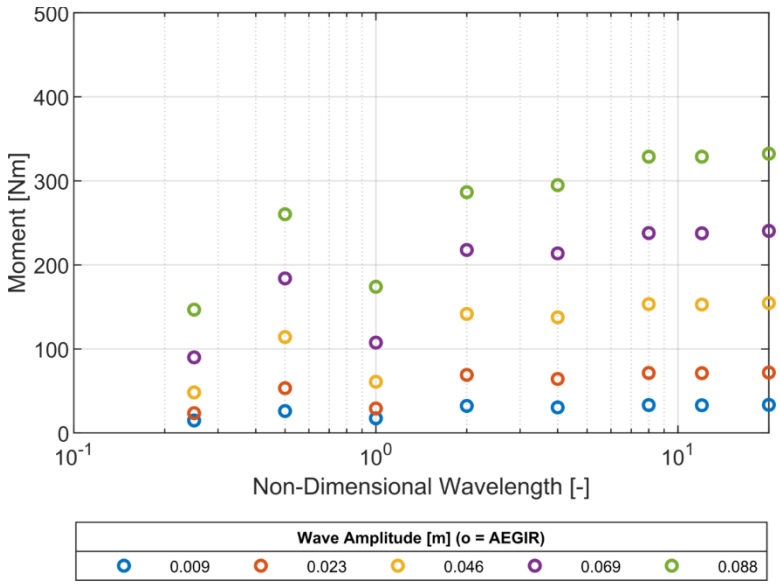

Figure 49. AEGIR Roll Moment Results for Beam Seas

b. Gazebo Results

Figure 50 clearly shows the effect of the rough discretization of the vessel in Gazebo. The roll moment is artificially large at all wavelengths longer than the beam-wise separation of the discretization points. Also seen is the convergence of all results as the wavelength increases far beyond the beam of the vessel.

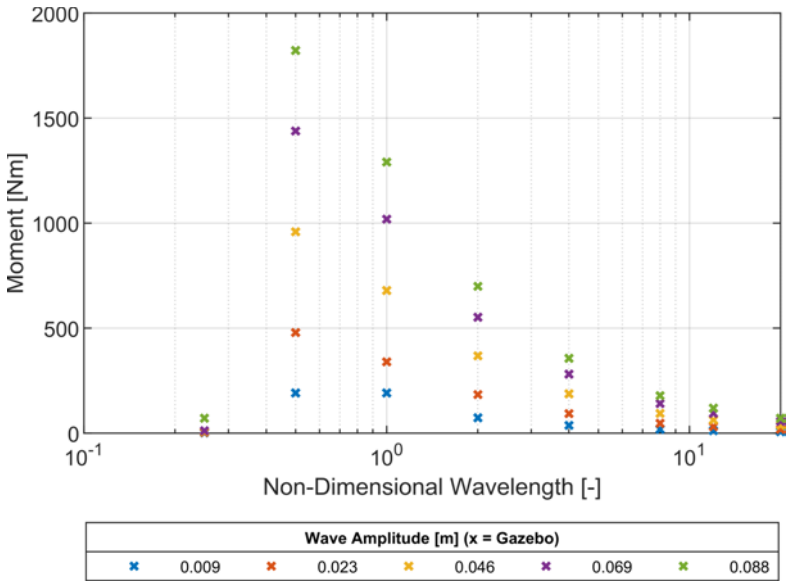

Figure 50. Gazebo Roll Moment Results for Beam Seas

c. Comparison

With the large difference behavior in the roll moment results, it is expected that the percentage difference comparison will not yield a region where the difference is steady. Figure 51 shows the percentage difference comparison for all wave cases.

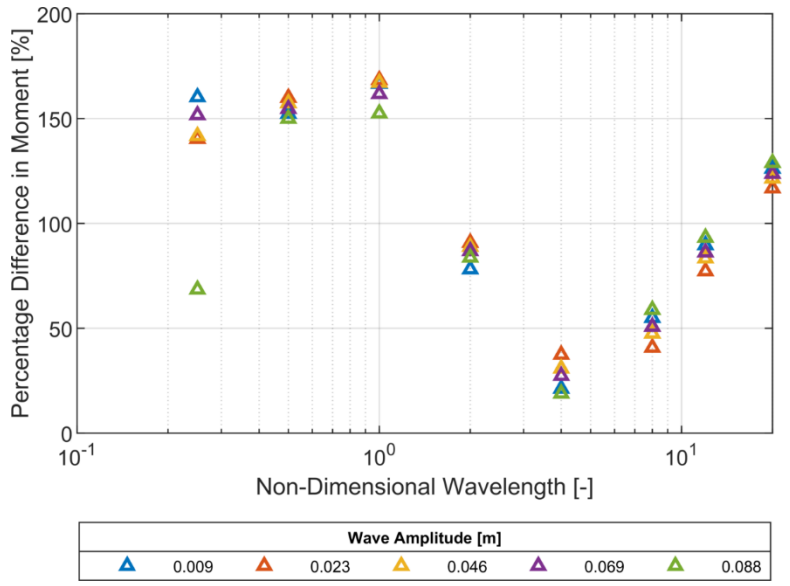

Figure 51. Roll Moment Comparison for Beam Seas

As with the pitch moment comparison, the results vary far beyond the 40–50% range in difference seen in the heave force difference. Some of this may be odd artifacts in the behavior of a catamaran that is rolling, which can have an odd coupling between heave and roll.

E. CONCLUSIONS

In head seas and beam seas, there are some conclusions that can be made that would potentially impact the vessel when allowed to be free in certain DOF. First, in head seas, there is a roughly constant difference between both heave force and pitch moment for wavelengths that are longer than the vessel length. This difference is about the same as the difference seen in the long wave verification, where the difference between AEGIR and Gazebo was on average about 35%. The average percent difference between AEGIR and Gazebo for the results generated from wavelength greater than the vessel length is also about 35%. This would potentially translate into a predictable difference between the heave and pitch motions in the same wave conditions. Second, roll performance in beam seas in Gazebo suffers worse than pitch performance due to the rough discretization of the Gazebo model. The difference between AEGIR and Gazebo for all cases where the NDW is less than one is greater than 150%, and while performs well for wavelengths near the vessel length, gets worse as the wavelength increases. There are also cases in both where Gazebo calculates no roll or pitch moment on the vessel when there should be in the wave field. The relative performance between AEGIR and Gazebo for several grouped wave cases are summarized in Table 7.

Table 7. Average Percent Difference for Head and Beam Sea Forces and Moments

	$\lambda < L$	$\lambda = L$	$\lambda = 2L$	$\lambda >> L$
Heave	80%	35%	40%	38%
Pitch	175%	90%	50%	25%
Roll	140%	160%	80%	125%

Bad	Poor	Good	Great

V. COMPARISON OF SIMULATED BODY MOTIONS

With an understanding of the contributions from individual force components, and the effect of wave period on the computed body forces of the vessel, the next step is to investigate the consequence of that forcing on a vessel that is free to move. This investigation will continue to simulate a mathematically similar vessel in regular waves across a range of wave periods and amplitudes.

A. APPROACH

A similar approach to the forces and moments study is used to develop the model parameters, desired results, and set of test cases needed to study the linear and angular motions of the vessel model in regular waves.

1. Model Setup

In this stage of simulation, each method is setup to now allow vessel motion. Each model can support full six DOF motion, and can account for added mass, linear damping, and quadratic damping for each motion. Both Gazebo and AEGIR are setup to have the same values for the added mass, linear, and quadratic damping that are applicable for each motion case. Only the necessary values are input into each simulation for the calculation of the motions.

2. Comparison of Vessel Motion

As with the simulations that were run to determine the forces on the fixed vessel, the same approach is used in the isolation of motion planes. While this is a six DOF model, the vessel will be setup in each simulation to only compute motions in one plane at a time. For head seas testing, the vessel is only free in heave and pitch, and fixed in all other DOF. For beam seas testing, the vessel is only free in heave and roll, and fixed in all other DOF. The motion testing is focused on the DOF that have restoring forces, specifically heave, pitch, and roll, rather than those that do not, specifically surge, sway, and yaw. The desired results will focus on the peak amplitude for each of the free DOF, and observation of the phase between the forcing and the response across each test case.

B. TEST CASES

When choosing the test cases that would be implemented in simulation for the motion study, consideration was made to make some of the cases the same as the forces and moments test cases, to be able to make connections back to the forces and moments results. The range of both wave period and wave amplitude required modification for this set of simulations to be able to quantitatively realize the results.

1. Wave Parameter Selection

During the forces and moments simulations presented in Chapter IV, the amplitude of the incident wave was artificially limited to values less than the draft of the vessel, to avoid the case where the fixed vessel becomes suspended in space above the free surface of a wave trough. Because the vessel is now able to respond to wave forcing, this is no longer a constraint, and larger amplitude waves can be simulated. The new limitation placed on the anticipated waves requires that any wave must be less than the freeboard of the vessel. This is both a mathematical and a practical limitation. It avoids the case where the vessel would essentially become submerged, which the model is not set up to handle. Practically, this would represent a sea state that the vessel would likely not operate in.

The same wave periods are used, with one exception. Because of the behavior observed at wavelengths less than the vessel length, the shorter wave case was removed. This case was also removed due to the limitations it imposes on acceptable wave amplitudes at such short wavelengths.

2. Steepness Considerations

Because of the increased limit on the wave amplitudes used for these simulations, a greater consideration for the wave steepness in each case must be made. Using the same set of wave periods from the forces and moments testing, and the changed limitation on wave amplitude, new wave amplitudes are selected that result in wave steepness values less than 1/7. The full range of wave cases and their associated wave steepness values are contained in Table 8.

Table 8. Motion Testing Wave Cases

λ/L [-]	λ [m]	Wave Period [s]	Wave Amplitudes [m]				
			0.06927	0.08774	0.15	0.2	0.3
0.5	2.42	1.244	0.057	0.073	0.124	0.166	0.248
1	4.84	1.76	0.029	0.036	0.062	0.083	0.124
2	9.66	2.488	0.014	0.018	0.031	0.041	0.062
4	19.33	3.519	0.007	0.009	0.016	0.021	0.031
8	38.66	4.976	0.004	0.005	0.008	0.010	0.016
12	58.00	6.095	0.002	0.003	0.005	0.007	0.010
20	96.65	7.868	0.001	0.002	0.003	0.004	0.006

Wave Steepness:	Flat	Realistic	Steep

Here it is evident that there are only a few wave cases of concern that will still be simulated. All other cases fall within an acceptable range of wave steepness. Of the selected amplitudes, the two smallest were taken from the fixed vessel forces and moments simulations directly. The largest wave amplitude represents a value that is 90% of the freeboard of the vessel. Each of these 35 wave cases are implemented in Gazebo and AEGIR.

C. HEAD SEAS TESTING

Each of the wave cases is implemented with the seas approaching from the bow of the vessel. The vessel is set to zero forward speed and is only free to move in heave and pitch.

1. Heave

The heave motion results were collected from both simulations for each of the test wave cases. The heave motion is calculated at the center of gravity of the vessel.

a. AEGIR Results

As with the heave force investigation, it is expected that the heave motion result in AEGIR is in phase with the wave profile. It is also expected that as the wave period

increases, the heave motion amplitude would more closely match the wave amplitude. Extracting the maximum heave amplitude from each wave case is shown in Figure 52.

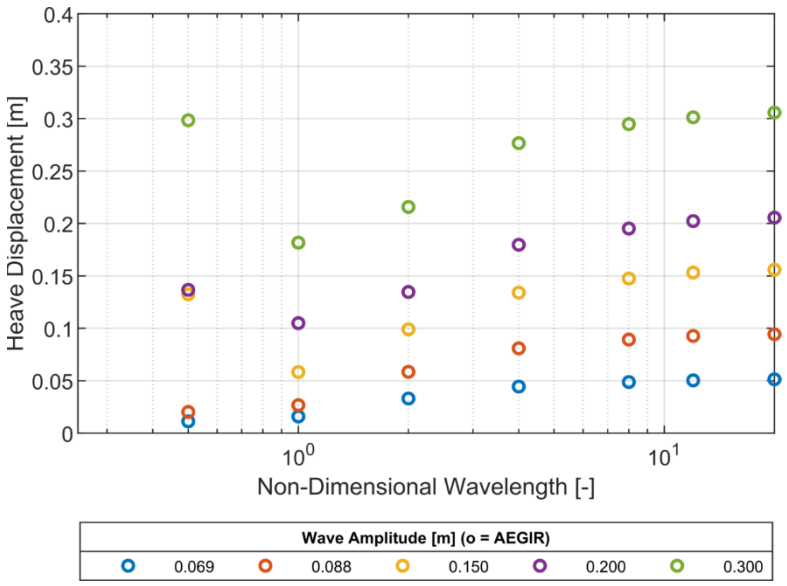

Figure 52. AEGIR Heave Displacement Results in Head Seas

There are several important observations than can be made from these trends. First, each of the results, as the wave period increases to the long wave period case, the motion of the vessel in heave approaches the wave amplitude, and the vessel is essentially following the wave profile. Second, the effect of wave steepness can be seen in the case where the NDW is less than unity, as the results are widely varied. The values for the tallest three waves can likely be discarded, as the wave steepness values exceed 1/7, indicating they are not physically realizable. Finally, the behavior of the heave motion is observed to have the same trends across the full range of wave amplitudes. Looking at the phase of the heave response for one of the wave cases, the 0.088-meter wave, also yields several observations. Figure 53 shows the very short period wave case.

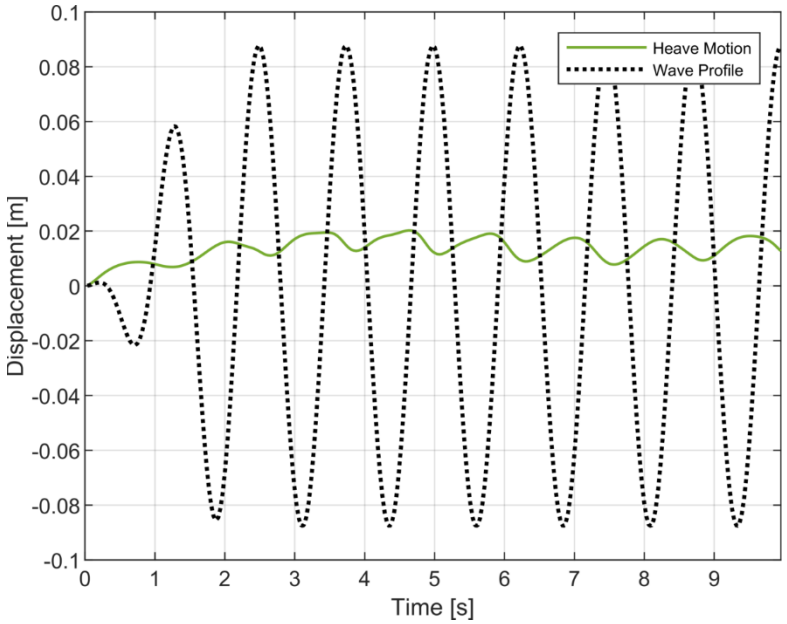

Figure 53. AEGIR Heave Response for 0.088-meter Wave at NDW=0.5

This plot shows an interesting phenomenon that is present at wavelengths less than the vessel length. Rather than the heave displacement oscillates about the mean position of the vessel, the static draft, the heave motion oscillates about a higher value. This essentially means that with these shorter waves, the vessel is buoyed up above its static draft, and oscillates about that new effective draft. Here it is also seen that the heave response is not sinusoidal or in phase with the wave profile, as the vessel appears to bounce along the small wave peaks. At higher wave amplitude this effect becomes more erratic.

Another interesting case is where the wavelength is twice the vessel length, which resulted in a significant damping of the heave response compared to the wave amplitude. This also results in the heave motion lagging behind the wave profile. The result also now appears sinusoidal. The time history showing these effects is contained in Figure 54.

Finally, when the wavelength is significantly longer than the vessel length, the heave response becomes purely sinusoidal, closer in phase to the wave profile, and has an amplitude very close to that of the incident wave. These effects are seen in Figure 55.

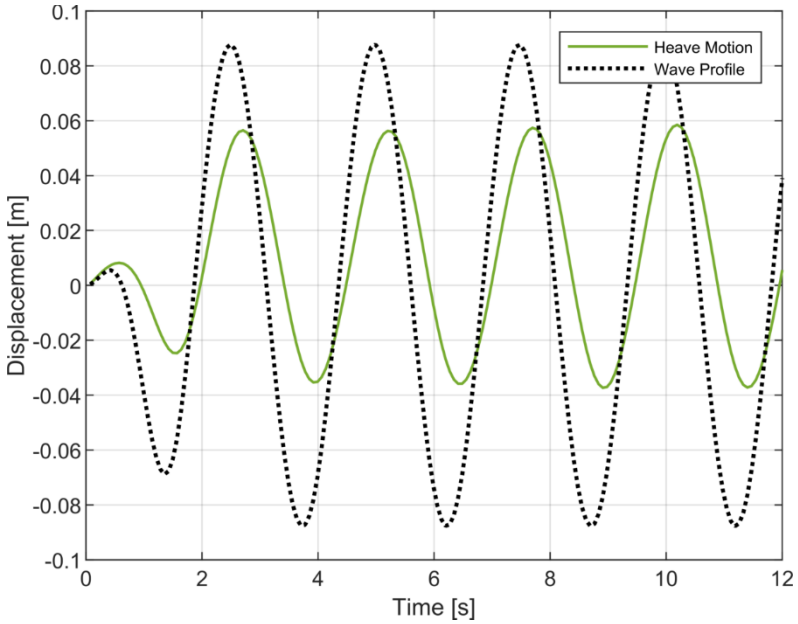

Figure 54. AEGIR Heave Response for 0.088-meter Wave at NDW=2

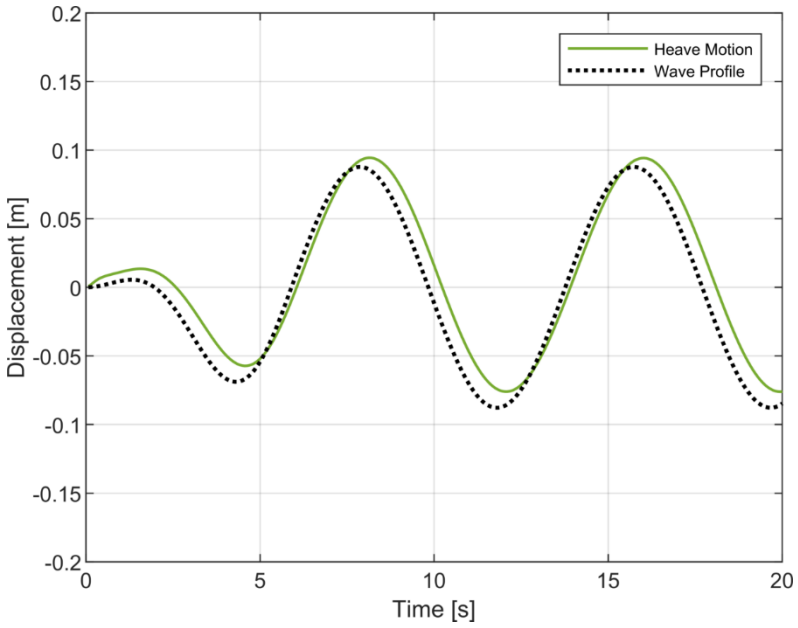

Figure 55. AEGIR Heave Response for 0.088-meter Wave at NDW=20

b. Gazebo Results

The heave response generated by Gazebo is also expected to be representative of the heave force results. Extracting the maximum value of the heave motion from each simulation result yields the heave motion across all wave cases, shown in Figure 56.

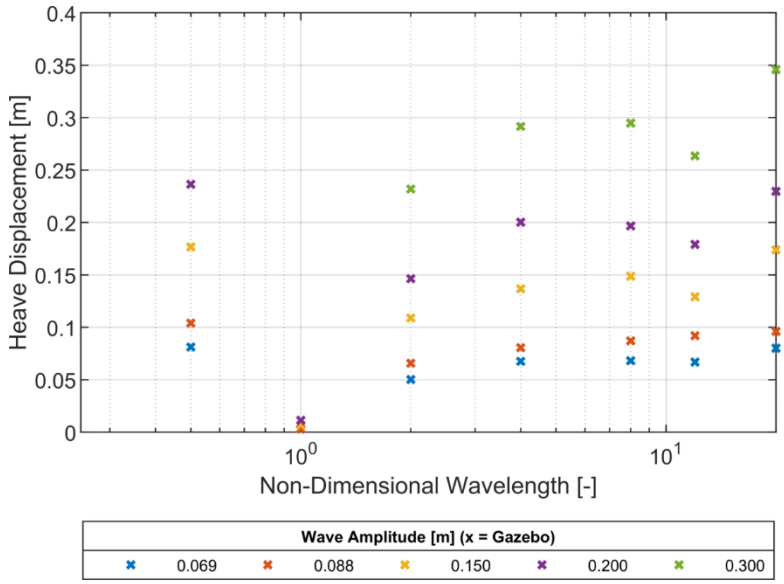

Figure 56. Gazebo Heave Displacement Results in Head Seas

These results highlight and reinforce several concepts observed in the Gazebo forces investigation. First, this reinforces that at increasing wavelengths, the resulting heave motion begins to converge towards the wave amplitude, but in these cases the longest two wavelengths did not exactly continue that trend. The departure of these results is unexplained but was investigated. Second, it was observed that at an NDW of unity, the heave motion, regardless of wave amplitude, all converged to nearly zero. The force study showed that the heave force was zero, hence no motion will result. Finally, when the wavelength is less than the vessel length, Gazebo overestimated the heave force, which here results in larger heave motions than expected. At increased wave amplitudes, while still within acceptable wave steepness limits, the heave motion did not seem to behave as expected. This may be a mathematical artifact of the discretization.

Looking closely at the response phase compared to the incident wave, it can also be observed how Gazebo responds to the varying wave period and its impact on the period of the heave response. Figure 57 depicts the shortest wavelength case.

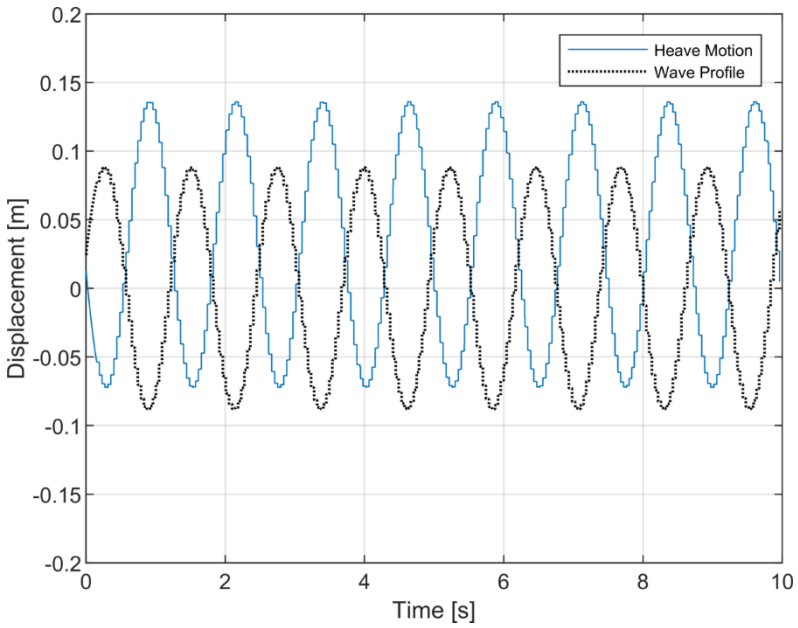

Figure 57. Gazebo Heave Response for 0.088-meter Wave at NDW=0.5

Clearly the peak heave displacement is larger than the wave profile, and the response is 180 degrees out of phase of the wave profile. For the case where the heave response appeared severely damped when the wavelength is equal to the vessel length, the time history reflects a very small, irregular response compared to the wave elevation, shown in Figure 58. As the wavelength increases, it is observed that the heave response becomes in phase with the wave elevation, as shown in Figure 59. It is also noted that in the presentation of this data, both the wave elevation and heave response appear jagged and are made up of a series of steps. This is due to a time rounding issue in the recording of the data from Gazebo and is not indicative of any physical response of the vessel, or does it affect the qualitative analysis of the response.

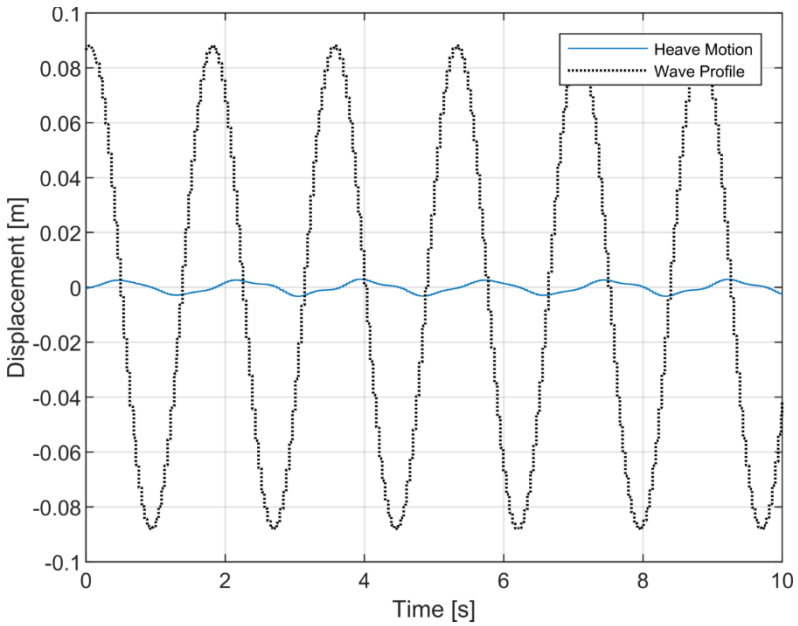

Figure 58. Gazebo Heave Response for 0.088-meter Wave at NDW=2

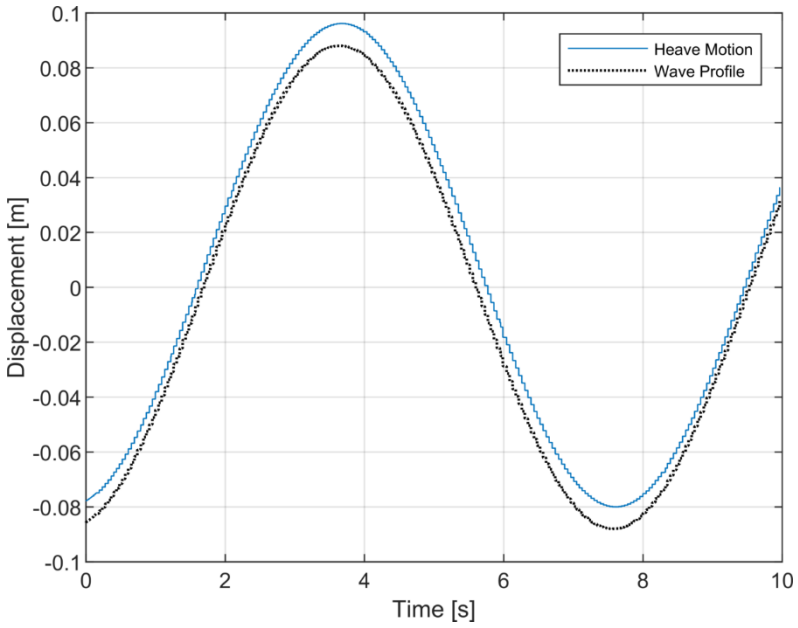

Figure 59. Gazebo Heave Response for 0.088-meter Wave at NDW=20

c. Comparison

Having simulated identical wave conditions in both Gazebo and AEGIR and extracting the same type of information, comparing both methods should highlight some of the same themes and limitations. Figure 60 shows the percentage difference comparison between both methods across all tested wave cases.

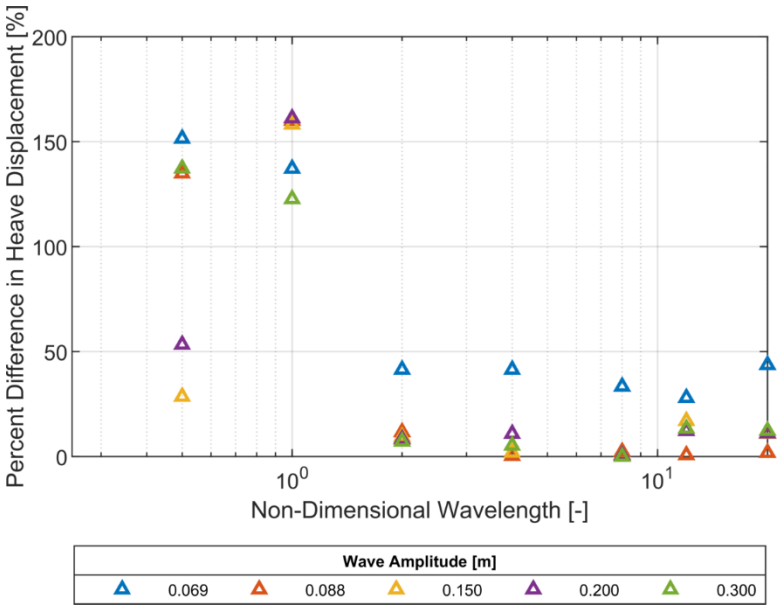

Figure 60. Heave Motion Result Comparison for Head Seas

As expected, the larger differences in heave motion between the two simulations are at the shortest wavelengths. At a wavelength equal to the vessel length, the difference is that largest but is also tightly clustered, caused by the large under-prediction by Gazebo. While the maximum difference between the two methods seems very high, closer examination of the range in which the performance of the heave motion was much closer yields a more promising result. This same data, displayed at a different scale, is shown in Figure 61.

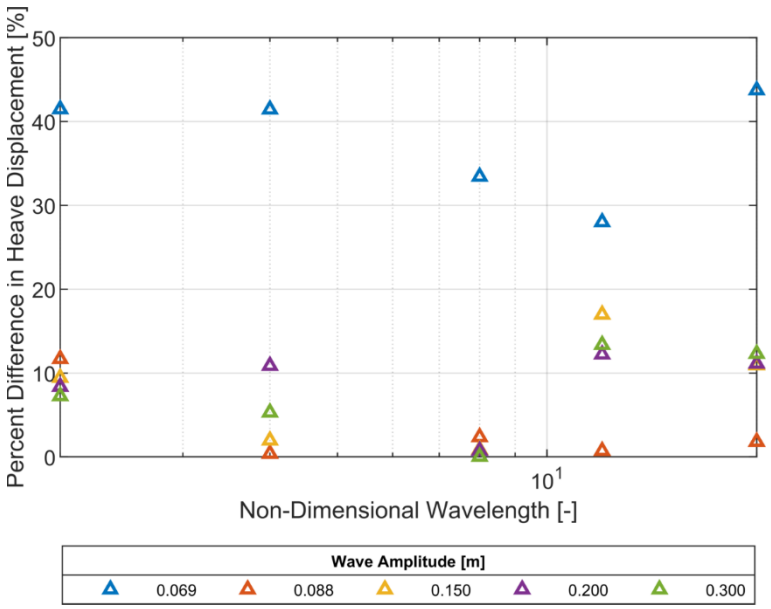

Figure 61. Heave Motion Comparison for Selected Wavelengths in Head Seas

Here, all wave cases exhibit a difference below 50%. Recalling from the heave force comparison, the largest difference in the heave force was calculated at the smallest wave amplitude for this range of wavelengths, which is also evident here. In fact, most of the selected wave amplitudes have a difference that is less than 20%, which out-performs the prediction from the heave force comparison. The difference in motion is not as severe as the difference in forcing. Had the Gazebo results shown the same trend at longer wavelength heave motion converging toward the wave amplitude, the differences indicated would have decreased as well.

2. Pitch

During the same head seas simulations, the pitch data was collected and converted into degrees for easier visualization. Because this is an angular result, comparing against the wave elevation, the wave profile for each plot is not to scale and only serves as a visual cue for the peak and trough of each wave. Because of the opposite sign convention between the Gazebo and AEGIR models for pitch, the absolute values of the pitch angle are directly compared.

a. AEGIR Results

When the simulations are run in AEGIR, the results for pitch are returned directly in time series. Because of the shape of the bow, individual results are not expected to be symmetrical about the static position of the vessel. The overall results across all test cases are show in Figure 62.

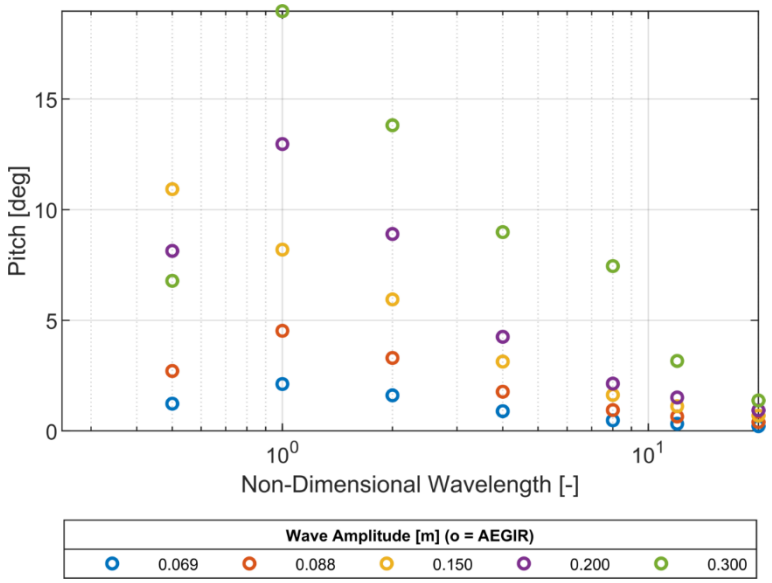

Figure 62. AEGIR Pitch Results in Head Seas

Because of the wave steepness limitations that exist, some of these results would not likely be experienced by the vessel. These results for the most part do reflect the anticipated trends. As the wavelength increases for a given wave amplitude, the resulting maximum pitch that the vessel experiences decrease as the wave steepness decreases. At much shorter wavelengths, the pitch is very large until the wavelength is less than the vessel length, which can then be expected to approach zero as the waves become smaller and affect the vessel less, as seen in the heave motion results for small amplitude waves. By examining the same cases as the heave motion results, the nature of the phasing between the wave profile and the pitch angle can be determined. Figure 63 contains results from a short wavelength, small amplitude case.

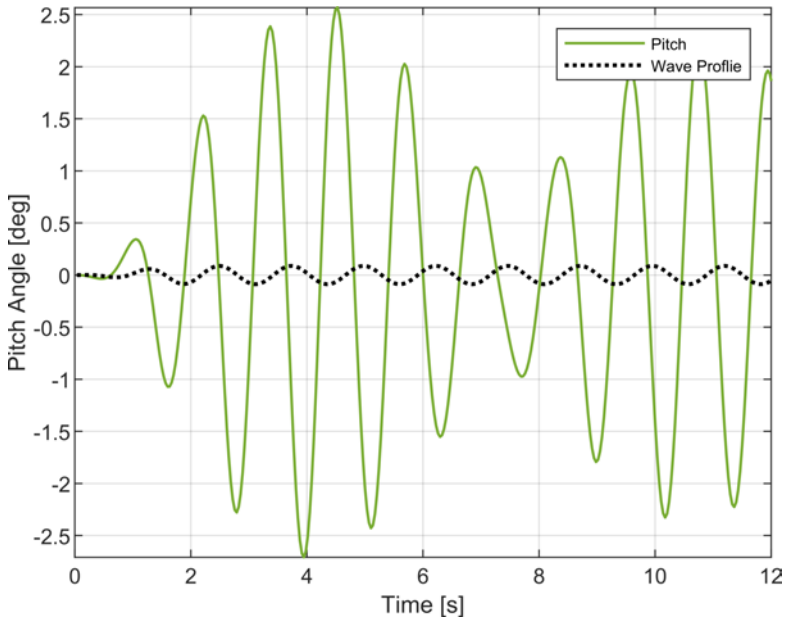

Figure 63. AEGIR Pitch Response for 0.088-meter Wave at NDW=0.5

As seen with the heave results, short wavelengths also have a distinct effect on the behavior of the pitch response. Here it is seen that there are two components to the oscillation. One components response is about the same frequency of the wave, while the other has about a 7 second period. This is a result of the vessel response being out of phase with the incident wave, where the response is slowly amplified over several seconds and then damped. This similar behavior would be expected for most wave cases with short wave periods. The other two cases highlight how this behavior is not present at wavelength longer than the vessel length, as the vessel has time and space to respond to each wave individual and has a regular sinusoidal response. These two cases also show how the wave phasing evolves as the wavelength increases. Longer period waves, regardless of amplitude, generally converge towards a case where the pitch angle is 90 degrees out of phase of the wave elevation, which would put it in phase with the calculated wave slope for each instance in time. These behaviors are seen in Figure 64 and Figure 65.

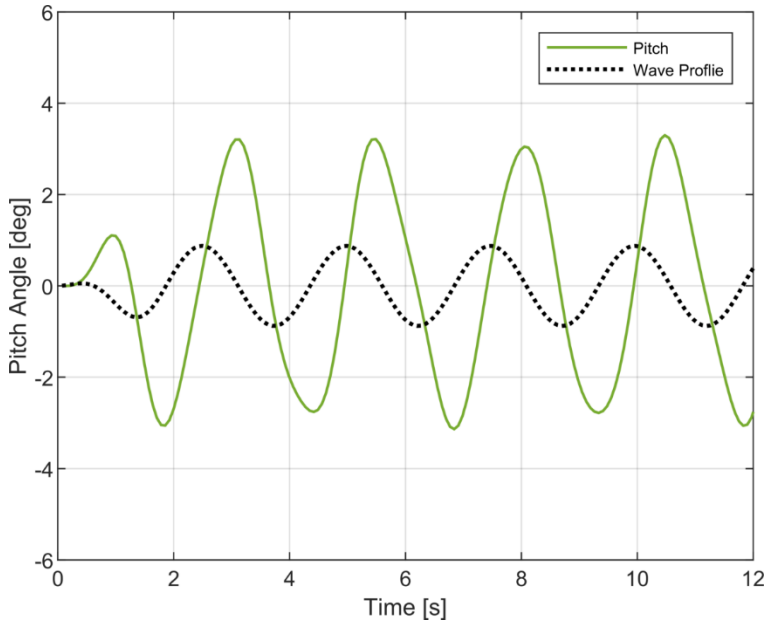

Figure 64. AEGIR Pitch Response for 0.088-meter Wave at NDW=2

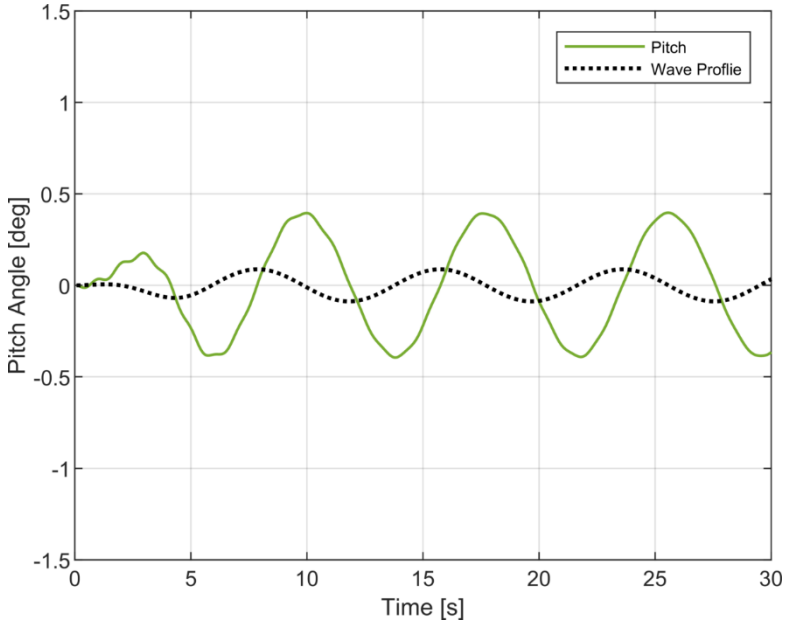

Figure 65. AEGIR Pitch Response for 0.088-meter Wave at NDW=20

b. Gazebo Results

Because of the rough sampling of the wave height along the vessel length and how the pitch is calculated, it is expected that some of the artifacts seen in the heave motion

results will be directly represented in the pitch as well. For all wave cases the maximum absolute value of the pitch is recorded and displayed in Figure 66.

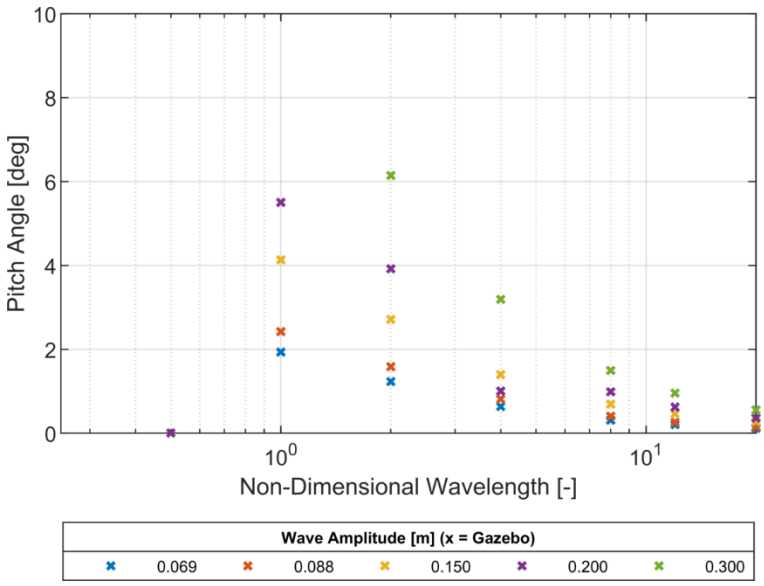

Figure 66. Gazebo Pitch Results in Head Seas

First, because two of the test cases at the shorter wavelengths for the 0.3-meter wave exceeded the steepness limitations, the results were very erratic and extremely large. Those two values were thus removed. Second, there appears to be no pitch in the case where the wavelength is less than the vessel length, which stems from the calculation of almost no force at the discretization points and thus no moment and no pitch angle. The rest of the results follow the expected relationship between the wave steepness and the pitch and converge towards the wave steepness at very long wavelengths. Checking the relationship between increased wavelength and the phasing between the wave profile and the pitch, it is evident that across all wave amplitudes the pitch motion approaches 90 degrees out of phase of the wave elevation, which would put the pitch in phase with the wave steepness. This result is evident in the comparison between Figure 67 and Figure 68.

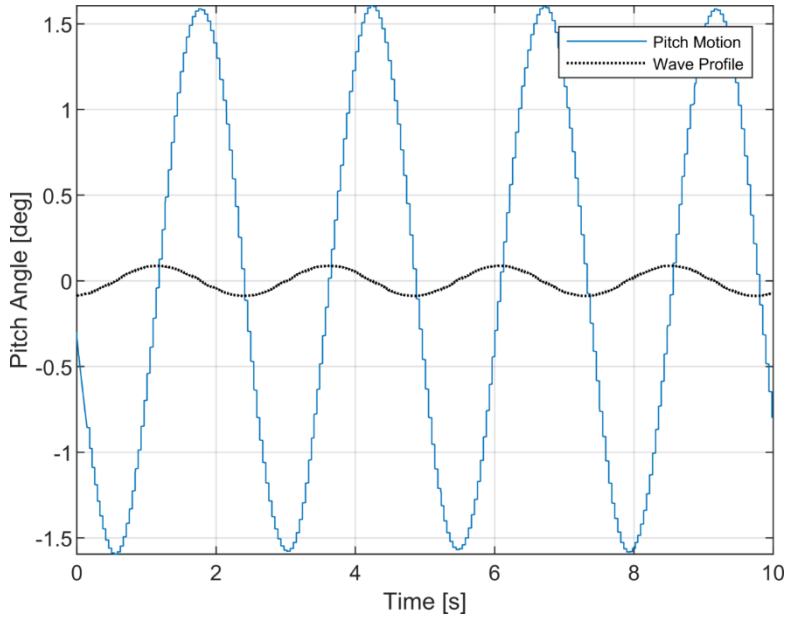

Figure 67. Gazebo Pitch Response for 0.088-meter Wave at NDW=2

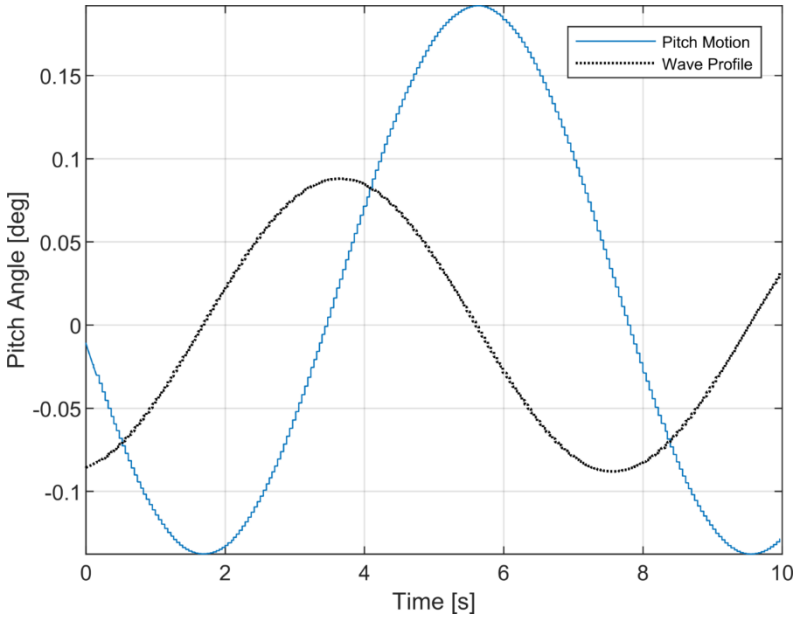

Figure 68. Gazebo Pitch Response for 0.088-meter Wave at NDW=20

c. Comparison

By extracting the absolute value of the pitch response amplitude from each wave case simulation, the difference in the sign convention between the two models is negated,

and the results can be directly compared. Figure 69 contains the difference between the two simulation methods across all wave cases.

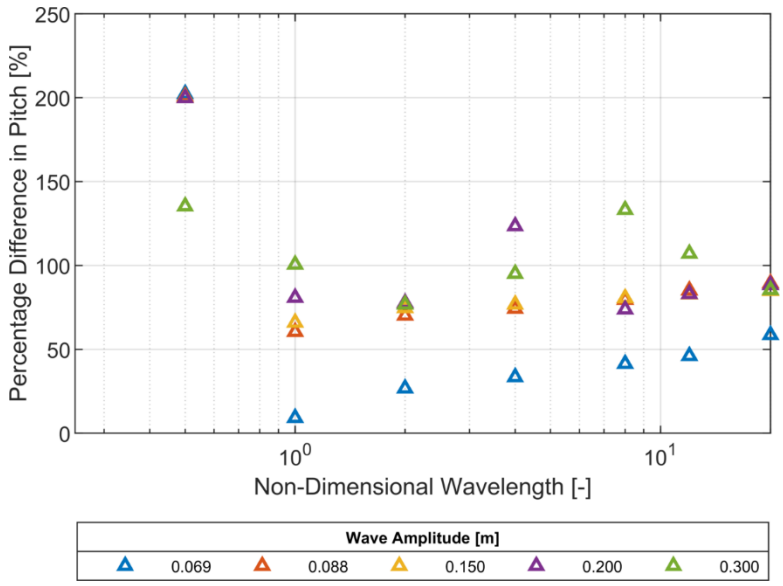

Figure 69. Pitch Motion Comparison for Head Seas

Again, due to the under-calculation made by Gazebo at short wavelengths, the difference is very large. At small wave amplitudes, as the wavelength increases, so does the difference. However, although these differences appear very large, in general these are differences between very small angular displacements.

D. BEAM SEAS TESTING

Each of the wave cases is implemented with the seas approaching from the starboard beam of the vessel. The vessel is set to zero forward speed and is only free to move in heave and roll.

1. Heave

The heave motion is collected for each wave case. Because the seas are now approaching from the beam, the individual heave motions from each pontoon will be out of phase with each other but should be equivalent. For each time step, the average heave

motion between the two pontoons is calculated, as the point of interest is the point between the two pontoons.

a. AEGIR Results

The AEGIR results for heave are comparable to the heave motion from the head seas testing. They won't match up exactly, as none of the waves are short enough to be equal to the beam of the vessel. Figure 70 shows the heave results for all wave cases.

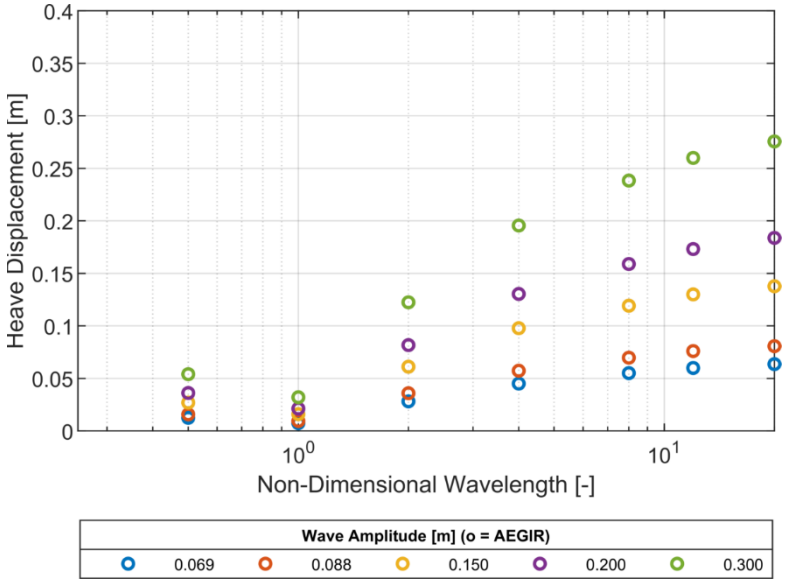

Figure 70. AEGIR Heave Results in Beam Seas

The results continue to reflect the expected behavior of each wave case. As an example, one of the time histories clearly shows the phase relationship between the incident wave and the heave motion, which again appears as nearly in phase for longer wavelengths, as expected. This result is shown for one wave case in Figure 71.

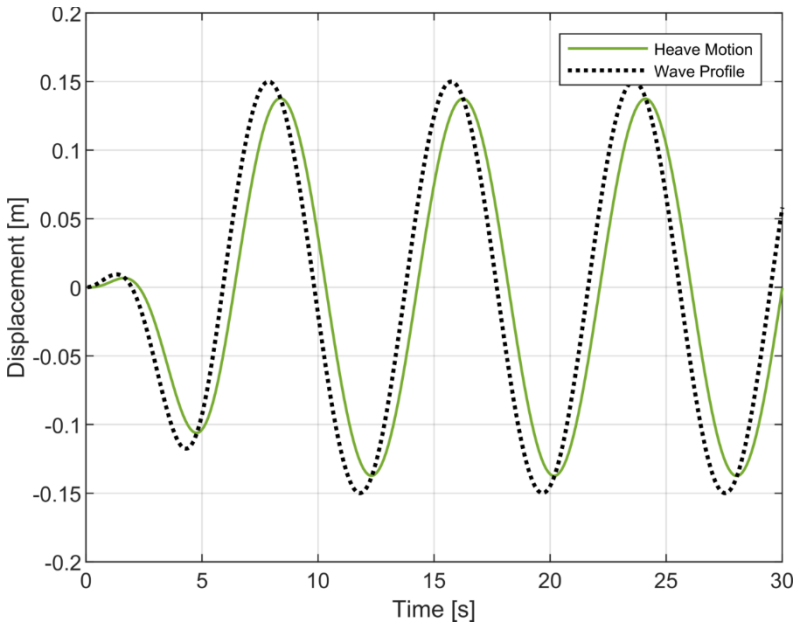

Figure 71. AEGIR Heave Response for 0.088-meter Beam Wave

b. Gazebo Results

The Gazebo heave results also continue to represent many of the common traits found across different simulations. Figure 72 shows the results from each wave case.

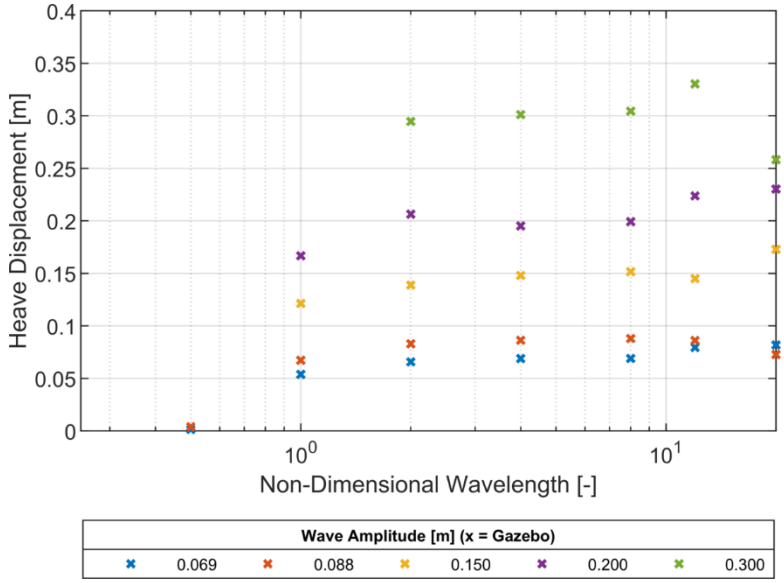

Figure 72. Gazebo Heave Results for Beam Seas

The beam seas results also highlight that at a specific NDW, which in this case is where the wavelength is equal to the distance between the two discretization points of the Gazebo model. This case is where zero heave motion is calculated, as shown. Also represented is the differing behavior from expected when at very long wavelengths. Looking at one specific case to check the phase characteristics yields the same expectation from the head seas testing where the heave motion is nearly in phase with the wave elevation for long period waves. This case is shown in Figure 73.

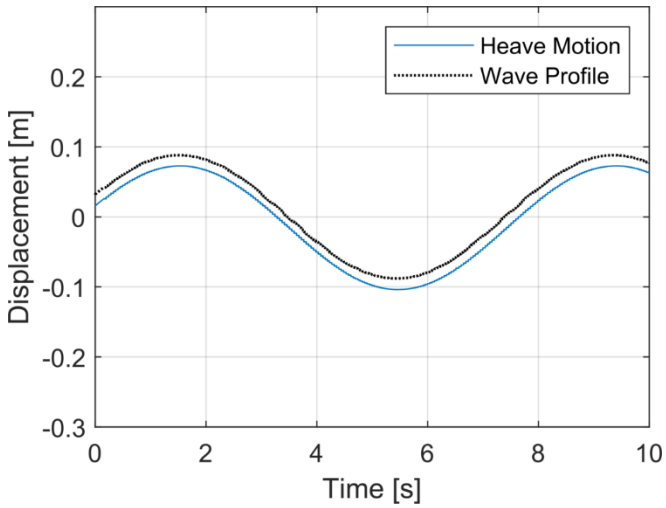

Figure 73. Gazebo Heave Response for 0.088-meter Beam Wave

c. Comparison

The comparison of results between Gazebo and AEGIR should also be representative of the heads seas testing comparison, but again will not be the same for each NDW because of the difference in direction. Figure 74 shows the comparison of results from the beam seas testing. This shows a steady decrease in the difference as the wavelength increases. Here it can be seen that the results do not match up with the head seas results, and that the difference is generally much larger, but for NDW of greater than four, the percent difference appears to be like the head seas results at about 25%.

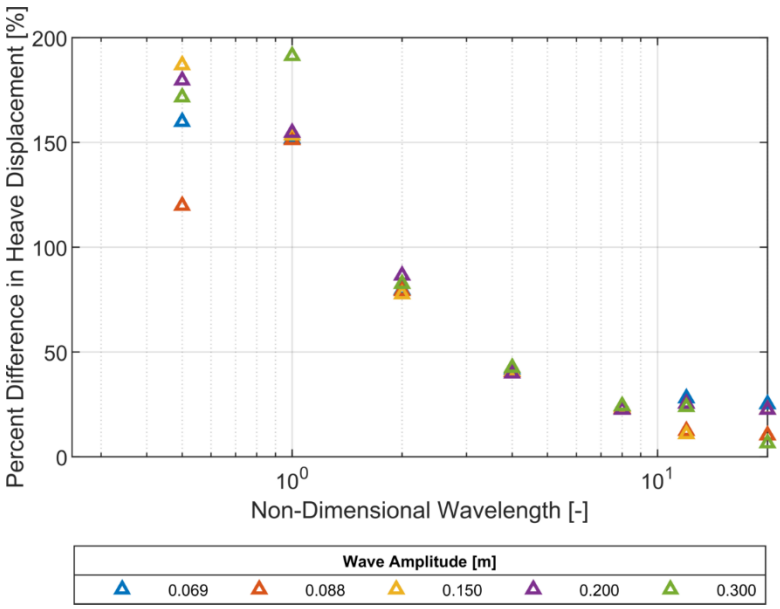

Figure 74. Heave Motion Comparison for Beam Seas

2. Roll

The greatest point to completing the beam seas testing is to observe how each simulation performs in calculating the roll of the vessel. Roll for a catamaran hull is slightly more difficult to model and calculate as the two hulls must be modeled as rigidly connected and the roll motion is therefore coupled.

a. AEGIR Results

As with the pitch results, the absolute value of the roll angle is taken into consideration for comparison. The AEGIR results for roll are contained in Figure 75. These results mirror the relationship seen in the head seas test between the wave steepness and the angular displacement, which in this case is roll. Each of the wave amplitudes experience a decrease in roll as the wavelength increases. Another fact that this highlighted is that for every wave case tested, the result showed very small amounts of roll were experienced by the vessel. This is attributed to the catamaran design, highlighting the significant platform stability.

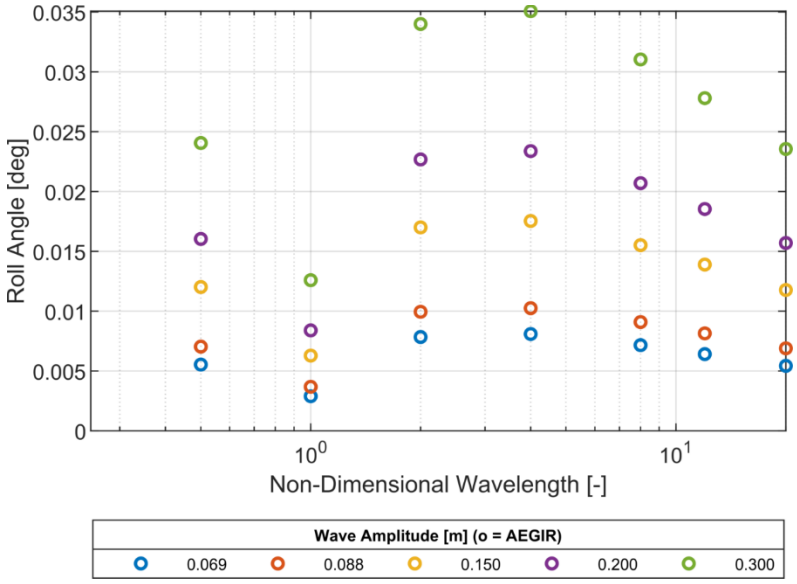

Figure 75. AEGIR Roll Results for Beam Seas

b. Gazebo Results

Gazebo exhibits the same type of response that was present in the pitch results. The same relationship between the wave steepness and the angular displacement is present as the wave period increases. One simulation had an outlier that was not found to have a stable solution with the current configuration, which is still displayed as the smallest NDW at the 0.15-meter wave. Figure 76 shows the results across all waves cases.

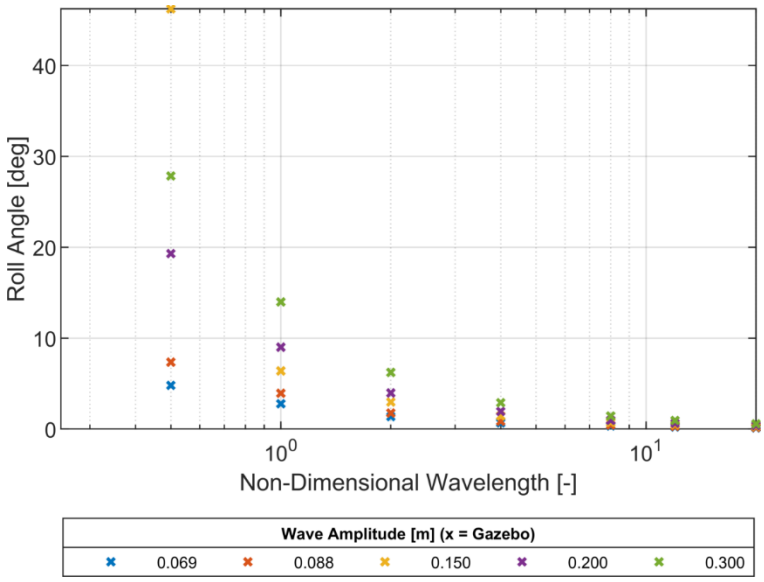

Figure 76. Gazebo Roll Results for Beam Seas

c. Comparison

The significant difference in the roll angles between the two simulations, at several orders of magnitude, is thus far the least accurate modeling of any of the DOF. Because Gazebo is using such rough approximations for the calculated forces, the resulting rotational motions seem to be exaggerated. Figure 77 shows the resulting percentage difference between the two simulation methods for roll. While the data does show the expected trend towards a lower percentage difference at the long wavelengths, all values fall with 180-200% difference between AEGIR and Gazebo. Wave amplitude seems to have no effect on the difference, though this may be because the values are so different that the change is not appreciated at this scale. Regardless, roll motion will likely produce a large amount of simulation inaccuracy in any case that it not purely head seas.

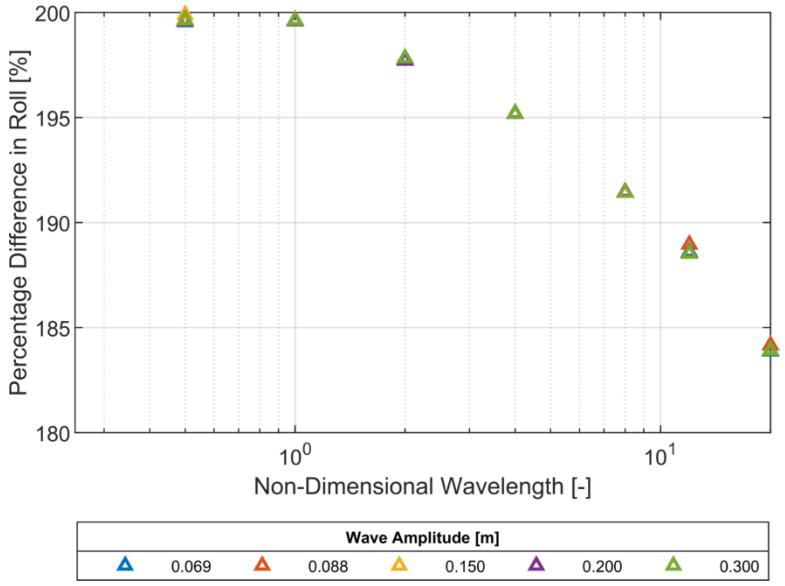

Figure 77. Roll Motion Comparison in Beam Seas

E. OBLIQUE SEAS TESTING

Each of the wave cases is implemented with the seas approaching from the forward starboard quarter. The vessel is set to zero forward speed and is free to move in heave, pitch, and roll. This will highlight the coupling between each of the free DOF in the simulation and see how each simulation handles motion in two planes simultaneously.

1. AEGIR Results

Each oblique sea wave case was run through AEGIR and the pitch, roll, and heave data is collected. Because the two pontoons are encountering each wave at a different time, each of the collected DOF is averaged between the centers of gravity. These results are not expected to match exactly to either the head seas of beam seas testing, as the encounter frequency in each direction is different than the actual wave period because of the oblique nature of the waves. Figure 78 contains the heave results for all wave cases, Figure 79 contains the pitch results, and Figure 80 contains the roll results.

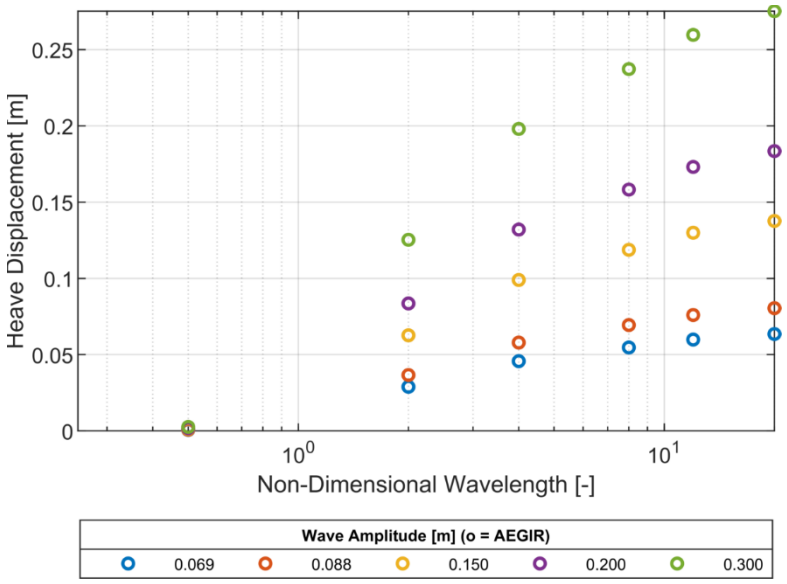

Figure 78. AEGIR Heave Results for Oblique Seas

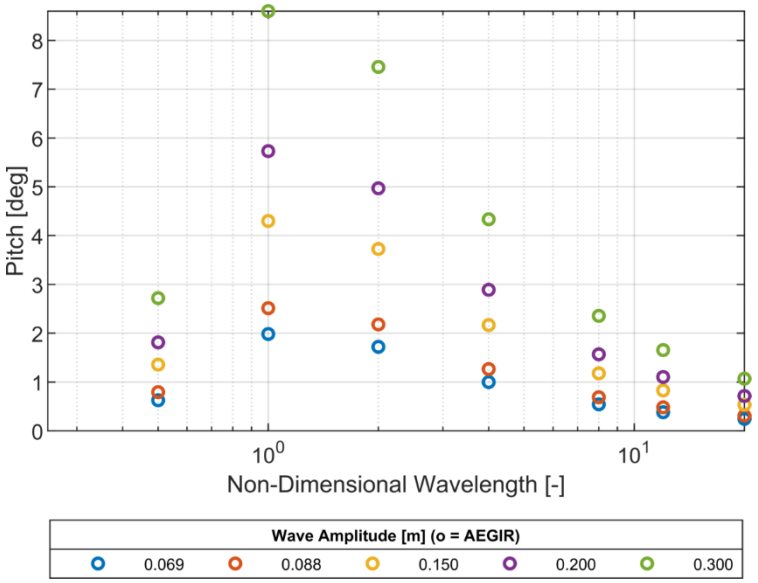

Figure 79. AEGIR Pitch Results for Oblique Seas

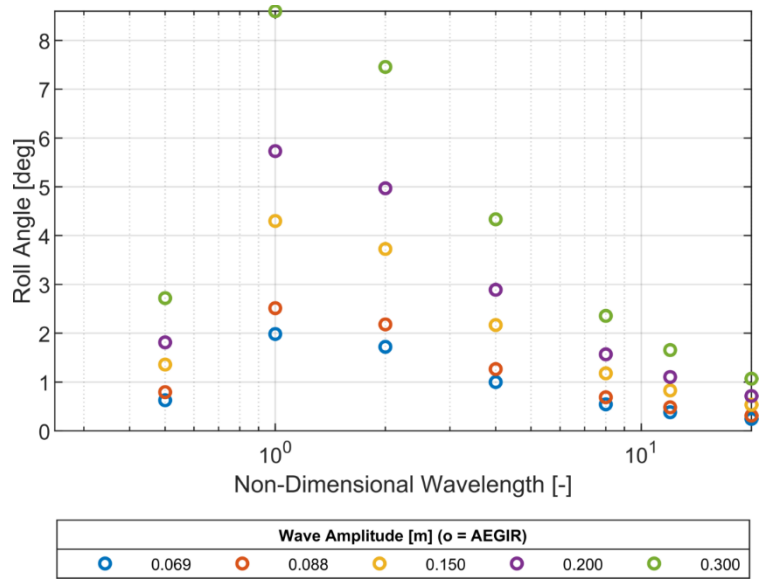

Figure 80. AEGIR Roll Results for Oblique Seas

2. Gazebo Results

The oblique sea wave cases are also run through Gazebo. Figure 81 contains the heave results, Figure 82 contains the pitch results, and Figure 83 contains the roll results.

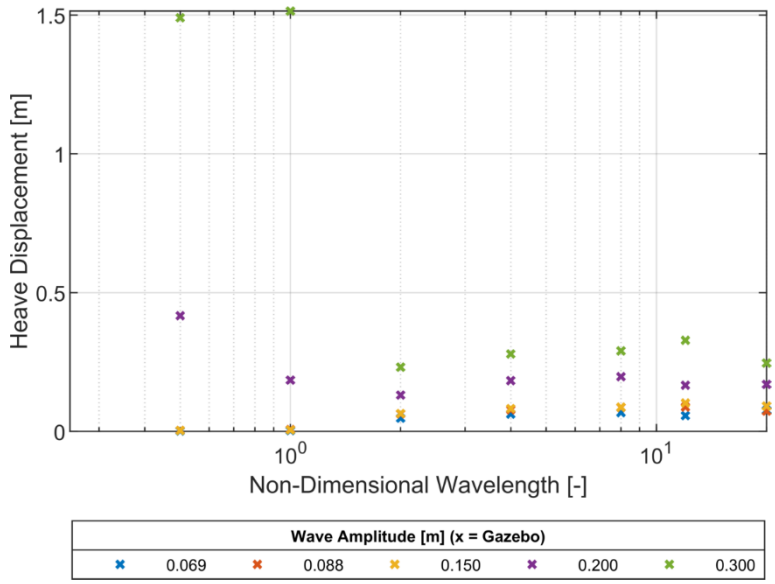

Figure 81. Gazebo Heave Results for Oblique Seas

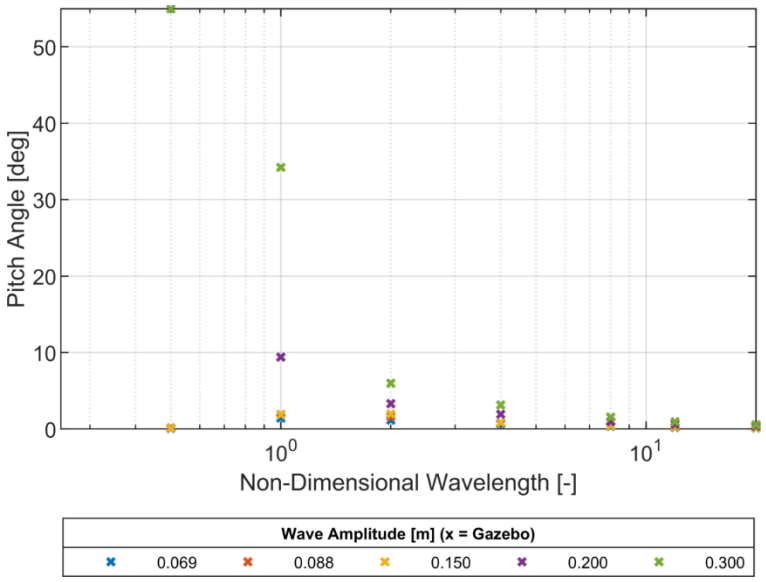

Figure 82. Gazebo Pitch Results for Oblique Seas

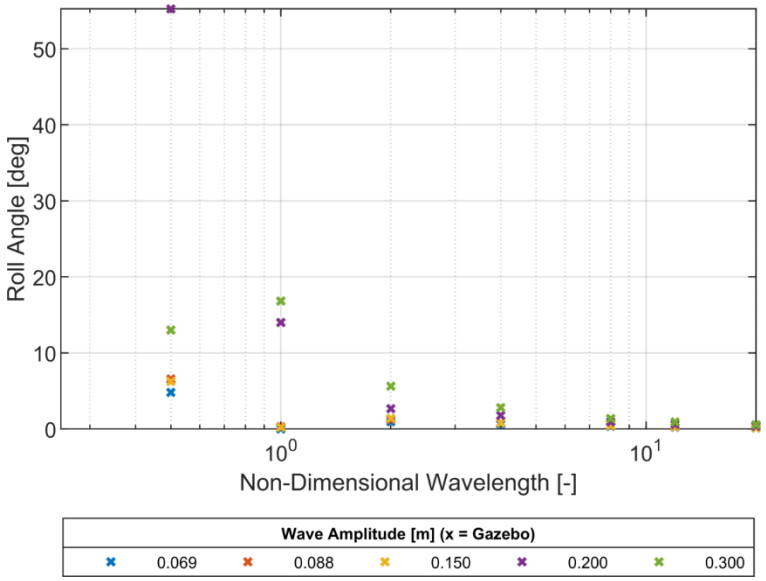

Figure 83. Gazebo Roll Results for Oblique Seas

3. Comparison

The focus of this test was to see if the differences in the two methods were exaggerated when an additional DOF was added to the simulation. Ideally, the differences would remain the same regardless of the number of DOF being computed or the direction

of the waves. The percentage difference of in each DOF is calculated and notionally compared to the previous two studies in head seas and beam seas. Figure 84 contains the heave results, Figure 85 contains the pitch results, and Figure 86 contains the roll results.

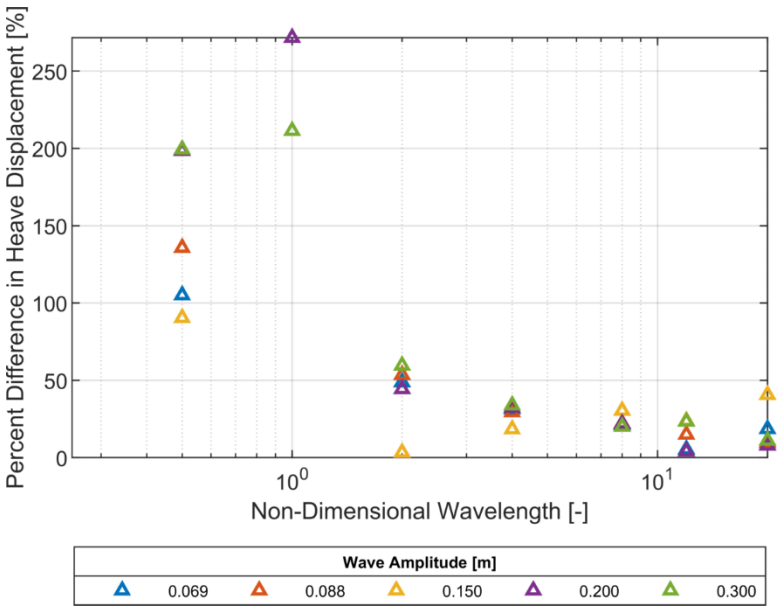

Figure 84. Heave Results Comparison for Oblique Seas

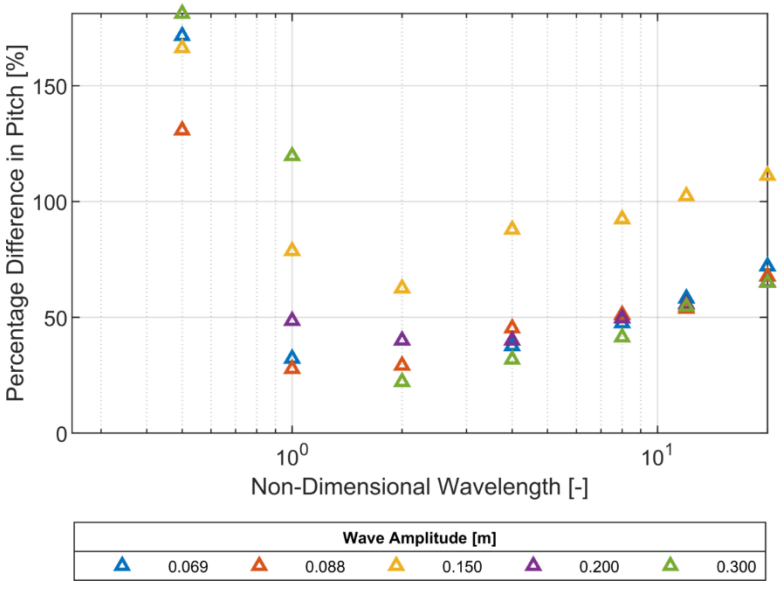

Figure 85. Pitch Results Comparison for Oblique Seas

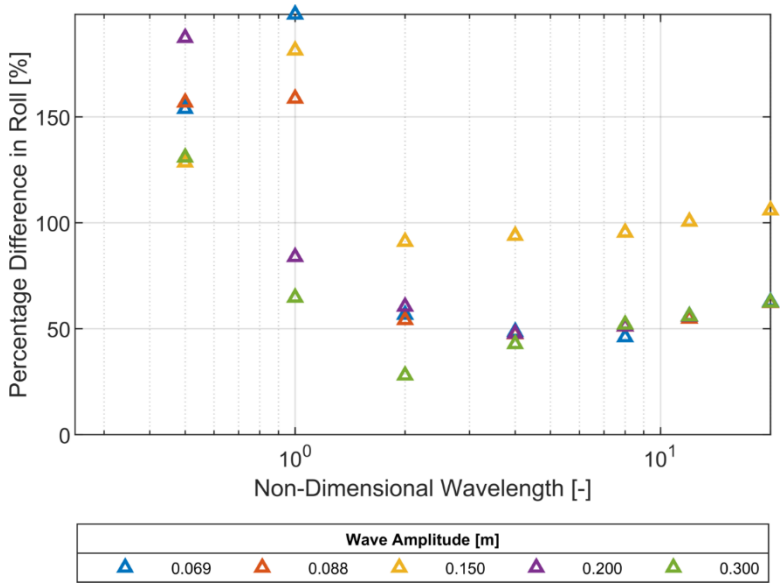

Figure 86. Roll Results Comparison for Oblique Seas

From these results it is evident that none of the DOF suffered large differences due to the addition of the third DOF, or the different incident angle. The Gazebo simulations still do not perform well for short wavelengths.

F. CONCLUSIONS

Conducting motion testing in two isolated planes and then in one couple scheme has highlighted previously observed trends as well as introduced new ones. Each simulation has yielded performance results in both the motion calculation and computational time realms.

1. Motion Performance

The overall performance of each Gazebo simulation against the AEGIR simulation is relatively acceptable. It is important to highlight is that while the force and moments were quite different, the resultant motions were very similar in many cases. While large percentage difference results seem very high, many of the differences observed are between very small motions, and thus even small differences can seem largely exaggerated when compared, while still staying with a comparable order of magnitude. Most importantly, each wave case produced predictable and repeatable motion simulations, that were

representative of the forces and moments simulations. The relative performance between AEGIR and Gazebo across several different wave categories is summarized in Table 9.

Table 9. Average Percent Difference for Head and Beam Sea Motion

	$\lambda < L$	$\lambda = L$	$\lambda = 2L$	$\lambda >> L$
Heave	100%	150%	15%	15%
Pitch	170%	80%	70%	70%
Roll	200%	200%	197%	185%

Bad	Poor	Good	Great

While much of this does not fall within a good or better relative rating, when the same ratings are applied to the oblique wave case, some improvement can be seen. The comparisons for the oblique case are summarized in Table 10.

Table 10. Average Percent Difference for Oblique Wave Motion

	$\lambda < L$	$\lambda = L$	$\lambda = 2L$	$\lambda >> L$
Heave	140%	250%	50%	25%
Pitch	170%	70%	50%	60%
Roll	150%	140%	60%	60%

Bad	Poor	Good	Great

2. Temporal Performance

Each time a simulation was run in Gazebo or AEGIR, the simulation duration and total computational runtime was noted. Gazebo conveniently produces a number that is called the Real-Time Factor (RTF), which displays the percentage of real time that the simulation is running at. Regardless of simulation duration or wave case, the simulation always ran at an RTF of 98 percent. This RTF was produced when the program was run headless, where all processes are running but no GUI is used, and data is simply recorded for analysis or playback. This method significantly reduced the required computational resources as each vessel motion does not need to be animated and displayed on the screen.

Because running Gazebo simulations with the GUI is very graphics intensive, it generally produced an RTF of 46%. To note, if running headless or with very high-performance graphics cards, Gazebo can run faster than real time.

When AEGIR is setup to run, it provides a recommended time step and simulation duration that is primarily based on the domain size and the wave characteristics. For every simulation that was run for motion cases, this recommendation was always taken. Thus, there is not a direct relationship between the simulation duration and the computation time, as the time step is variable. However, this does provide an idea of the required computational resources required and the relative difference between AEGIR and Gazebo, which uses a fixed time step for computation. Figure 87 contains representations of the time requirements for different simulations.

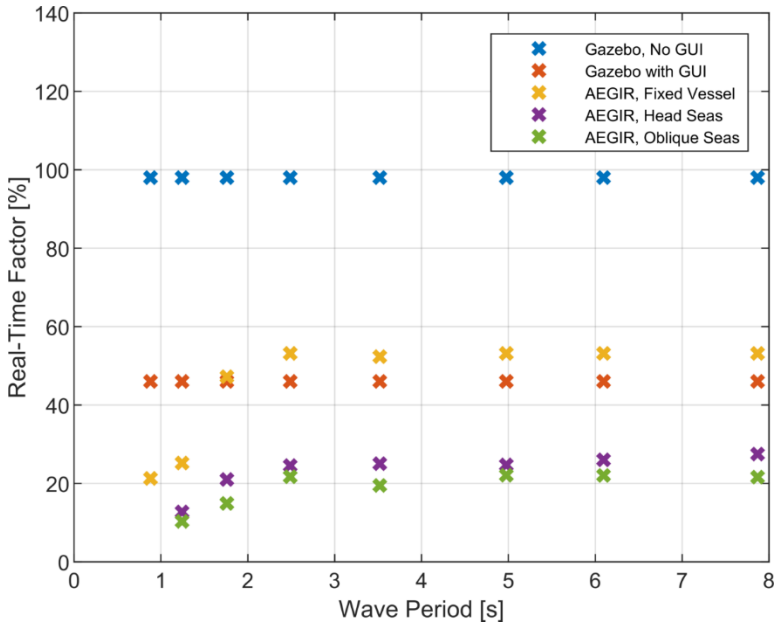

Figure 87. Real-Time Factor of Various Simulation Conditions

These performance parameters were based on two completely difference computers. AEGIR was run on a high-performance, overclocked desktop machine, specifically assembled to run graphics-intensive operations. Gazebo was run on an average performance laptop computer with no separate graphics card.

THIS PAGE INTENTIONALLY LEFT BLANK

VI. CONCLUSIONS

Based on the aggregated data, quantitative analysis and qualitative observations, this research has met a series of conclusions. This final section will focus on identifying the capabilities and limitations of this study, its results, and the impact on autonomy development, while also providing suggestions for the use and improvement of the Gazebo environment.

A. APPLICATION OF SIMULATION METHODS

1. Acceptable Wave Parameters

One of the most important conclusions gleaned from this study is the clear limitation on wave parameters than can be implemented in the Gazebo simulation. For this hull form, the limits were identified and tested for acceptable combinations of wave period and wave amplitude. Short period waves had a clear impact on the way Gazebo performed and provided the largest deviation from AEGIR.

Wave steepness was a concern, especially when the vessel was freed in several degrees of freedom. If waves were too steep, the vessel motions became more of impulsive responses, and exceeded reasonable reactions, such as heaving above the wave height, or rolling past the steepness of the waves. Wave steepness for implemented wave cases should be no greater than 1/7 and would not be interesting and produce meaningful results for steepness less than 1/300.

Finally, the vessel geometry will potentially constrain the acceptable wave parameters, though waves that were taller than the freeboard were not tested in full motion cases. Figure 88 shows the recommended limitations on wave parameters for use with the WAM-V.

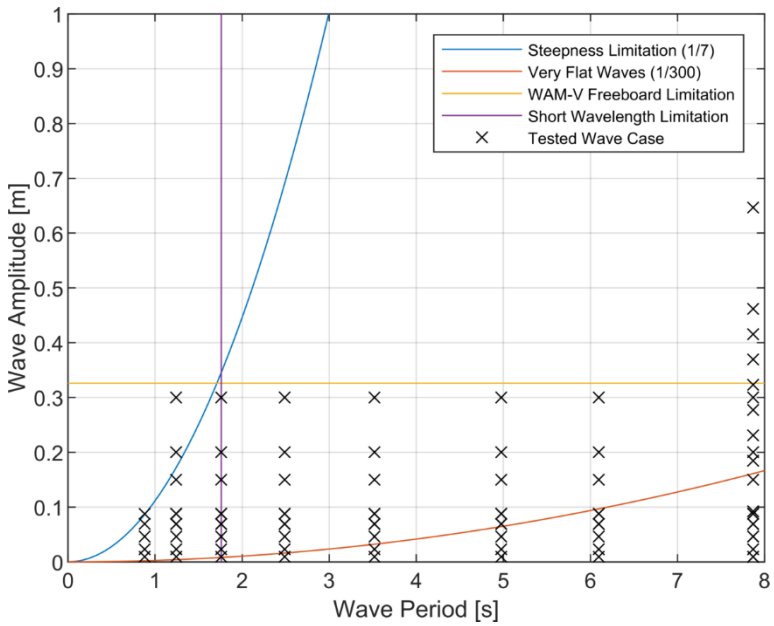

Figure 88. Wave Parameter Limitations and Recommendations

These limitations would naturally be a concern when trying to simulate a full spectrum of ocean waves, which are represented by a sum of monochromatic wave components. With a distinct band of wavelengths that aren't well handled in Gazebo, this has the potential of eliminating a large amount of energy from a desired wave spectrum if that band of wavelengths had to be avoided. However, even with these limitations, for a fully developed, single peak wave spectra that generally represents the deep ocean, the loss of the short period wave band would not hamper the ability to full simulate wave spectra up to Sea State 4. As seen in Figure 89, the lower limit to the wave period cuts off a portion of the spectra in which there is very little energy, and as seen, Gazebo has little problem simulating very long ocean waves. Thus, even with the short period limitation, fully developed seas can be simulated with the appropriate combination of component waves.

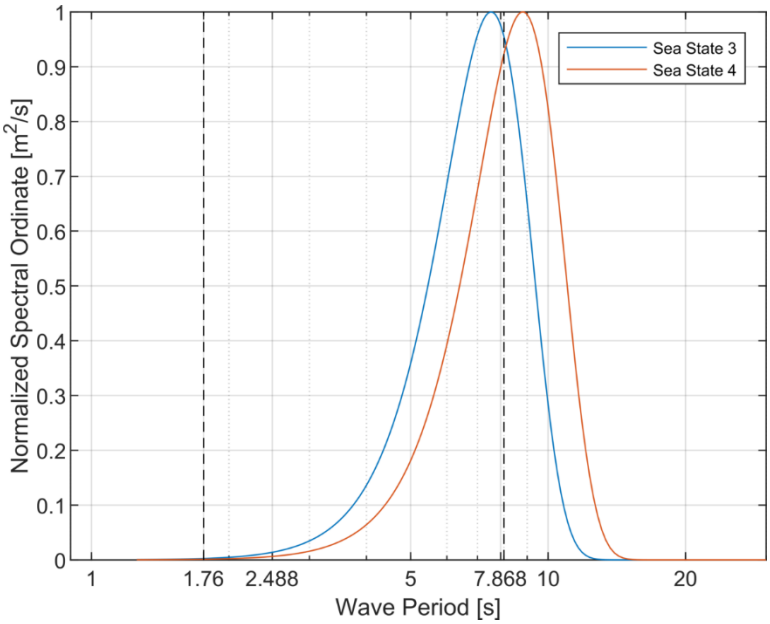

Figure 89. Wave Period Limitation Effects on Sea Spectrum Bandwidth

2. Fidelity

Overall, the trade-off between fidelity and the accuracy of result was not a large sacrifice. Gazebo was able to produce consistent results, albeit with limitations, that were close in performance to AEGIR. Some of the more complex forces and phenomenon, such as the viscous forces, wave forces, and forces from radiation and diffraction that AEGIR takes into account did not seem to have extremely large effects on the overall motions of the WAM-V for the wave regimes considered here, as the motions seemed to be driven primarily by the static buoyancy model of determining the forces. For the wave cases testing in the fixed DOF cases, the contribution of these more complex forces was between 8% and 15% of the overall forces imparted on the vessel by the waves. Gazebo is certainly applicable for many parts of the development of a vessel, mostly concerning control and autonomy, but does not have enough modeling fidelity for the design of hulls from a naval architecture standpoint. Deep studies into the more complex wave dynamics and interactions with the hull would be best suited for AEGIR.

3. Real-Time Performance

The value of being able to perform a simulation of this complexity in near real time cannot be understated. While there are many applications where the higher-fidelity mathematical answer is desired; however, in the development of autonomy, having a simulation system that can accept environmental disturbances, simulate motions, and then implement control in real time is of far greater value. The value in being able to physically see a simulation during runtime is also valuable to the developer, as often qualitative measures for the performance of autonomous systems can influence important development decisions and provide a logical guide towards making quantitative assessments. The steady performance of the Gazebo simulation across a wide range of simulation conditions suggests that a significant amount more of complexity can be added to the system without hampering the real-time performance.

B. FUTURE WORK

1. Potential Gazebo Improvements

The strongest limitation on the use of the Gazebo simulation environment for this application is the short wavelength performance. This performance is due to the small number of points at which the wave height is measured and thus the forces are calculated and applied. The number of sections that the hull should be discretized into, and the number of points where forces are applied in the Gazebo model should be largely increased. The increase isn't arbitrary – there should be enough points along the hull in length and beam so that the highest frequency wave can still be captured. The number of discretization points should be large enough to be able to capture several points along each wave crest and trough, for every wave that is incident along the hull. This number is also influenced by the shortest wavelength expected for the wave. For the wave cases that were tested, the smallest wave period was 0.88 seconds, which corresponds to a 1.21-meter wave. This means there are four total waves along the length of the hull. If there needs to be four points per wave to describe two zero-crossings, a peak, and a trough, the minimum number of points that the length of the hull should have is 16. The same principle could be applied to the beam, but the number of points should be beam-wise along each demi-hull.

Another low complexity improvement to the Gazebo model would be to change the shape of the hull to a cylindrical shape instead of the simple rectangular prism. From the geometric verification it was clearly seen that the cylindrical approximation performed significantly closer to the AEGIR results than a rectangular prism approximation. This would likely eliminate a lot of the percentage difference between the two methods.

2. Further Studies

This study was developed with its own goals in mind, but also set up to be easily expanded. A very limited number of wave cases were used across each section of the study, which could always be expanded. There are sections of the test matrix that could stand to be investigated further. While there were a few cases where wave periods beyond the original set were testing to investigate phenomenon happening at the intermediate periods, this was not done exhaustively. This is especially important to do at the short wave periods, as not every aspect of the vessel interaction with waves at anything but even number NDWs is understood. If any modifications to the Gazebo plugin were to be made, this entire study, or some sections, could be reproduced to investigate the impact on the Gazebo performance and to see if there was any change in the difference between Gazebo and AEGIR.

A next area of study not addressed in this research is the use of irregular waves in both simulations. Work would need to be done to ensure a statistically determined wave field would be implemented the same way in both simulations, and all results would be focused on statistics of the responses. Effort could be made to develop another plugin that could generate a probabilistic wave field, without the user having to manually type a series of component waves or understand completely how to select those waves. Also, not testing but another large area of study is the testing of omni-directional waves, where this study only focused on regular waves travelling in one direction.

Another next area of study could be the implementation of controlling algorithms within this environment that would control motions in a plane other than the surge-sway-yaw plane. This could include pitch or roll stability control, vision-based wave navigation in waves, or station-keeping in a complex, moving seaway. There are also studies that could be conducted involving the investigation of motion of typical sensor performance, and how

the changes in the motion impact sensor performance, and whether a difference of 35% in the motion drastically impacts the sensor performance, driving the need for a better simulation model.

C. FINAL REMARKS

This study has made every attempt to unify two realms of engineering in the development of an autonomous surface vessel – that of Naval Architecture and Seakeeping, and that of Controls and Autonomy. One of the major goals at the outset of this work was to garner a deeper understanding of a complex simulation environment that has had decades of combined effort into its development and use that understanding to try and make just a small part of a larger, open-source simulation world better. If even a small part of this study is used, expanded upon, reproduced, or cited in the continued development of open source tools for the greater robotics community, the goal has been met. Both simulations are powerful, and both are necessary for a truly holistic development cycle.

APPENDIX. DATA REPOSITORY

This appendix contains general organization and explanation of all the data, code, and resources available for further study. All material is located at the following URL: https://nps.box.com/s/k9kayvr2fwrreu9vazhby1x77vhjwher

The chart below shows each of the test sets that were run, most of which are name matched in the individual folders.

Case ID	# of Amplitudes	# of Periods	Direction	Fixed Modes						Test Mode	Notes
				x	y	z	θ	φ	ψ		
Test 1	1	1	180							Motion	Single Hull
Test 2	1	1	180							Motion	Both Hulls
Test 3	5	4	180							Motion	Initial Testing
Test 4	3	3	180	x	x	x	x	x	x	Force	Initial Testing
Test 5	3	3	180	x	x	x	x	x	x	Force	Detail Testing
Test 6	8	1	180	x	x	x	x	x	x	Force	Initial Fixed Amp
Test 7	4	8	180	x	x	x	x	x	x	Force	Fixed Steepness
Test 8	1	5	180	x	x	x	x	x	x	Force	Initial long wave test
Test 8B	11	1	180	x	x	x	x	x	x	Force	Detailed long wave test
Test 8C	11	1	90	x	x	x	x	x	x	Force	Detailed long wave test
Test 9	6	8	180	x	x	x	x	x	x	Force	Detailed force test
Test 10	12	8	180	x	x	x	x	x	x	Force	Detailed force test
Test 11	5	8	180	x	x	x	x	x	x	Force	Final Head Seas Test
Test 11B	1	25	90	x	x	x	x	x	x	Force	Detail for short periods
Test 11C	5	8	180	x	x	x	x	x	x	Force	Final Beam Seas Test
Test 11D	1	25	90	x	x	x	x	x	x	Force	Detail for short periods
Test 12A	3	7	180	x	x		x		x	Motion	Initial Head Seas
Test 12B	3	7	180	x	x		x		x	Motion	Final Head Seas
Test 12C	3	7	90	x	x			x	x	Motion	Initial Beam Seas
Test 12D	3	7	90	x	x			x	x	Motion	Final Beam Seas
Test 12E	5	7	135	x	x				x	Motion	Oblique Seas

Gazebo folders contain MATLAB data files that can be imported and directly used in their structure format. AEGIR folders contain the namelists, solutions and geometries used in each test. These namelists and solutions can be reloaded via NavaSim. The MATLAB folder is also organized by each test set. The Functions folder must be set to the MATLAB path for any code to run.

THIS PAGE INTENTIONALLY LEFT BLANK

LIST OF REFERENCES

[1] Mattis, James. Summary of the 2018 National Defense Strategy. Department of Defense, Washington, D.C. (2018).

[2] Pandey, Jyotsna and Hasegawa, Kazuhiko. "Study on Manoeuverability and Control of an Autonomous Wave Adaptive Modular Vessel (WAM-V) for Ocean Observation," 2015 *International Association of Institutes of Navigation World Congress (IAIN)*, pp. 1–7. Prague, Czech Republic, October 20-23, 2015. DOI 10.1109/IAIN.2015.7352248. URL https://ieeexplore.ieee.org/document/7352248.

[3] Yeo, Dong Jin, Cha, Moohyun, and Mun, Duhwan. "Simulating Ship and Buoy Motions Arising from Ocean Waves in a Ship Handling Simulator," *Simulation* Vol. 88 No. 12 (2012): pp. 1407–1418. URL https://doi.org/10.1177/0037549712452128.

[4] Farrell, Phillip. "Ship Dynamics Identification Using Simulator and Sea Trial Data." Technical Report No. 2002-015. Defence R&D Canada, Toronto, Canada. 2002.

[5] "2018 Maritime RobotX Challenge Task Descriptions and Specifications," version 4.0, robonation, last modified December 05, 2018, URL https://www.robotx.org/images/RobotX_2018_Tasks-FINAL_v4.0.pdf.

[6] "21st Annual International Robosub Competition Mission and Scoring," version 1.5, robonation, last modified July 17, 2018, URL https://www.robonation.org/sites/default/files/2018%20RoboSub_2018%20Mission%20and%20Scoring_v01.50.pdf

[7] "2018 Maritime RobotX Rules and Requirements," version 4.0, robonation, last modified December 05, 2018, URL https://www.robotx.org/images/RobotX_2018_Rules-FINAL_v4.0.pdf

[8] Schnieders, Joseph. "Comparison Study of Low-Level Controller Techniques for Unmanned Surface Vessels." Master's Thesis Number 30384, Naval Postgraduate School, Monterey, California. 2018. URL https://calhoun.nps.edu/handle/10945/59581.

[9] Pace, Dale. "Modeling and Simulation Verification and Validation." *Johns Hopkins APL Technical Digest* Vol. 25 No. 2 (2004): pp. 163-172. URL https://www.jhuapl.edu/techdigest/TD/td2502/Pace.pdf.

[10] Chou, Ching-Tang, and Fu, Li-Chen. “Ships on Real-Time Rendering Dynamic Ocean Applied in 6-DOF Platform Motion Simulator.” *CACS International Automatic Control Conference,* pp.1235–1240. Taichun, Taiwan, 2007. URL https://www.semanticscholar.org/paper/Ships-on-Real-time-Rendering-Dynamic-Ocean-Applied-Chou-Fu/cc8c97565abfa71cd6f53c6ab1787392f1a7bb37?navId=paper-header.

[11] Cieutat, Gonzato, and Guitton. “A New Efficient Wave Model for Maritime Training Simulator,” *Proceedings Spring Conference on Computer Graphics*, pp 202–209. Budmerice, Slovakia, 2001. DOI 10.1109/SCCG.2001.945355. URL http://ieeexplore.ieee.org/document/945355/.

[12] Heins, Peter, Jones, Bryn, and Taunton, Dominic. “Design and Validation of an Unmanned Surface Vehicle Simulation Model.” *Applied Mathematical Modeling* Vol. 48 No.1 (2017): pp. 749–774. DOI 10.1016/j.apm.2017.02.028. URL https://linkinghub.elsevier.com/retrieve/pii/S0307904X17301245.

[13] Krishnamurthy, Khorrami, and Fujikawa. “A Modeling Framework for Six Degree-of-Freedom Control of Unmanned Sea Surface Vehicles.” *Proceedings of the 44th IEEE Conference on Decision and Control,* pp 2676–2681. Seville, Spain, 2011. DOI 10.1109/CDC.2005.1582567. URL http://ieeexplore.ieee.org/document/1582567/

[14] Peterson, Andrew, Ahmadian, Mehdi, Craft, Michael, and Shen, Andrea, 2013, “Simulation and Scale-Testing to Improve the Next Generation of Wave-Adaptive Modular Vessels,” *Proceedings of the 2013 Grand Challenges on Modeling and Simulation Conference. Toronto, Canada,* 2013. URL https://www.researchgate.net/publication/262239838_Simulation_and_scale-testing_to_improve_the_next_generation_of_wave-adaptive_modular_vessels.

[15] Sargent, Robert. “Verification and Validation of Simulation Models.” *Proceedings of the 2011 Winter Simulation Conference,* pp. 183–198. Phoenix, Arizona, 2011. URL https://dl.acm.org/citation.cfm?id=2431538

[16] Timperley, Christopher, Afzal, Aafsoon, Katz, Deborah, Hernandez, Jam, and Le Goues, Claire. “Crashing Simulated Planes Is Cheap: Can Simulation Detect Robotics Bugs Early?” *2018 IEEE 11th International Conference on Software Testing, Verification and Validation (ICST),* pp 331–342. Vasteras, Sweden, 2018. DOI 10.1109/ICST.2018.00040. URL https://ieeexplore.ieee.org/document/8367060.

[17] Ueng, Shyh-Kuang, Lin, David, and Liu, Chieh-Hong. “A Ship Motion Simulation System.” *Virtual Reality* Vol. 12 No. 1 (2008): pp. 65–76. DOI 10.1007/s10055-008-0088-8. URL https://link.springer.com/article/10.1007%2Fs10055-008-0088-8.

[18] Smith, Julianna. “Hundreds of teams from around the globe go robot to robot in 2018 robonation competitions.” AUVSI Foundation, last modified October 24, 2018, https://www.auvsi.org/hundreds-teams-around-globe-go-robot-robot-2018-robonation-competitions.

[19] Datla, Raju, and Kim, Hong Yoon. “Evaluation of a CFD Program AEGIRTM for Bare Hull Resistance and Seakeeping Prediction Capability.” Technical Report No. 2009/010. Naval Surface Warfare Center Carderock, West Bethesda, Maryland. 2009.

[20] Sarda, Edoardo, Qu, Huajin, Bertaska, Ivan, and von Ellenrieder, Karl. “Station-Keeping Control of an Unmanned Surface Vehicle Exposed to Current and Wind Disturbances,” *Ocean Engineering* Vol. 127 No. 1 (2016): pp. 305–324. DOI 10.1016/j.oceaneng.2016.09.037. URL https://www.sciencedirect.com/science/article/pii/S0029801816304206?via%3Dihub.

[21] Fossen, Thor. “A Nonlinear Unified State Space Model for Ship Maneuvering and Control in a Seaway.” *International Journal of Bifurcation and Chaos* Vol. 15 No. 9 (2005): pp. 2717–2746. DOI 10.1142/S0218127405013691. URL https://www.worldscientific.com/doi/abs/10.1142/S0218127405013691.

[22] Fossen, Thor. *Handbook of Marine Craft Hydrodynamics and Motion Control*, John Wiley & Sons, Ltd, Chichester, UK (2011).

[23] “Robotic Operating System: CoreComponents,” Open Source Robotics Foundation, last modified August 8, 2018, http://wiki.ros.org/ROS/Introduction.

[24] Navatek, Ltd. *Aegir User Guide*, Navatek, Ltd., Newport, Rhode Island (2018).

[25] “16’ WAM-V USV for RobotX 2016,” Marine Advanced Research, Inc., last modified November, 2015, https://www.robotx.org/images/files/RobotX2016SpecsFINALNov2015.pdf.

[26] Bingham, Brian. “Gazebo USV Plugins, Theory of Operation,” Github, last modified February 26, 2018, https://github.com/bsb808/robotx_docs/blob/master/theoryofoperation/theory_of_operation.pdf.

[27] Navatek, Ltd. *AEGIR Theory Guide*. Navatek, Ltd., Newport, Rhode Island (2018).

THIS PAGE INTENTIONALLY LEFT BLANK

INITIAL DISTRIBUTION LIST

1. Defense Technical Information Center
   Ft. Belvoir, Virginia

2. Dudley Knox Library
   Naval Postgraduate School
   Monterey, California